

Development and Analysis of Control Strategies for a 1 MW/3.2 MWh Energy Storage System at Avista Utilities

February 2020

PNNL

Jan Alam, Patrick Balducci, Trevor Hardy

WSU

Faculty:

Anjan Bose, Chen-Ching Liu, Anurag Srivastava, Yin Xu

Graduate Students:

Thomas J. Morrell, Venkatesh Venkatramanan, Yue Zhang,
Catherine Liu

DISCLAIMER

This report was prepared as an account of work sponsored by an agency of the United States Government. Neither the United States Government nor any agency thereof, nor Battelle Memorial Institute, nor any of their employees, makes **any warranty, express or implied, or assumes any legal liability or responsibility for the accuracy, completeness, or usefulness of any information, apparatus, product, or process disclosed, or represents that its use would not infringe privately owned rights.** Reference herein to any specific commercial product, process, or service by trade name, trademark, manufacturer, or otherwise does not necessarily constitute or imply its endorsement, recommendation, or favoring by the United States Government or any agency thereof, or Battelle Memorial Institute. The views and opinions of authors expressed herein do not necessarily state or reflect those of the United States Government or any agency thereof.

PACIFIC NORTHWEST NATIONAL LABORATORY
operated by
BATTELLE
for the
UNITED STATES DEPARTMENT OF ENERGY
under Contract DE-AC05-76RL01830

Printed in the United States of America

Available to DOE and DOE contractors from the
Office of Scientific and Technical Information,
P.O. Box 62, Oak Ridge, TN 37831-0062;
ph: (865) 576-8401
fax: (865) 576-5728
email: reports@adonis.osti.gov

Available to the public from the National Technical Information Service
5301 Shawnee Rd., Alexandria, VA 22312
ph: (800) 553-NTIS (6847)
email: orders@ntis.gov <<https://www.ntis.gov/about>>
Online ordering: <http://www.ntis.gov>

Development and Analysis of Control Strategies for a 1 MW/3.2 MWh Energy Storage System at Avista Utilities

February 2020

PNNL

Jan Alam
Patrick Balducci
Trevor Hardy

WSU

Faculty:

Anjan Bose, Chen-Ching Liu, Anurag Srivastava, Yin Xu

Graduate Students:

Thomas J. Morrell, Venkatesh Venkatramanan, Yue Zhang, Catherine Liu

Prepared for
the U.S. Department of Energy
under Contract DE-AC05-76RL01830

Pacific Northwest National Laboratory
Richland, Washington 99354

Summary

This report documents the work performed by Pacific Northwest National Laboratory (PNNL) and Washington State University (WSU) supporting an effort to develop control strategies for a 1 MW/3.2 MWh energy storage system (ESS) at Avista Utilities (Avista). The ESS project is funded through the Washington Clean Energy Fund (CEF) program administered by the Washington State Department of Commerce (DOC). A tri-party Cooperative Research and Development Agreement (CRADA), namely the CRADA 360, was created in 2015 to facilitate this work.

A three-level control architecture was envisioned by PNNL for the Avista ESS project: (a) the highest level is the optimization controller for supporting market services; (b) the middle level is a real-time controller that will accept schedules created by the optimization controller and will create real-time dispatch signals adhering to the electrical system conditions; and (c) the bottom level is a local controller that will perform the actual charge/discharge control based on the commands received from the real-time controller with any modification necessary to manage any local situation, such as a contingency.

Four tasks were identified to accomplish the ESS controller development and implementation work under CRADA 360. Task 1 was intended to build the various use cases of interest for Avista for processing and decision-making through the optimization controller. Economic evaluation performed using forecasts of price and load/generation could be vulnerable to forecasting uncertainties. Task 2 was designed to understand the impacts of uncertainties on ESS optimal operation, value streams, and designing a control strategy to manage the impact of uncertainties. The ESS is installed at a physical location within the Avista network and, therefore, it will have impacts on the local network operation. Task 3 was designed for modeling and simulation of the Avista network to assess those impacts. Task 4 was intended to assist Avista in the deployment of control strategies for the ESS. While PNNL and WSU performed initial development and analysis of control strategies, Avista took a different approach for implementation. Therefore, the concepts and architecture developed by PNNL were not directly pursued for field deployment.

Various use cases relating to bulk transmission system (e.g., energy shifting, system capacity support, ancillary services), distribution system (e.g., load-shaping, volt-var control, outage mitigation, microgrid operation), and a co-optimized operation of the ESS for a bundle of use cases were modeled using PNNL Battery Storage Optimization Tool (BSET). This tool was developed under a separate agreement (CRADA 352) to support economic benefit evaluation of ESS for a set of CEF projects. In the CRADA 360 project, BSET was envisioned as the core computing module for the optimization controller (the highest level in the three-level control architecture mentioned in the paragraph above) that will generate charge/discharge commands for optimally controlling the ESS for various use cases.

To accommodate for the uncertainties in price, a standard deviation of error of the price is incorporated in optimization formulation of the controller through allowable deviation in battery state of charge (SOC) caused by use case operation at every instant of time. For periods with high uncertainty, the allowable SOC deviation will be more restricted and, hence, the amount of energy transacted will be limited, while for periods with low standard, implying the forecast is more accurate, larger energy transactions will be permitted.

Modeling and simulation of the relevant portion of the Avista distribution network has been performed to incorporate the network characteristics and constraints with ESS control strategy. The network model available from Avista in Synergi software was converted into a GridLAB-D™ model for a research-oriented analysis. A lumped dynamic model of the Avista system was also created by making assumptions on dynamic performance parameters of the system components. Three strategies for distributing Area Control Error (ACE) signals between the lumped approximation of the conventional generators in Avista and the ESS were studied in the event of various system changes (e.g., step increase and ramping of load demand). The strategies could be described in simple terms as follows: (a) static strategy where the ACE signal is distributed based on a user-defined factor (for instance 70 percent to the conventional generator and 30 percent to the ESS); (b) proportionality-based strategy where the ACE is divided according to the available energy in the ESS; and (c) a priority-based strategy where the ACE is fully allocated to the ESS if sufficient energy is available in the ESS. It was observed that a priority-based ACE signal distribution strategy produced best output in terms of minimizing the power system frequency deviation in the event of a system change (e.g., step change or ramping of road demand).

The GridLAB-D model was also used for assessing how the reactive power capability of the ESS inverter will be used for locational voltage support within the Avista network. A volt-var control strategy using the voltage sensitivity of the relevant location with the reactive power output of the inverter has been developed and tested using daylong time series power flow simulations over multiple days in winter and summer. Appreciable voltage improvement was observed in simulation results for both seasons.

The analyses performed by PNNL and WSU suggest that the ESS installed at Avista network could support the network and tap into various revenue streams by controlling the real and reactive power output through appropriate control strategies. PNNL also proposed a high-level road map for implementation of the strategies developed under CRADA 360. While these strategies have not been deployed in the field, as Avista pursued a different implementation pathway, the analysis performed by PNNL and WSU could provide generally useful knowledge for ESS control strategy development.

Acronyms and Abbreviations

ACE	Area Control Error
AGC	Automatic Generation Control
AMI	Advanced Metering Infrastructure
BESS	Battery Energy Storage System
BSET	Battery Optimization Tool
CEF	Clean Energy Fund
CRADA	Cooperative Research and Development Agreement
DMS	Distribution Management System
DOC	Department of Commerce
DOE	Department of Energy
ESS	energy storage system
Hz	hertz
IDA	Independent AGC Signal Distribution
kVA	kilovolt amps
ms	millisecond
MVA _r	mega volt amps (reactive)
MW	megawatt
MWh	megawatt hours
PI	Proportional Integral
PNNL	Pacific Northwest National Laboratory
PriDD	Priority AGC Signal Distribution
ProDD	Proportional AGC Signal Distribution
PV	photovoltaic
SDA	Static AGC Signal Distribution
SOC	state of charge
WSU	Washington State University

Contents

- Summary ii
- Acronyms and Abbreviations..... iv
- Contents v
- 1.0 Introduction 1
 - 1.1 Background and Objective 1
 - 1.2 Tasks 2
 - 1.3 Project Benefit to Stakeholders 2
 - 1.3.1 Washington State DOC 3
 - 1.3.2 Avista Utilities 3
 - 1.3.3 U.S. Department of Energy and PNNL 3
 - 1.4 Report Organization 3
- 2.0 Energy Storage Controller – General Considerations 5
 - 2.1 Need for Optimized Dispatch 5
 - 2.2 Limitations of Comprehensive Optimization Controller 5
 - 2.3 Handling Fast-Response Services 6
- 3.0 Controller Architecture 7
 - 3.1 Controller Description 7
 - 3.1.1 Optimization Controller 7
 - 3.1.2 Real-Time Controller 8
 - 3.1.3 Local Controller 8
 - 3.1.4 Controller Implementation Division 9
 - 3.2 Optimization Controller Net Energy Estimates 9
- 4.0 Controller vs. Economic Analysis..... 11
 - 4.1 BSET Optimization..... 11
 - 4.2 Optimization Controller vs. BSET 12
- 5.0 Handling Forecasts and Uncertainty 13
 - 5.1 Proposed Optimization Controller Development..... 13
 - 5.2 Optimization with Uncertainty 14
 - 5.3 Optimization with Uncertainty Across Multiple Services 14
- 6.0 Controller Development Process 16
 - 6.1 Prototype Development..... 16
 - 6.1.1 Optimization Controller 16
 - 6.1.2 Real-Time Controller 16
 - 6.1.3 Local Controller 17
 - 6.2 Prototype Controller Testing 17
 - 6.3 Production Controller Integration..... 17

7.0	Distribution Network Model Development	18
7.1	Background.....	18
7.2	Overview of the Problem.....	18
7.2.1	Main Issues	18
7.3	Software Comparison	19
7.4	Synergi – GridLAB-D Conversion.....	19
7.4.1	Overview	19
7.4.2	Conversion Program.....	20
7.5	Smart Meter Data.....	22
7.6	Node Allocation from Smart Meters to Synergi and GridLAB-D Nodes.....	23
7.6.1	Node Allocation Overview.....	23
7.6.2	Procedure.....	23
7.6.3	Mapping Program.....	23
7.6.4	Aggregation Program	23
7.7	Developing Player Files to Play Back Measurements into GridLAB-D.....	24
7.7.1	The Need for Player Files.....	24
7.7.2	MATLAB Player File Generator Algorithm	24
7.8	Overall Model – Simulation and Analysis	25
7.9	Conclusion	30
8.0	ESS Real Power Control Strategy for Frequency Support	31
8.1	Motivation	31
8.2	AGC Signal Distribution Strategies	31
8.3	Analysis	33
8.3.1	Single Area Program	33
8.4	Results.....	34
8.4.1	Avista System with 10-MW BESS Subjected to a 20-MW Load Step Increase	34
8.5	Avista System with 1.31-MW BESS Subjected to a 20-MW Load Step Increase.....	39
8.6	Avista System with 1.31-MW BESS Subjected to a 3.33-MW Load Ramp Increase.....	43
8.7	BESS Performance When Operating in Island Mode	47
8.8	Conclusions	49
9.0	ESS Reactive Power Control Strategy for Voltage Support	50
9.1	Introduction.....	50
9.1.1	Abstract.....	50
9.2	Methodology Description.....	50
9.2.1	Voltage Sensitivity Analysis.....	50
9.3	Reactive Compensation Strategy of Battery.....	51

9.4	Simulation Guide.....	51
9.5	Initial Test on Turner 117 Model on September 14, 2016.....	52
9.5.1	Basic Information of Feeder Turner 117	52
9.5.2	Voltage Profile of Feeder Turner 117.....	53
9.5.3	Voltage Sensitive to Reactive Power	54
9.6	Volt-Var Control Strategy with Battery.....	54
9.7	Performance of the Proposed Strategy	55
9.8	Simulation Results for Clear Data without PV – Winter Data Testing on Turner 117	57
9.8.1	Simulation Results for January 12, 2017	57
9.8.2	Simulation Results for January 13, 2017	58
9.8.3	Simulation Results for January 14, 2017	59
9.8.4	Simulation Results for January 15, 2017	60
9.8.5	Simulation Results for January 16, 2017	61
9.9	Simulation Results for Clear Data without PV – Summer Data Testing on Turner 117	62
9.9.1	Simulation Results for August 22, 2017	62
9.9.2	Simulation Results for August 23, 2017	63
9.9.3	Simulation Results for August 24, 2017	64
9.9.4	Simulation Results for August 25, 2017	65
9.10	Simulation Results for Clear Data without PV – Autumn Data Testing on Turner 117	66
9.10.1	Simulation Results for October 12, 2017	66
9.10.2	Simulation Results for October 13, 2017	67
9.10.3	Simulation Results for October 14, 2017	68
9.10.4	Simulation Results for October 15, 2017	69
9.11	Statistical Analysis of ESS Controller.....	70
9.12	Validation of a Constant K Value for Winter Season	71
9.13	Simulation Results without PV	72
9.13.1	PV Installation Location	72
9.13.2	Voltage Control Results for Different Levels of PV Penetration.....	73
9.14	Simulations Conclusion.....	77
10.0	Conclusion	78
11.0	References.....	80

Figures

Figure 1.	CRADA 360 Relationships and Tasks.....	1
Figure 2.	Proposed Controller Architecture	7
Figure 3.	BSET Optimization with Data Inputs and Outputs	11
Figure 4.	Controller Architecture with Data Inputs and Outputs.....	12
Figure 5.	Flowchart for Node and Branch Conversion from Synergi to GridLAB-D.....	20
Figure 6.	Flowchart for Mapping and Aggregation Procedure	24
Figure 7.	GridLAB-D Real Power vs. DMS Measurements at the Substation for Winter Case	26
Figure 8.	GridLAB-D Reactive Power vs. DMS Measurements at the Substation for Winter Case	26
Figure 9.	Fall Data MW Output	27
Figure 10.	Fall Data Mega Volt Amps (reactive) (MVAR) Output.....	27
Figure 11.	Summer Data MW Output.....	28
Figure 12.	Summer Data MVAR Output.....	28
Figure 13.	MW Seasonal Comparison	29
Figure 14.	MVAR Seasonal Comparison	29
Figure 15.	Static AGC Signal Distribution (SDA).....	32
Figure 16.	Proportional AGC Signal Distribution (ProDD)	32
Figure 17.	Priority AGC Signal Distribution (PriDD).....	32
Figure 18.	AGC Signal Distribution Block Diagram for SDA, ProDD, and PriDD	32
Figure 19.	Independent AGC Signal Distribution (IDA).....	33
Figure 20.	AGC Signal Distribution Block Diagram for IDA	33
Figure 21.	Single Area Block Diagram without BESS.....	34
Figure 22.	Single Area Block Diagram with BESS.....	34
Figure 23.	Smoothed ACE (close up on largest magnitude ACEs) in MW vs. Seconds.....	35
Figure 24.	Smoothed ACE (over whole simulation time) in MW vs. Seconds	35
Figure 25.	ACE (close up on largest magnitude ACE) in MW vs. Seconds	36
Figure 26.	Mechanical Power Output of Equivalent Generator in MW vs. Seconds.....	36
Figure 27.	Mechanical Power Output of Equivalent Generator and Smoothed ACE in MW vs. Seconds.....	37
Figure 28.	BESS Power Output in MW vs. Seconds	37
Figure 29.	System Frequency Close Up in Hertz (Hz) vs. Seconds.....	38
Figure 30.	System Frequency in Hz vs. Seconds.....	38
Figure 31.	Smoothed ACE (close up on largest magnitude ACE) in MW vs. Seconds	39
Figure 32.	Smoothed ACE (over whole simulation time) in MW vs. Seconds	40
Figure 33.	ACE (close up on largest magnitude ACE) in MW vs. Seconds	40
Figure 34.	Mechanical Power Output of Equivalent Generator in MW vs. Seconds.....	41

Figure 35. Mechanical Power Output of Equivalent Generator and ACE in MW vs. Seconds.....41

Figure 36. BESS Power Output in MW vs. Seconds42

Figure 37. System Frequency close up in Hz vs. Seconds.....42

Figure 38. System Frequency in Hz vs. Seconds.....43

Figure 39. Smoothed ACE (over whole simulation time) in MW vs. Seconds44

Figure 40. Mechanical Power Output of Equivalent Generator in MW vs. Seconds.....44

Figure 41. Mechanical Power Output of Equivalent Generator and ACE in MW vs. Seconds.....45

Figure 42. BESS Power Output in MW vs. Seconds45

Figure 43. System Frequency Close Up on Ramp Settling Frequency in Hz vs. Seconds.....46

Figure 44. System Frequency in Hz vs. Seconds.....46

Figure 45. System Frequency Comparison Between Load Step Increase and Load Ramp in Hz vs. Seconds.....47

Figure 46. Turner 117 Screenshot48

Figure 47. Turner 116 Screenshot49

Figure 48. Topology of Feeder Turner 117.....52

Figure 49. The Deviation Between DMS Measurement and Aggregated Smart Meters Measurement53

Figure 50. The Voltage Profile Along the Feeder at a Relative Heavy-Load Time53

Figure 51. The Schedule of Reactive Power of Battery, Average Battery Voltage Before Reactive Power Control and Target Voltage Value for the Target Day55

Figure 52. Voltage Profile Comparison Between Cases with and without BES Control55

Figure 53. Average Voltage at Battery Bus Before and After BESS Control.....56

Figure 54. Voltage of Three Phases at the Bus with Lowest Voltage with and without BESS Control.....56

Figure 55. Average Battery Voltage Before and After Reactive Power Control (left) and the Schedule of Reactive Power of Battery for January 12, 2017 (right)57

Figure 56. Voltage Profile Comparison Between Case with and without BESS Control for January 12, 201757

Figure 57. Average Battery Voltage Before and After Reactive Power Control (left) and the Schedule of Reactive Power of Battery for January 13, 2017 (right)58

Figure 58. Voltage Profile Comparison Between Case with and without BESS Control for January 13, 201758

Figure 59. Average Battery Voltage Before and After Reactive Power Control (left) and the Schedule of Reactive Power of Battery for January 14, 2017 (right)59

Figure 60. Voltage Profile Comparison Between Case with and without BESS Control for January 14, 201759

Figure 61. Average Battery Voltage Before and After Reactive Power Control (left) and the Schedule of Reactive Power of Battery for January 15, 2017 (right)60

Figure 62. Voltage Profile Comparison Between Case with and without BESS Control for January 15, 201760

Figure 63. Average Battery Voltage Before and After Reactive Power Control (left) and the Schedule of Reactive Power of Battery for January 16, 2017 (right)61

Figure 64. Voltage Profile Comparison Between Case with and without BESS Control for January 16, 201761

Figure 65. Average Battery Voltage Before and After Reactive Power Control (left) and the Schedule of Reactive Power of Battery for August 22, 2017 (right)62

Figure 66. Voltage Profile Comparison Between Cases with and without BESS Control for August 22, 201762

Figure 67. The Average Battery Voltage Before and After Reactive Power Control (left) and the Schedule of Reactive Power of Battery for August 23, 2017 (right)63

Figure 68. Voltage Profile Comparison Between Cases with and without BESS Control for August 23, 201763

Figure 69. Average Battery Voltage Before and After Reactive Power Control (left) and the Schedule of Reactive Power of Battery for August 24, 2017 (right)64

Figure 70. Voltage Profile Comparison Between Cases with and without BESS Control for August 24, 201764

Figure 71. Average Battery Voltage Before and After Reactive Power Control (left) and the Schedule of Reactive Power of Battery for August 25, 2017 (right)65

Figure 72. Voltage Profile Comparison Between Cases with and without BESS Control for August 25, 201765

Figure 73. Average Battery Voltage Before and After Reactive Power Control (left) and the Schedule of Reactive Power of Battery for October 12, 2017 (right)66

Figure 74. Voltage Profile Comparison Between Cases with and without BESS Control for October 12, 201766

Figure 75. The Average Battery Voltage Before and After Reactive Power Control (left) and the Schedule of Reactive Power of Battery for October 13, 2017 (right)67

Figure 76. Voltage Profile Comparison Between Cases with and without BESS Control for October 13, 201767

Figure 77. Average Battery Voltage Before and After Reactive Power Control (left) and the Schedule of Reactive Power of Battery for October 14, 2017 (right)68

Figure 78. Voltage Profile Comparison Between Cases with and without BESS Control for October 14, 201768

Figure 79. Average Battery Voltage Before and After Reactive Power Control (left) and the Schedule of Reactive Power of Battery for October 15, 2017 (right)69

Figure 80. Voltage Profile Comparison Between Cases with and without BESS Control for October 15, 201769

Figure 81. Power Factor Improvement for October 15, 2016.....70

Figure 82. Reactive Power Schedule of BESS Generated by Constant K and Separated K for Each Voltage Range at January 15, 201772

Figure 83. PV Location and Connected Node ID.....72

Figure 84. Real Power Demand for January 16 w/wo a 750 kVA PV Panel (left); the PV Output and the Real Power Demand Difference w/wo PV Panel Penetration73

Figure 85. Average Battery Voltage Before and After Reactive Power Control (left) and the Schedule of Reactive Power of Battery for January 16, 2017 with 75 kVA PV (right)74

Figure 86. Voltage Profile Comparison Between Case with and without BESS Control for January 16, 2017 with 75 kVA PV74

Figure 87. Average Battery Voltage Before and After Reactive Power Control (left) and the Schedule of Reactive Power of Battery for January 16, 2017 with 750 kVA PV (right)75

Figure 88. Voltage Profile Comparison Between Case with and without BESS Control for January 16, 2017 with 750 kVA PV75

Figure 89. Average Battery Voltage Before and After Reactive Power Control (left) and the Schedule of Reactive Power of Battery for January 16, 2017 with 3000 kVA PV (right)76

Figure 90. Voltage Profile Comparison Between Case with and without BESS Control for January 16, 2017 with 3000 kVA PV76

Figure 91. Voltage of Three Phases at the Bus with Lowest Voltage with and without BESS Control for 3000 kVA PV Penetration Case77

Tables

Table 1. Comparison of Synergi and GridLAB-D Voltages25

Table 2. Comparison of Synergi and GridLAB-D Currents25

Table 3. The Sensitivity Table for September 16, 2016 Case54

Table 4. The Sensitivity Table for January 12, 2017 Case57

Table 5. The Sensitivity Table for January 13, 2017 Case58

Table 6. The Sensitivity Table for January 14, 2017 Case59

Table 7. The Sensitivity Table for January 15, 2017 Case60

Table 8. The Sensitivity Table for January 16, 2017 Case61

Table 9. The Sensitivity Table for August 22, 2017 Case.....62

Table 10. The Sensitivity Table for August 23, 2017 Case.....63

Table 11. The Sensitivity Table for August 24, 2017 Case.....64

Table 12. The Sensitivity Table for August 25, 2017 Case.....65

Table 13. The Sensitivity Table for October 12, 2017 Case66

Table 14.	The Sensitivity Table for October 13, 2017 Case	67
Table 15.	The Sensitivity Table for October 14, 2017 Case	68
Table 16.	The Sensitivity Table for October 15, 2017 Case	69
Table 17.	Power Factor Improvement from ESS Controller for All Test Cases.....	70
Table 18.	The Sensitivity Table for January 12 to 16, 2017 Cases.....	71
Table 19.	The Sensitivity Table for January 16, 2017 Case with 75 kVA PV	73
Table 20.	The Sensitivity Table for January 16, 2017 Case with 750 kVA PV	74
Table 21.	The Sensitivity Table for January 16, 2017 Case with 3000 kVA PV	75
Table 22.	The Sensitivity Table for January 12 to 16, 2017 Cases.....	76

1.0 Introduction

1.1 Background and Objective

Avista Utilities (Avista) is an investor-owned, vertically integrated utility serving approximately 340,000 electricity customers in Washington State and Idaho. More than 50 percent of the electrical energy served by Avista comes from hydro- and wind-based clean generation resources. Avista was one of the first utilities to be funded through the Washington Clean Energy Fund (CEF) program, launched in 2015 by the Washington State Department of Commerce (DOC). A vanadium-redox flow battery system rated at 1 megawatt (MW)/3.2 megawatt hours (MWh) was installed by Avista under this funding scheme. To understand and evaluate the value streams energy storage systems (ESSs) could bring for Avista, an analytics program led by Pacific Northwest National Laboratory (PNNL) was launched through a Cooperative Research and Development Agreement (CRADA), namely CRADA 352. A Battery Storage Evaluation Tool (BSET) was developed and enhanced under this agreement. A parallel effort was launched under a different agreement, CRADA 360, to utilize the knowledge gained from the analytics program to realize the value streams through appropriate control strategies and an implementation platform. A tri-party agreement among PNNL, Washington State DOC, and Avista was signed to facilitate this work. PNNL led both efforts and engaged Washington State University (WSU) through a subcontract on the control strategy development under CRADA 360. The schematic diagram in Figure 1 illustrates the relationship between CRADA 360 and 352 through BSET.

The objective of this report is to document the effort undertaken by PNNL and WSU in developing the control strategies for Avista ESS under CRADA 360. Since a different implementation pathway was pursued by Avista, the report does not contain any field implementation results and lessons.

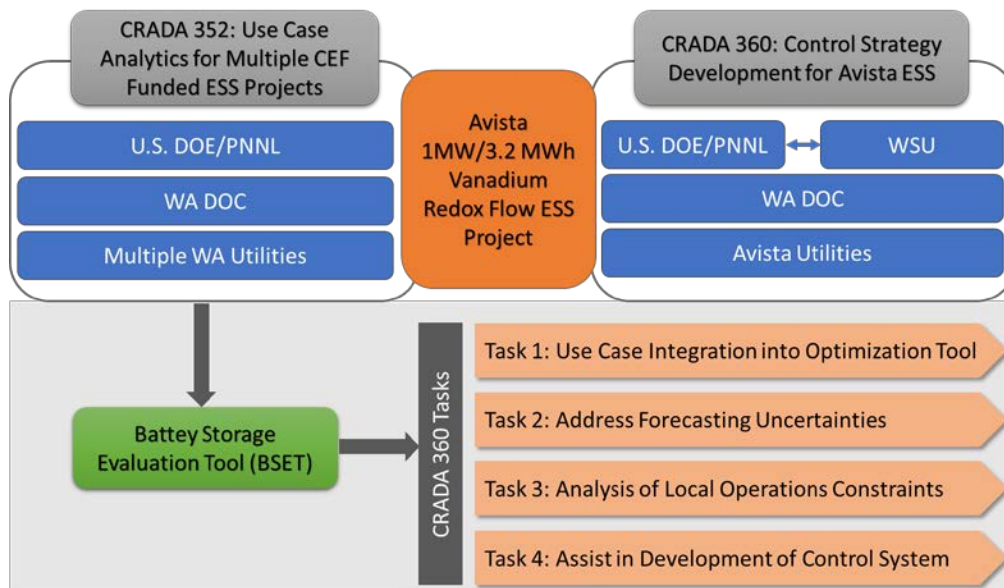


Figure 1. CRADA 360 Relationships and Tasks

1.2 Tasks

Four tasks were defined to achieve the goals of the control strategy development effort, as illustrated in Figure 1.

Task 1: Use Case Integration into Optimization Tool

The purpose of this task was to model and evaluate the economic use cases of the ESS for Avista through the BSET, developed by PNNL. This tool can determine the dispatch signals for ESS to maximize the operational value of multiple use cases through co-optimization. Various engineering (e.g., ESS parameters) and financial (e.g., electricity price) information is incorporated in modeling the use cases of interest.

Task 2: Address Forecasting Uncertainties and Perform Sensitivity Analysis

To address the uncertainty of load, price, and renewable energy in-feed, this task applied the Monte Carlo method and determined uncertainty with respect to developments in the grid, markets, and storage, including energy prices, balancing signal, balancing reserve requirements, and system load. The BSET model can also be used to explore the sensitivity of the results to varying key assumptions, including discount rates, energy prices, balancing service prices, ESS capacity for mitigating outages, and changes in the ESS energy and power capacities.

Task 3: Perform Analysis of Local Operations Constraints on Value Proposition

In this task, PNNL worked with Avista and WSU to characterize the network constraints associated with local operations of the ESS for achieving economic benefit. The results of these simulations revealed areas of operational concern such as American National Standards Institute voltage violations, excessive voltage regulator action, and distribution feeder loss increase, among others. WSU developed steady-state and dynamic models of the Avista network for the analyses required for this task.

Task 4: Assist in Development of Control System

PNNL intended to assist Avista in the integration of optimization algorithms into a more comprehensive control system that recognizes operational constraints and objectives beyond value maximization of the ESS. The plan was to provide the optimal control strategy (based on value) to Avista for their adaptation, extraction, or merger with other control system development efforts. The control system must be integrated with the control of the distribution system and the ESS. Avista was supposed to lead this effort, with support from PNNL and other project partners (e.g., UniEnergy Technologies, WSU). PNNL intended to provide assistance in evaluation of the control system, specifically focusing on the degree to which services valued in Task 1 are realizable in the developed control system. PNNL intended to re-evaluate the value attainable for the ESS based on the Avista implemented control system and validate/calibrate the optimal selection of services following completion of an initial set of ESS performance tests.

1.3 Project Benefit to Stakeholders

The project was anticipated to benefit the main stakeholders in a multitude of ways, as described below.

1.3.1 Washington State DOC

To maximize the value of the CEF program, Washington DOC and grant recipient utilities worked with PNNL in a separate project to evaluate specific storage functions, which will be implemented and tested individually, and then combined and tested in paired or potentially higher-aggregated multiple services. The CRADA 360 project was expected to assist in refining the accuracy and implementation of economic dispatch through incorporation of lessons learned from research conducted in this project with a field-deployed control system and evaluating their performance, thereby building the business case for ESS through the development of new algorithms and tools for optimizing ESS operation. This framework and its application for the demonstration project is expected to inform and empower other utilities in Washington State and in the region, storage technology developers, and state regulators to prudently and confidently pursue the deployment of energy storage.

1.3.2 Avista Utilities

The proposed energy storage solution, when combined with the Pullman smart grid project of Avista, will enhance reliability, increase efficiency and provide direct customer benefit. The CRADA 360 project was expected to enable Avista to test both supply- and load-side use cases and then dispatch storage for optimal operation while computing the benefits of all available opportunities. In addition, it was anticipated to provide learning opportunities to refine the accuracy and implementation of economic dispatch through incorporation in a field-deployed control system. Through the development of new algorithms and tools for controlling, optimizing, and evaluating ESS operations in order to maximize system benefits, energy storage could be an important asset in the supply-demand equation. The concepts and tools developed under this project could be applied to storage, customer-owned assets, and other distributed resources, the characteristics of which are known but could be involved in a power system that is in optimal configuration at all times. Avista will have the opportunity to explore the incorporation of energy storage as a distribution asset in their distribution management system, a step toward harvesting the increasing value of the smart grid at the distribution and customer levels.

1.3.3 U.S. Department of Energy and PNNL

It was anticipated that the project will expand the U.S. Department of Energy (DOE) examination and documentation of energy storage technology development with the goal of developing advanced battery technologies by performing economic and engineering analyses that explore the valuation and business case for storage applications within the transmission and distribution grid. A primary benefit of this project will be the creation of new algorithms and tools for controlling and optimizing ESS operations and for more accurately accommodating electrical behavior and limitations in economic dispatch. The project will enable PNNL to advance grid and storage analytics on behalf of DOE, allowing highly detailed analyses seeking optimal operation of an ESS providing numerous services.

1.4 Report Organization

The report integrates the work performed by PNNL and WSU for development of ESS control strategy for Avista ESS. Chapters 2 through 6 contain the work performed by PNNL in developing high-level concepts for the control strategy, including architecture, approach to address uncertainty, and guidelines for controller field deployment. Chapters 7 through 9 document the work performed by WSU in modeling and analysis of the impacts of real and

reactive power output from the ESS on Avista distribution network. Details of the network modeling approach and validation results are presented in Chapter 7. Chapter 8 documents ESS real power control strategies for enhancing the dynamic performance of the network in the events of load change. A reactive power control strategy is developed in Chapter 9 for supporting network voltage in various scenarios including high load and solar photovoltaic (PV) penetration. A summary of the work performed, and important findings are presented in the Conclusion in Chapter 10.

2.0 Energy Storage Controller – General Considerations

ESSs have the potential to improve the operating capabilities of the electricity grid. Their ability to store energy and deliver power can increase the flexibility of grid operations while providing the reliability and robustness that will be necessary in the grid of the future—one that will be able to provide for projected increases in demand and the integration of clean energy sources while being economically viable and environmentally sustainable. Energy storage has received a great deal of attention in recent years. Entrepreneurs are working enthusiastically to commercialize myriad promising technologies, and venture capitalists and the U.S. government are investing in this space. The technologies show promise, but it remains difficult to evaluate and measure the benefits that ESS could provide.

2.1 Need for Optimized Dispatch

ESSs have a wide variety of value streams they can provide. Because of their inherent ability to shift energy exchanges across time, utilizing them to their greatest value necessarily involves the use of optimization software that can schedule the charging and discharging of the ESS for a specified period of time into the future (the optimization period). Using historical pricing and system data, it is possible to estimate the potential value of the ESS if it were to be used in that precise, optimal manner. That is, if it is assumed that perfect forecasts were available for all economic and electrical data, an optimizer could determine the absolute best-case value generated by the ESS.

2.2 Limitations of Comprehensive Optimization Controller

PNNL has previously developed optimization software to generate optimal ESS dispatch schedules for a limited number of services to help define the total potential value generated by an ESS. This software will form the basis for the optimization controller, but differences between these two applications will require the software to be modified in particular ways.

Some of the services that ESSs provide require changes in charge/discharge power on a relatively short time scale. If engaged in frequency regulation, for example, a new charge/discharge power is defined every four seconds (typically). If acting as an uninterruptible energy source, the ESS may need to ramp to full output power in milliseconds if it detects a disturbance in the grid. In these kinds of situations, the time required to send the relevant system data to the optimizer, have the optimizer generate the optimal dispatch schedule, and communicate this dispatch signal back to the ESS, is likely to exceed the amount of time required to realize the value of some of these services. Furthermore, in cases such as outage mitigation, there is no need for the optimization to be involved in the provisioning of said service. When an outage event occurs, the ESS should respond immediately, regardless of what the optimization engine has determined it would be doing if an outage was not taking place.

In evaluating the potential value of the ESS optimally engaging in a variety of services, the input data is historical, and the optimizer operates under the assumption of perfect foresight. If a real-time optimization-based controller were to operate, it would require forecast data for all required inputs, some of which may not exist at all (the Automatic Generation Control [AGC] signal in frequency regulation, for example). Furthermore, any forecasts that are available will have uncertainty (which may or may not be quantified). Any optimization effort that ignores this uncertainty may produce a mathematically correct optimal schedule but one where the slightest

deviation from the forecasted inputs produces dramatically lower values. A more appropriate optimization algorithm would incorporate input signal uncertainties and produce a dispatch schedule that finds the highest value for a specified amount of risk.

2.3 Handling Fast-Response Services

Given the limitation of communication time, computation time, and the response time required by the service, some of these services could be considered “fast-response” and are unable to be dispatched directly by an optimizer. Thinking more generally about the services offered, they can be divided into three categories based on the data and response-speed required.

1. **Market Services** – Market services are those services that can be valued and fully dispatched by an optimizer. These services have values typically defined by a market, and their dispatch is infrequent enough that the delays due to communication and computation do not significantly impact their provision. Furthermore, the optimal dispatch of the service is only affected by market forces rather than being defined or influenced by electrical system conditions. Energy arbitrage is a perfect example of a market service; the market period is typically one hour, the value of the service is only defined by the market, and the ESS does not need to be aware of any electrical system conditions to correctly value and dispatch the service. With only a forecast of market prices, the optimizer can fully schedule an ESS for energy arbitrage.
2. **Operational Services** – Operational services are services whose provision is only triggered by local system conditions, and the required response time for provision of these services is much faster than the communication and computation time required by a remote optimizer. The value for these services must be fixed or known *a priori* to the provision of the service. Using an ESS for outage mitigation is an example of an operational service. The value for the ESS providing outage mitigation is largely determined by the loads on the system (particularly if there is a specific high-value customer it will be serving) and can be fully assessed prior to any outage. When an outage begins, the ESS will need to respond within milliseconds to provide continuity of service, much faster than existing communication and computation systems could respond to provide an optimal response to the outage. Furthermore, no optimization is necessary in provisioning operational services, as their value is pre-determined and whether the ESS will provide said services would be similarly pre-determined. In provisioning these services, all that is required is the triggering event (likely unique for each service) for the ESS to immediately engage.
3. **Hybrid Services** – Hybrid services are those whose value is based on market conditions but are provisioned based on electrical system conditions. The timing of the provision of these services is determined by the optimizer, but the moment-by-moment operation is defined by system conditions. These services require the engagement of the optimizer, as it will determine if it is financially optimal to engage in a given service (as in the case of market services) but must rely on electrical system conditions to determine the specific charge/discharge pattern (as in the case of the operational services). Frequency regulation is an example of a hybrid service. Based on the market and/or regional generator availability, the optimizer may determine that the best value for ESS activity is to perform frequency regulation (versus, for example, energy arbitrage). The optimizer cannot, in a timely manner, determine the charge/discharge activity of the ESS for frequency regulation, as the needs of the electrical system are redefined every four seconds (typically). Instead, software separate from the optimizer must be engaged that takes the appropriate input signals (frequency, AGC, ACE, etc.), quickly computes the charge/discharge levels, and communicates them to the ESS.

3.0 Controller Architecture

To accommodate the time-constraints imposed by the computing and communication infrastructure, the proposed controller architecture requires splitting the software into three distinct hierarchical portions:

1. Optimization Controller
2. Real-Time Controller
3. Local Controller.

Figure 2 shows the design of the controller that is being proposed to handle the three types of services described in section 2.3.

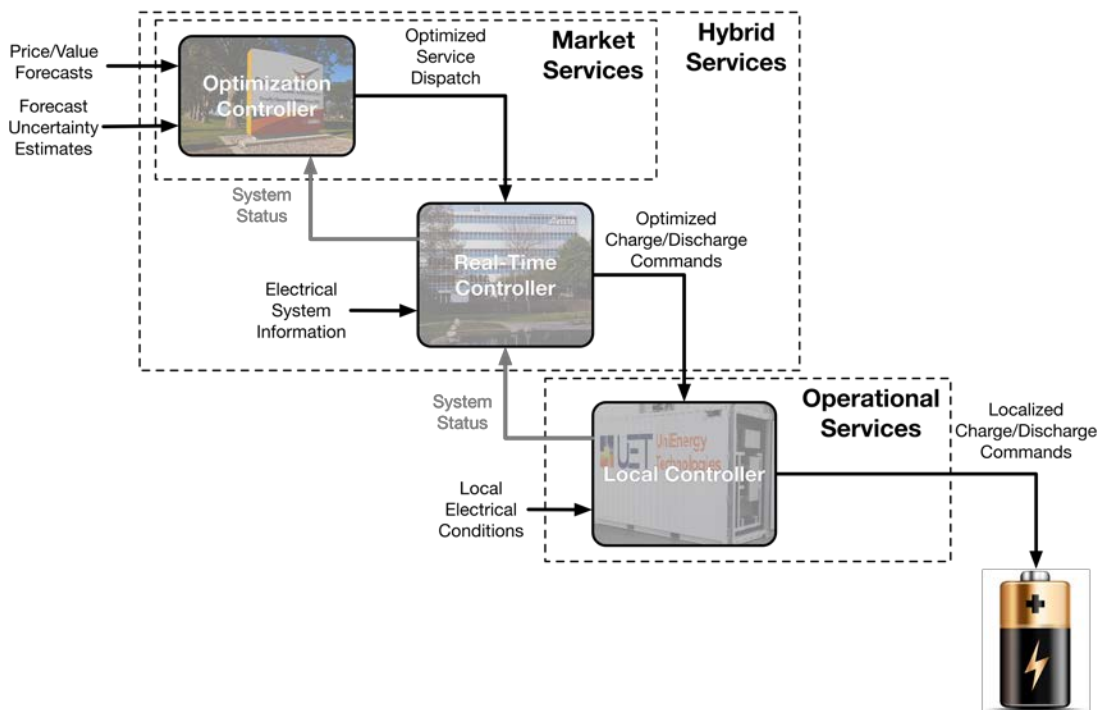


Figure 2. Proposed Controller Architecture

3.1 Controller Description

3.1.1 Optimization Controller

The optimization controller requires forecasts for all dispatchable services (i.e., services in which provisioning is optional) and computes the optimal scheduling of said services for the duration of the optimization period. For market services, such as energy arbitrage, it determines the charge/discharge schedule directly; for hybrid services, it simply defines when these services will be engaged. In either case, the output of the optimization controller is passed to the real-time controller for further refinement and dispatch to the ESS.

The optimization controller will generate new dispatch schedules at a frequency commensurate with the update frequency of the price forecasts it uses as inputs. When the optimization controller generates a new dispatch schedule, it must also receive any newly updated forecasts and ESS system information, particularly SOC.

Additionally, previous work with the existing optimization engine at PNNL shows that generating new dispatch schedules more frequently, with only the ESS SOC being updated each time, provides greater dispatch schedule accuracy and total value. These more frequent re-optimizations ensure that the gap between the optimization controller's estimate of the ESS SOC and the actual SOC are minimized, which prevents the optimization controller from dispatching services the ESS is unable to provide. The exact frequency of optimized schedule generation will be determined based on the available limitations of the computing and communication infrastructure.

3.1.2 Real-Time Controller

The real-time controller is responsible for taking the output of the optimization controller and generating the real-time charge/discharge commands for the ESS to execute. For market services, no extra computation is involved, as the optimization controller has already fully defined the charge/discharge schedule. For any hybrid services, it is the responsibility of the real-time controller to generate the charge/discharge commands, as needed, based on the current electrical system state or similar signal. For example, if the optimization controller has specified that for the next hour, the highest value service is frequency regulation, the real-time controller would perform (for example) a simple multiplication of the AGC signal by a pre-defined factor to translate AGC into charge/discharge commands that are then sent on to the ESS. The generation of this command would occur every four seconds to match the update frequency of the AGC.

Each hybrid service would have its own unique algorithm that could be executed quickly enough to appropriately provision the given service. Using the example of frequency regulation, if it were not possible to calculate the charge/discharge command and communicate this to the ESS in a timely manner (something on the order of four seconds), then this service would have to be provisioned in another manner.

The real-time controller will incorporate the research and analysis by WSU regarding the dispatch of reactive power for optimal voltage management. As the reactive power output from the inverter in the ESS is only limited by the real power dispatch, the value generated through reactive power has virtually no cost. It is anticipated that the work by WSU will provide algorithms that can be used to most optimally utilize the reactive power capacity of the inverter. These algorithms will not require input from the optimization controller but rather will generate a secondary schedule for reactive power that can be overlaid with the real power schedule generated by the optimization controller.

3.1.3 Local Controller

The local controller receives commands from the real-time controller and executes them directly with the ESS system. Commands from the real-time controller are over-ridden in the provisioning of an operational service such as outage mitigation. In these cases, communication and computation delays would be too large to inform the real-time controller of the beginning of an operational event, and the local controller must immediately respond on its own to provision

the service. It is assumed that the local controller will be sited with the ESS so as to be as responsive as possible.

The triggering condition for the provision of an operational service must be defined and coded into the local controller as well as release conditions that define when the operational service event is over and commands from the real-time controller can resume their execution. If multiple operational services are possible, a prioritized ranking of the services must be made in the event that triggering conditions for multiple services occur simultaneously.

3.1.4 Controller Implementation Division

Though implied in this discussion and Figure 2, the physical location of these three controllers does not necessarily have to be in three distinct locations. The limitations of the communication and computation systems have the largest impact on what physical divisions, if any, need to exist in the controller implementation. The local controller is assumed to be sited with the ESS to provide the fastest response, but if very low latency communication between the ESS and the local controller exists, this is not necessarily the case. The two could be co-located either at the ESS or at a control center. In either case, the two controllers would have approximately immediate access to the data they needed and the ability to communicate their respective commands in a timely manner.

Similarly, if adequate computation and communication infrastructure existed, the optimization controller could be physically located with the real-time and/or local controller. The optimization controller needs access to all necessary forecasts and hardware on which to run the relatively computationally intensive optimization routine. Since the communication latency is less of an issue, the primary concern would likely be data security, as forecasted values would likely be considered highly sensitive.

3.2 Optimization Controller Net Energy Estimates

In the case of all non-market services, for the optimization controller to operate effectively, it must have the ability to calculate the SOC of the ESS at each decision point in the optimization (typically once an hour for each hour in the optimization period). To do this, it must be able to determine the net energy exchange between the ESS and the electrical grid during the times a given service could be scheduled. Such energy impacts influence the optimizer; if a given service requires 50 percent of the ESS capacity for one hour of operation and provides \$100 of value, while another service requires 30 percent of the ESS capacity but provides \$95 of value, the optimizer will choose the latter, as it provides more value per unit of energy transferred.

When the optimizer is used for lifetime economic evaluation, it is fully aware of the ESSs virtual operation for every second of the evaluation period. Modifying this optimization engine for real-time operation requires that the charge/discharge commands for some services be defined outside the optimization controller. Some means of estimating the net energy exchange must be developed to enable the optimizer to work effectively.

For market services, the price forecast is sufficient for full optimal dispatch of the service as the power transfer of the ESS is defined and the optimizer is able to estimate the SOC of the ESS for the duration of the provision of that service. No further estimate of the net energy exchange is required.

Hybrid services, due to the real-time controller defining the charge/discharge schedule, are more complex. In addition to the price forecast, an estimate of the SOC impact as a function of when the service is provisioned must be calculated. For some services, such as frequency regulation, the impact on SOC could be relatively minimal due to the typically energy-neutral nature of the regulation signal. For other hybrid services, the impact on SOC may be a function of time of day, system load, voltage at the ESS, outdoor temperature, etc.

Developing these models will rely on results from the baseline and use-case testing data. Analysis of the data will be used to determine the sensitivity of each service to various factors (e.g., power level, temperature, etc.). These models will allow simple estimates of the net energy transaction for each service. For example, it may be discovered that over one hour of frequency regulation, independent of system load or the range of power levels used in providing the service, the net loss of energy is 0.5 MWh. This information will be used by the optimization controller as it computes the highest value dispatch signal.

Operational services are, by nature, completely outside the scope of the optimization controller and, as explained previously, override the commands sent by the real-time controller (which itself receives commands from the optimization controller). At the conclusion of the provision of one of these operational services, the optimization controller must be informed of the impact on SOC due to the operational event, so that the formation of the next dispatch schedule incorporates the current state of the ESS.

4.0 Controller vs. Economic Analysis

4.1 BSET Optimization

The optimization controller proposed above bears a strong resemblance to the software tool being used in related work being done in CRADA 352, commonly called BSET. BSET is being used to provide an assessment of the total economic potential of the ESS as it engages in a variety of services.

The core of BSET is an optimization engine of which the primary goal is to define the charge/discharge schedule of the ESS for the duration of the economic assessment. As shown in Figure 3, to do this, the optimization engine must know

1. The price for each service it will offer. For the economic analysis, these are historical prices.
2. Service-specific signals. For services such as energy arbitrage, the output of the ESS is wholly defined by the state of the ESS (how much energy it holds), and its power rating and such additional signals are not required. For services such as frequency regulation, the output of the optimization engine is defined not only by the state and rating of the battery, but also the regulation signal that must be followed. In cases such as these, when the optimization engine chooses frequency regulation as the most beneficial service, it uses the provided regulation signal to define a second-by-second dispatch of the ESS, calculating the changing SOC on a similar time scale.

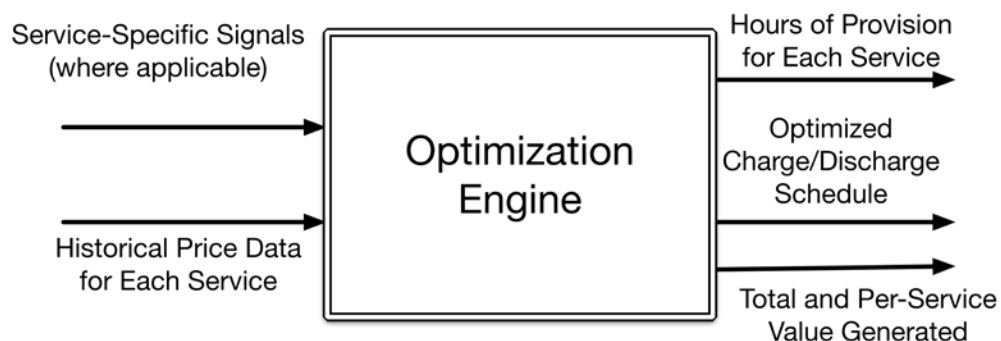


Figure 3. BSET Optimization with Data Inputs and Outputs

From these inputs, the optimization engine is able to fully define the hypothetical charge/discharge schedule of the ESS for the entire duration of the analysis period (typically one year). In addition to this schedule, the ESS is also able to provide other related information about the ESS such as the number of hours it engaged in each service over the analysis period and the revenue generated by each service.

It is worth noting that, traditionally, the economic analysis provided by BSET assumes perfect foresight. That is, the historical prices and required output signals are assumed to be perfectly accurate and entirely reflect reality. It also assumes that the operation of the BSET does not affect the price of the services it engages in; that is, the ESS is assumed to be a price-taker.

4.2 Optimization Controller vs. BSET

The core goal of the ESS Controller is very similar to that of BSET: determine the charge/discharge schedule that will maximize the value of the ESS. And to that end, the inputs to the two are similar in principle. The specific signals used, though, are quite different because the controller must work with forecasts and estimates about the future state of the ESS and the economic and electrical environment in which it will be operating. Figure 4 shows how the proposed controller architecture affects the data requirements.

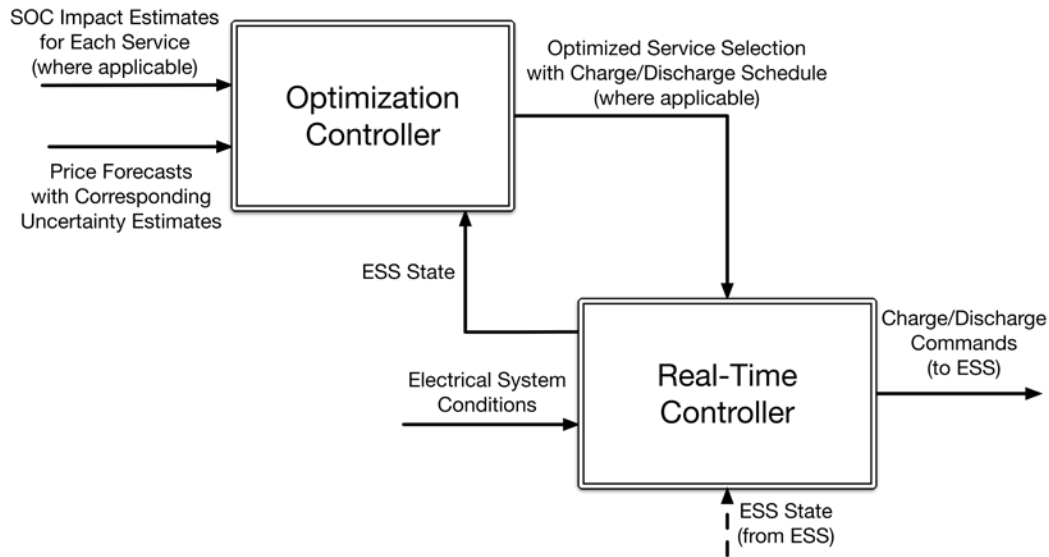


Figure 4. Controller Architecture with Data Inputs and Outputs

Additionally, the service-specific signals used for economic evaluation are not available as forecasts, so the optimization controller is unable to define the specific charge/discharge pattern for these services. Instead, it uses SOC-impact estimates when calculating which services to dispatch and leaves the definition of specific charge/discharge pattern to the real-time controller. The real-time controller, using electrical system information, will fill in the holes of the charge/discharge schedule created by the hybrid services. The real-time controller will likely need to periodically update the ESS SOC estimated by the optimization controller with the actual SOC measured by the ESS itself.

These differences between BSET and the optimization controller will require a separate version of software to be created for the optimization controller; using BSET with new input files will not be sufficient. These changes are not expected to be extensive, though, and in discussion with the BSET developers, are not anticipated to be difficult or time-consuming.

5.0 Handling Forecasts and Uncertainty

5.1 Proposed Optimization Controller Development

By definition, the optimization controller can only schedule services that have forecasts associated with them. At present, the only forecasts available to PNNL from Avista are the system energy price and system load. It is proposed that the incorporation of uncertainty into the optimization controller focus on the energy price forecasts due to its fundamental value to the system as a whole. For the purposes of discussion, the case of energy arbitrage will be used as an example.

Energy arbitrage is a service an energy storage device can engage in where it purchases energy (charges) at a low price and sells it (discharges) at a high price. The difference in the price between the low and high price periods (ignoring the efficiency of the ESS) and the amount of energy transferred at these prices define the value the ESS will generate during a given period (for example, 24 hours). This optimization problem could be generally stated as:

$$\underset{P_t}{\text{maximize}} \quad \sum_t P_t \lambda_t \quad (1)$$

subject to:

ESS power capacity limits
 ESS energy capacity limits
 ESS efficiency characteristics

where

P_t is the power exchange for period t (positive for discharge)
 λ_t is the price of energy forecasted for period t

This problem can be easily solved by a number of optimization techniques, assuming a forecast of the upcoming prices is provided. The optimization engine assumes that these forecast prices are 100 percent correct and produces the single mathematically optimal charge and discharge pattern for the energy storage device. If a slightly different price schedule was provided, such as from another forecasting source, the optimization engine could also generate the mathematically optimal schedule, and there is no guarantee that it would resemble in any way the previously generated schedule. All that would be guaranteed is that both schedules would be the single best schedule for their respective price forecasts.

The obvious problem with this approach is that the forecasted price is not 100 percent accurate, and deviations between the forecasted and actual price will have a potentially very large impact on the total revenues for the optimization period. The goal of this part of the project is to add some awareness of the uncertainty in each forecasted value, such that the optimization engine (along with an expression of the owner's risk appetite) would generate schedules that could be appropriately risk-averse. For example, if the owner is very risk-averse, periods with high prices but also high uncertainty would not be scheduled for discharge, so that the owner was less exposed to risk if prices were actually much lower than forecasted.

5.2 Optimization with Uncertainty

To try to incorporate an awareness of the uncertainty in a point forecast, the objective function is preserved, but the constraints are modified as shown.

$$\underset{P_t}{\text{maximize}} \sum_t P_t \lambda_t \quad (2)$$

subject to:

$$\Delta\text{SOC} < \frac{r}{\sigma_{t,\lambda}} \quad (3)$$

ESS power capacity limits
 ESS energy capacity limits
 ESS efficiency characteristics

where

P_t is the power exchange for period t (positive for discharge)

λ_t is the price of energy forecasted for period t

$\sigma_{t,\lambda}$ is the standard deviation of the error for the price forecast for period t

r is the risk tolerance factor defined by the user

This formulation of the optimization problem includes the standard deviation of the error in the forecast price as a limiting factor on the change of the SOC for the upcoming period. For periods with high uncertainty (as expressed by the standard deviation of the forecast error) the allowable deviation will be more restricted. The amount of energy transacted will be limited given the potential for energy prices to widely vary from the forecast and have significant impact on the overall total profit from the operation of the energy storage device. For periods where the standard deviation is lower, implying the forecast is more accurate, larger energy transactions are permitted.

Very large values of r effectively negate the effects of the standard deviation of the forecast error, removing the intended limitation due to uncertainty. Very small values of r allow the uncertainty effect to be dominant, removing the ability of the optimizer to schedule the energy storage device based on energy prices and constraining transactions to periods with low uncertainty. If r is excessively small, the total amount of energy transacted could be very limited, as all periods are deemed to have excessive amounts of uncertainty. The meaningful range for values of r must be determined experimentally by running the optimizer with a static set of prices and uncertainties (from historical data) and evaluating the output of the optimizer for values of r that produce desirable effects. This range of r will be normalized to more easily managed scale for users, such as zero to ten.

5.3 Optimization with Uncertainty Across Multiple Services

The above example discusses how uncertainty in the price forecast could be incorporated into an optimizer with a single use case, that of energy arbitrage. That use case is solely reliant on the price forecast and, thus, the constraint on uncertainty in that forecast is appropriate. For other use cases, though, the price of energy may not be a factor in the realization of said use case. For example, limiting the demand on a distribution feeder below a certain level to allow the deferment of equipment upgrade is completely independent of price. When the demand

reaches a certain level, the energy storage device must step in, regardless of the price of energy, to prevent the equipment from being overloaded. In this case, we would not want the optimizer to be prevented from transacting large amounts of energy because of the uncertainty in the price forecast for that period.

Thus, use cases that are not dependent on the price forecast will not be subject to constraints imposed by the uncertainty in the price forecast. Discussion with those developing and implementing the optimization controller have indicated that it will be possible to incorporate a constraint on energy transactions based on forecast uncertainty, as outlined in Equation 2, for only those services that incorporate energy price into their valuation.

6.0 Controller Development Process

6.1 Prototype Development

6.1.1 Optimization Controller

The controller being developed is highly related to the development of the optimizer for evaluating the total economic benefits of the ESS and some of the use-case testing. Though each of these applications has slightly different inputs and outputs, all make use of the same optimization engine that will value each of the use cases in the same way. In addition to this engine, the differences in expected inputs and outputs will require customization of the interface to the engine and/or adjustments to its structure to accommodate the unique aspects of each application. The prototype optimization controller, unlike the optimizer used for economic evaluation and possibly the use-case testing, will run frequently, likely once a day. For each run, the most recent forecast will be downloaded, the optimization re-run, and an updated dispatch schedule uploaded to the real-time controller located at Avista.

To enable the dispatch of hybrid services, estimates of the net energy impact for each hybrid service will need to be made. Early results from the use case testing and software tools developed to aid that effort have provided preliminary estimates for use by the optimization controller.

Expected challenges in the development of the prototype optimization controller:

1. The optimization engine will need to be modified to accommodate uncertainty estimates and SOC impacts for hybrid services. These modifications will be taking place in parallel to the work from CRADA 352 to improve the internal battery model. The technique outlined above has been vetted by BSET developers but has not been implemented or verified.
2. Relatedly, the communications protocols (e.g., schedule file format, data transfer frequency) may need to be modified to accommodate automated operation and comprehensive service provision. It is expected some of these issues will be resolved as a part of testing for use case 7.

6.1.2 Real-Time Controller

The development of this portion of the prototype controller will entirely be done by Avista, with guidance from PNNL. It is anticipated that much of the prototype development will take place as a natural part of the use-case testing, but there will likely be extensions or modification required.

The algorithms to generate the individual charge/discharge commands for each of the hybrid services will need to be defined. The use-case testing, thus far, has confirmed that the required algorithms for each use case are generally not complex and implemented with no great difficulty.

The incorporation of the WSU reactive power dispatch algorithms may be challenging. The nature and complexity of their models and algorithms will impact the difficulty of the integration.

Expected challenges in the development of the prototype real-time controller:

1. Rewriting schedule file parser to accommodate the dispatch of multiple services.
2. Incorporation of the reactive power dispatch algorithms from WSU.

6.1.3 Local Controller

As of this writing, there is no local controller in any form associated with the ESS. The provision of fast-response services, such as outage mitigation, requires some form of low-latency controller. At this time, it is not anticipated that a local controller will be a part of the final deliverable.

6.2 Prototype Controller Testing

The testing of Use Case 7 (Optimal Utilization of Energy Storage) provides an ideal opportunity to test the effectiveness of the prototype controller while accomplishing the goals of the use-case testing. It will be possible to make all of the changes to the existing optimization software and IT infrastructure prior to the full testing of the prototype. Such changes, though, must be done in a way that will not interfere with the ongoing use-case testing. It is expected that the prototype controller will not be complete in time for testing during the first round of use-case testing, and thus, the target date for completion will be the second round of testing.

If it is decided to evaluate the prototype controller outside the use-case testing, the ESS can be reserved for an appropriate amount of time (approximately one week) in which the testing can be done.

The prototype controller will be evaluated fundamentally in its ability to execute the optimization when given all required inputs, generate a dispatch schedule for upload, translate the dispatch signal into charge/discharge commands, and have the ESS execute these commands. The quality of the optimization will have already been evaluated as part of the use-case analysis work, and much of the data transfer protocol changes can be tested prior to an integrated test.

6.3 Production Controller Integration

The algorithms developed as part of the prototype development and the experience gained as part of the prototype testing will result in a knowledge base that will allow an Avista-identified vendor to develop and implement a production-level controller. PNNL will assist this vendor in understanding the prototype code and architecture. Avista will make all final decisions about the production controller. The algorithms and information to be transferred largely consist of

1. BSET-based optimization controller algorithm, including incorporation of uncertainty estimates. Part of the deliverables for CRADA 360 is a report on this matter.
2. Price uncertainty estimates and the algorithms used to develop them. Part of the deliverables for CRADA 360 is a report on this matter.
3. Estimates of the net energy transfer for each of the hybrid services based on analysis of the use-case data.

7.0 Distribution Network Model Development

7.1 Background

A portion of The Battery Optimization Project required the Battery Energy Storage System (BESS) analysis to be done in GridLAB-D™, a power distribution system simulation software package developed by DOE at PNNL with time-varying loads. The characteristics of the distribution system in question, the feeders Turner 116 and Turner 117, were stored in a Microsoft Access database in the DNV GL Synergi Electric format. This Synergi model represented the feeders with historical energy demand data as the loads, while this project was chiefly interested in using sampled smart-meter power demand data taken at the customers' meter terminals. GridLAB-D and Synergi access their model information differently, so a method of converting the useful data from Synergi to GridLAB-D was required.

7.2 Overview of the Problem

In order to analyze the effect the BESS would have when involved in Integrated Volt/Var Control, Conservation Voltage Reduction, and Energy Arbitrage, the feeder model for Turner 117 needed to be translated from the Synergi Electric format to the GridLAB-D format. The foundation for a Synergi Electric feeder model is found in an Access database with different datasheets storing different specifications. Examples of these sheets are the “Nodes,” “Branch,” “Sectionalizers,” “Regulator,” and “Loads” tables. GridLAB-D differs from Synergi, in that the accepted data is stored in GLM files, text files that follow the GridLAB-D format. An additional obstacle is that certain model instances allowed in Synergi are not allowed in GridLAB-D. One example of this is the modeling of “jumper” configurations (for example, when a set of single-phase loads are connected to two phases, with one of the one phase open). This configuration is useful for modeling restoration efforts during a fault scenario. Such a configuration is possible in Synergi, but GridLAB-D does not allow single-phase loads to be connected to more than one phase. Efficiently translating between the two software packages requires a medium to host both sets of data and functions to typecast the data object, as well as an experienced power systems background.

7.2.1 Main Issues

- The Synergi Electric feeder model is represented as an Access database, while the GridLAB-D software requires model data represented in a text-file format.
- Synergi Electric load data is represented as average energy-demand data assigned to a branch segment, while the smart-meter data is timestamped, complex power load demand associated with a latitude and longitude location.
- Units for a set of data in Synergi may be different for the same data object in GridLAB-D.
- Topologies allowed in Synergi are not allowed in GridLAB-D.

The sections below discuss the differences between Synergi Electric feeder model and GridLAB-D feeder model requirements and the solution WSU developed to efficiently translate from the Synergi Electric format to the GridLAB-D format.

7.3 Software Comparison

In this section, a comparison between Synergi Electric and GridLAB-D and their applicable uses is discussed.

Synergi Electric is a software package used by Avista Utilities' Distribution System Planning Department to validate recommendations for distribution system upgrades. Synergi is a distribution system modeling and analysis software, part of the larger Synergi software package. Synergi is developed by DNV-GL. Synergi can be used to accurately model and analyze polyphase power distribution systems. It provides accurate models for distribution system components such as transmission lines, transformers, capacitors, voltage regulators, tap changing transformers, and motors. Synergi solves the network solution using a custom algorithm based on established methods and provides detailed reports. It also provides various tools for planning studies such as tools for load growth and various load allocation techniques.

The Synergi manual brings out the key difference between this software and other modeling software. Synergi uses an object-oriented design that allows the system to model the distribution system accurately and extensively without matrix-based modeling limitations. Hence this software provides support for detailed device models. Every model has terminals that connect to the distribution feeder and respond to voltage and current variations just like real devices. For devices such as regulators or capacitors, the device module handles its own inner workings and responds to the changes in the distribution feeder.

GridLAB-D is an open source power distribution system modeling and analysis tool developed by PNNL for DOE. It provides detailed models for various power system components, with active development for more devices and upgrades to existing models. It also provides support for various control techniques based on established algorithms from literature. For example, it provides the option of solving the network solution using the Forward-Backward sweep method or Newton-Raphson method, as desired by the user.

GridLAB-D uses an advanced algorithm to simultaneously solve the power system by solving the states for all the different devices at the same time and not sequentially. The advantages of this method over other simulators (as provided by their manual) are

1. It handles unusual situations much more accurately
2. It handles widely disparate time scales, ranging from sub-seconds to many years
3. It is very easy to integrate with new modules and third-party systems.

GridLAB-D is an ideal tool for research purposes, as it offers the flexibility to develop complex models and implement user-developed algorithms for various control purposes. It is also suitable for the objectives of this project, which requires the development of a custom voltage control scheme for the BESS and its implementation and analysis for a distribution feeder.

7.4 Synergi – GridLAB-D Conversion

7.4.1 Overview

The objectives of the project required the conversion of the power system topology data from Synergi to GridLAB-D. This is because

1. GridLAB-D offers the flexibility of a modular environment, which is useful for making changes to the system quickly.
2. The source code is available for everyone to edit, as required. This offers the flexibility to edit the battery model, as required, and make it more detailed if necessary.
3. The open source nature of the software also offers the chance to develop modules and controls that can be used by other researchers to validate the results and re-use it in other projects.
4. Synergi only offers the option of a steady state snapshot of power flow, while GridLAB-D is capable of simulating the system for various timescales.
5. It is easier to deploy user-developed control algorithms in GridLAB-D, as the control algorithm can be written in a supported third-party platform and then used in the simulation.
6. GridLAB-D offers the use of player files and schedules that can be used to play back real data from field measurements into the simulation. This allows us to develop a time-series, measurement-based model.

The Synergi Electric to GridLAB-D conversion program consists of a set of MATLAB scripts that take in the data (in the form of an Access database) from Synergi, imports into MATLAB, and then provides the different GLM files for nodes, lines, and such as output. A flowchart describing the entire process is shown in Figure 5.

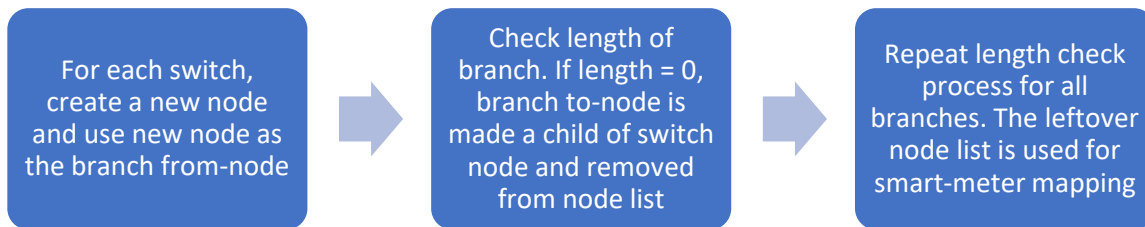


Figure 5. Flowchart for Node and Branch Conversion from Synergi to GridLAB-D

The process starts with identifying the relevant information necessary to develop the GridLAB-D model from the Synergi database, then importing the data into an Excel sheet. The Excel sheet is convenient for MATLAB to read from, and the data is imported into the MATLAB workspace and different variables are created for different device models.

Once the data is loaded into MATLAB, various scripts are developed to modularly filter the data as necessary and format the data into the specifications of the GLM files.

7.4.2 Conversion Program

7.4.2.1 Considerations, Assumptions, and Data Requirements

The conversion program logic is as follows: first the switches script, second the overhead lines script, third the underground lines script, and finally the nodes script. The sub-programs must be executed in that order for reasons described later in this report. The remaining objects required to meaningfully model a real power system were either already present in an acceptable form for the GridLAB-D model, such as the regulators and capacitors, or were deemed unnecessary to model for the purpose and state of this project. Differentiating between circuit-breaking

equipment classes was deemed inconsequential: fuses were ignored and there was no differentiating between sectionalizers, reclosers, and circuit-breakers. A connection to the Bulk Electric Power System is assumed at the substation node. This node is designated as the swing node in the GridLAB-D model without considering a Thevenin equivalent impedance for the true swing node of the power system. The conversion package assumes the entire distribution system is modeled on a single, known voltage magnitude. This is of consequence because the step-up transformer for the BESS is not present in our model, nor are any pole-top transformers or pad-mounted transformers. An additional set of script(s) for modeling transformers on the distribution system can be built as the GridLAB-D transformer object is well defined and understood. The data required to begin the Synergi Electric to GridLAB-D conversion are the switch-device phase, the section-ID to which the switch is attached, the switch from-node, the “switch is closed” flag status, the “switch is gang-operated” flag status, and the nominal phase-to-ground voltage, the overhead branch and underground branch section-IDs, the length of each overhead and underground branch, the phase of each overhead and underground branch, the to- and from-node for each overhead and underground branch, and the line configuration for each overhead and underground branch. The overhead and underground lines programs both follow the same format. For this reason, only one section will be dedicated to their construction.

7.4.2.2 Switches Program

Running the switches program creates a “.glm” file titled “Switches117” in a specified directory. For every circuit-breaking switch present in the import data, a node is created to represent the to-node of the switch with matching phases and voltage-magnitudes. The GridLAB-D switch object is then made between the imported switch from-node and the newly created switch to-node, which is designated as “OPEN” or “CLOSED” depending on the status flagged by the import data. The program then edits the imported overhead and underground branches tables based on the created node and switch. If the corresponding branch length is greater than zero, the from-node of the branch corresponding to the switch is changed to the created switch node. The branch object relating to the switch is then generated in the GridLAB-D format with the given length, configuration, and phase data. If the branch length is equal to zero, a GridLAB-D node object is generated corresponding to the to-node of the branch. This node is then made a “child” of the branch from-node, which is the newly generated switch node. These steps eliminate the occurrence of parallel branches between nodes (an illegal situation in GridLAB-D) and facilitate the modeling of zero-impedance branches. The leftover data corresponding to the switch is deleted from the imported data, removing the possibility of defining a branch or node object twice. The MATLAB workspace is then saved in the current directory.

7.4.2.3 Branches Program

When a branch has a length greater than zero, a GridLAB-D branch object is created specifying the name of the branch, the supported phases, the from- and to-node, the branch length, and the branch configuration. If the branch has a length equal to zero, a GridLAB-D node object is created. This node object specifies the name of the node, the branch to-node, the supported phases, the nominal voltage magnitude, the ideal complex voltage solution target, and specifies the branch from-node as the parent node. The branch to-node and all its relevant information is deleted from the MATLAB workspace. The corresponding data is deleted, because a node that is the child of another node cannot be given a child, which is required for the load allocation process described later in this report. The MATLAB workspace is then saved in the current directory.

7.4.2.4 Nodes Program

The nodes program takes the leftover node data from the imported data and generates GridLAB-D node objects based on the corresponding characteristics. The node object specifies the node name, the supported phases, the nominal voltage magnitude, and the target complex voltage solution. The MATLAB workspace is then saved in the current directory.

7.5 Smart Meter Data

Beginning from March 2011, Avista Utilities started installation of “smart” meters in Pullman and Albion. Around 13,000 electric meters were installed. The smart meters provide greater visibility to the utility, for example, enabling them to monitor outages without having to wait for an individual customer to call in the outage.

For this project, the battery’s performance needs to be tested in various situations to study its impact on the system. The Synergi model only provides a steady state snapshot of the system, and the loading conditions are an averaged, filtered profile, which is not representative of any loading condition. The battery, on the other hand, needs to be tested for various loading conditions such as peak load and shoulder seasons. This necessitates the use of real-time data from the field to model the load in the simulation. The feeder has Distribution Management Systems (DMS) measurements, but this data is only available in two locations: the substation and at a switch that is approximately at the midpoint of the feeder. To accurately model the feeder, it would require distributing these two load values across the feeder according to some weighting factors. This method would introduce more assumptions into the modeling process, potentially making it less accurate. Hence, smart meters have been used to model the load.

The smart meters provide a compromise to the load modeling problem. The smart meters are already distributed across the feeder and provide measurement data collected at five-minute intervals. This data can be used to model the load in the simulation by aggregating the smart meters to nodes in the GridLAB-D simulation and using “player” files to play back the measurement data into the model.

However, the smart meter data is not without its problems. The smart meters are present at the customer level and are not directly connected to the feeder. This means that some detail and accuracy is lost, such as the model of the transformers going from the feeder to the consumer. Moreover, the smart meters themselves can be considered to be a recent technology and are not as established as the older SCADA measurements. The smart meters can provide voltage, real power, and reactive power measurements. However, the reactive power measurement is calculated rather than measured, and this has the potential to introduce errors into the model.

For the GridLAB-D model, the TUR 117 feeder has been modeled using the smart meter information. TUR 116 does not have full coverage by smart meters, and hence, TUR 117 has been chosen.

7.6 Node Allocation from Smart Meters to Synergi and GridLAB-D Nodes

7.6.1 Node Allocation Overview

The smart meter allocation program is a set of two sub-programs that take smart meter number, phase, location, and complex load information at each time step and aggregate the appropriate information to the closest node with corresponding phase. The set of programs executes without error if the location and phase of every smart meter reporting time-series loading is known, every load value is real number, and if the phase and location of every node in the system is known, and every smart meter listed on the system is reporting time-series load. This method assumes that the node nearest to a smart meter with matching phase corresponds to that smart meter's load point in the Synergi model. This may not be valid in general, as a Synergi node may be listed as a three-phase node but represent a three-phase main arterial with a single-phase load attached to it. If the error induced by this assumption is small, meaning there is a single-phase load electrically near the three-phase node, the misplaced voltage drop will not be consequential.

7.6.2 Procedure

For each Avista smart meter, the Euclidean Distance was calculated for every Synergi node using the formula in Figure 5. For the first Synergi node, the Euclidean Distance was stored along with the corresponding index. From then on, after the next Euclidean Distance was calculated for the next node in the list, the new distance was compared to the most recently stored distance value. If the new Euclidean Distance value was smaller than the previously stored value, the new value was stored along with its node's corresponding index. This method ensured that all possible nodes on the corresponding feeder were checked and that the nearest Synergi node was stored.

7.6.3 Mapping Program

The program compares the phase of a smart meter with all the nodes in the system. In the event of a match, the distance from the matched node to the smart meter is calculated. If it is the first node with matching phase, the smart meter number, node identifier, and distance are stored. If the selected node is not the first match, a comparison between the current calculated value and the stored value is done. If the stored node's distance is shorter than the current node's distance, the current match is discarded, and the program continues iterating through the remaining system nodes. If the current distance is shorter than the stored distance, the mapping table is updated with the current node's identifier and distance. In both cases, the program iterates through all the nodes to ensure every possible match is considered. Once the list of smart meters has been exhausted, the program concludes by exporting a Microsoft Excel Spreadsheet containing the mapping and saves the present MATLAB workspace in the current directory.

7.6.4 Aggregation Program

The next program takes the output of the mapping program and aggregates each smart meter's complex power load to its assigned node. This results in a table describing every assigned node's load per phase at every time-step, which totals to six tables. The program then sums up the six tables and graphs the results: A phase, B phase, C phase, and Total Watts per time-

step, and A phase, B phase, C phase, and total Volt-Amp Reactive per time-step. The MATLAB workspace is then saved in the current directory. Figure 6 depicts a flowchart for the mapping and aggregation program

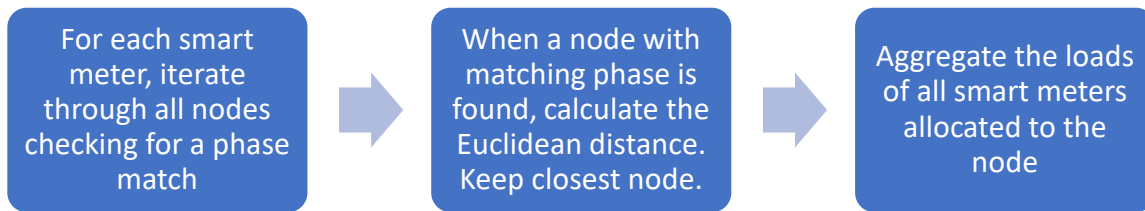


Figure 6. Flowchart for Mapping and Aggregation Procedure

7.7 Developing Player Files to Play Back Measurements into GridLAB-D

7.7.1 The Need for Player Files

In GridLAB-D, a player file provides the ability to update a single object variable at specified times (sourceforge wiki on players). This allows users of GridLAB-D to update an object's properties based on predetermined values. For this project, we used player files to update the load at each node, the regulator tap positions, and the capacitor switch states at five-minute intervals and the battery charging schedule at five-second intervals. After each update, the power-flow is resolved with the last solution's results as the initial conditions and the updated object values as the new boundary conditions to be met. We have inserted meters and recorders to measure the time-series model and verified that the loading changes as expected based on the player files. It is worth noting that the model does not make an abstraction for the battery SOC. Instead, the model uses charge and discharge schedules provided by either PNNL or Avista Utilities.

7.7.2 MATLAB Player File Generator Algorithm

The algorithm for creating GridLAB-D player files is the same regardless of which property is being updated. The program iterates through the number of desired objects with properties to be updated. A ".player" file is generated for every object's to-be-updated property at a specified address, and the amount of time steps is specified by the user. At the first time-step, the output specifies the date, time, and property value. The rest of the time-steps have the time step increment and the updated value. The loop concludes with the MATLAB program closing the ".player" file it has been writing in to.

7.7.2.1 Scripts

We have written MATLAB scripts generating player files for nodal loads: time-series real and reactive power loads per phase, and the capacitor switch states and substation voltage-regulator tap positions. In the case of the nodal loads, a file pointing the GridLAB-D program to the player files had to be written. This file iterates through the number of nodes with smart meter loads, creates a GridLAB-D load object, sets the corresponding node as the parent object of the load, specifies the supported phases, nominal voltage magnitude, and specifies the appropriate player file based on the phase configuration. The need for this additional parent-child

relationship with the nodes object is what required us to “pre-filter” the list of eligible nodes for loads at the beginning of the conversion.

7.8 Overall Model – Simulation and Analysis

The model developed by WSU for testing the performance of the battery for various scenarios is the TUR 117 smart meter data-based, time-varying model in GridLAB-D.

Table 1 and Table 2 show that the GridLAB-D model sufficiently matches with the steady state results produced by Synergi. However, we have also modeled the time series load from smart meters in the model. These results are discussed below.

Table 1. Comparison of Synergi and GridLAB-D Voltages

SectionID	Phase of Result	Synergi (kV)	GridLAB-D(kV)
ND_390-34270	A	7.67 \angle -0.02 ^o	7.67 \angle -0.02 ^o
ND_390-71389	A	7.67 \angle -0.14 ^o	7.64 \angle -0.41 ^o
ND_391-1025850	A	7.64 \angle -0.32 ^o	7.64 \angle -0.37 ^o
ND_391-1025856	A	7.64 \angle -0.32 ^o	7.64 \angle -0.37 ^o
ND_391-1025852	B	7.68 \angle -120.35 ^o	7.64 \angle -120.40 ^o
ND_391-1025853	B	7.68 \angle -120.35 ^o	7.64 \angle -120.40 ^o
ND_391-1025858	B	7.68 \angle -120.35 ^o	7.64 \angle -120.41 ^o
ND_391-1025851	C	7.62 \angle 119.57 ^o	7.64 \angle 119.57 ^o
ND_391-1025857	C	7.62 \angle 119.57 ^o	7.64 \angle 119.57 ^o
ND_391-1025854	C	7.62 \angle 119.57 ^o	7.64 \angle 119.57 ^o

Table 2. Comparison of Synergi and GridLAB-D Currents

Node ID	Phase of Result	Synergi (A)	GridLAB-D(A)
389-1194600-0	A	0.12 \angle -19.2 ^o	0.13 \angle -25.62 ^o
389-1194603-0	A	0.11 \angle -13.83 ^o	0.107 \angle -17.02 ^o
389-1194604-0	A	0.85 \angle -15.65 ^o	0.85 \angle -17.03 ^o
389-1194605-0	A	0.55 \angle -15.61 ^o	0.55 \angle -17.03 ^o
389-1195987-0	B	0.32 \angle -135.77 ^o	0.37 \angle -136.33 ^o
389-1195989-0	B	0.32 \angle -135.92 ^o	0.32 \angle -136.33 ^o
389-1195995-0	B	0.09 \angle -135.24 ^o	0.09 \angle -136.33 ^o
411-404602-0	C	0.83 \angle 105.99 ^o	0.84 \angle 107.69 ^o
411-907112-0	C	13.9 \angle 100.18 ^o	13.94 \angle 99.79 ^o
C-395-277266	C	17.9 \angle 100.66 ^o	18.0 \angle 99.97 ^o

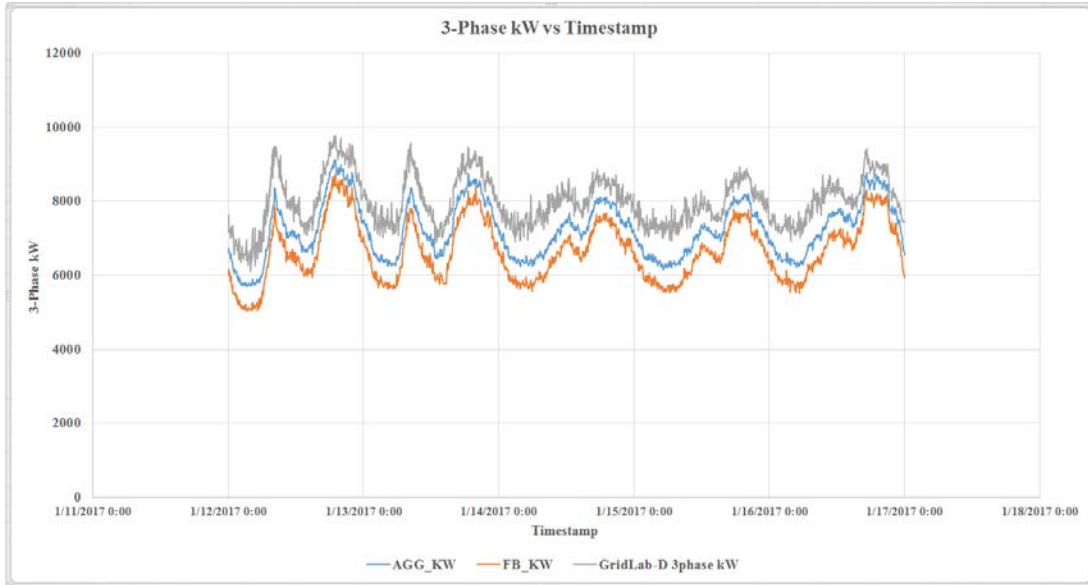


Figure 7. GridLAB-D Real Power vs. DMS Measurements at the Substation for Winter Case

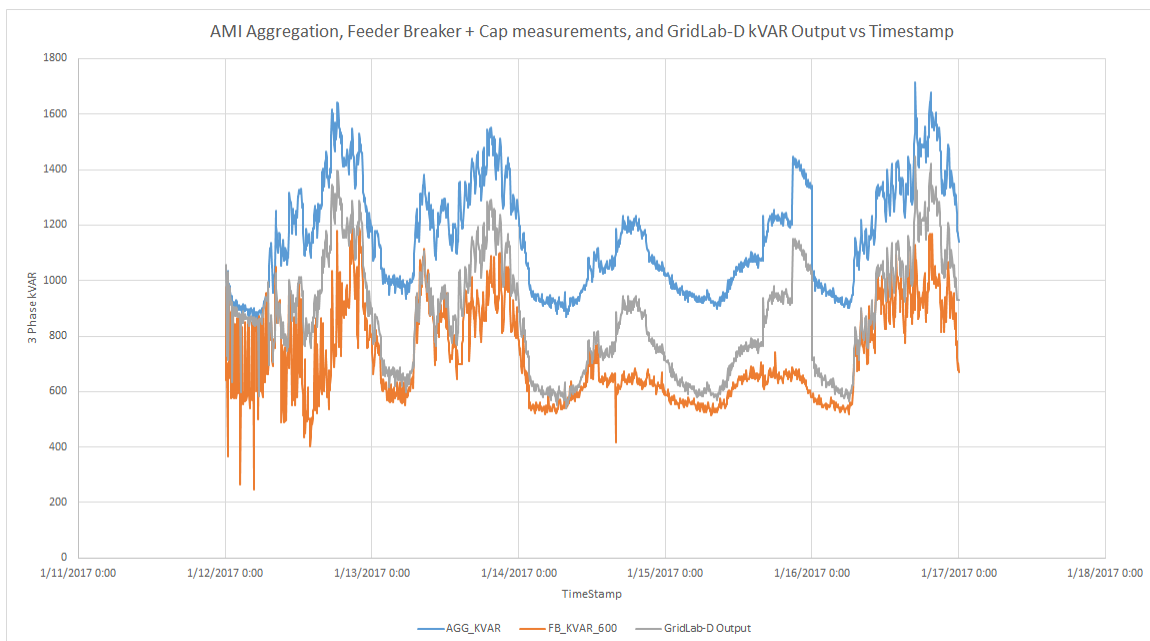


Figure 8. GridLAB-D Reactive Power vs. DMS Measurements at the Substation for Winter Case

As shown in Figure 8, the GridLAB-D model recreates the input Advanced Metering Infrastructure (AMI) data wave-shape. The problem arises from the AMI data having discrepancies from the feeder-breaker data. Some of these data discrepancies originate from the AMI meter accuracy, reporting frequency, noise in the communication channel, and calculation failures. A positive from the kVAR graph is the GridLAB-D output, when adjusted for the kVARs supplied by capacitor banks, correlates strongly with the feeder-breaker values. This strong correlation shows that the model is a valid tool for offline analysis and would be improved with more accurate input data. Figures 9 through 14 present a few snapshots of GridLAB-D model validation results.

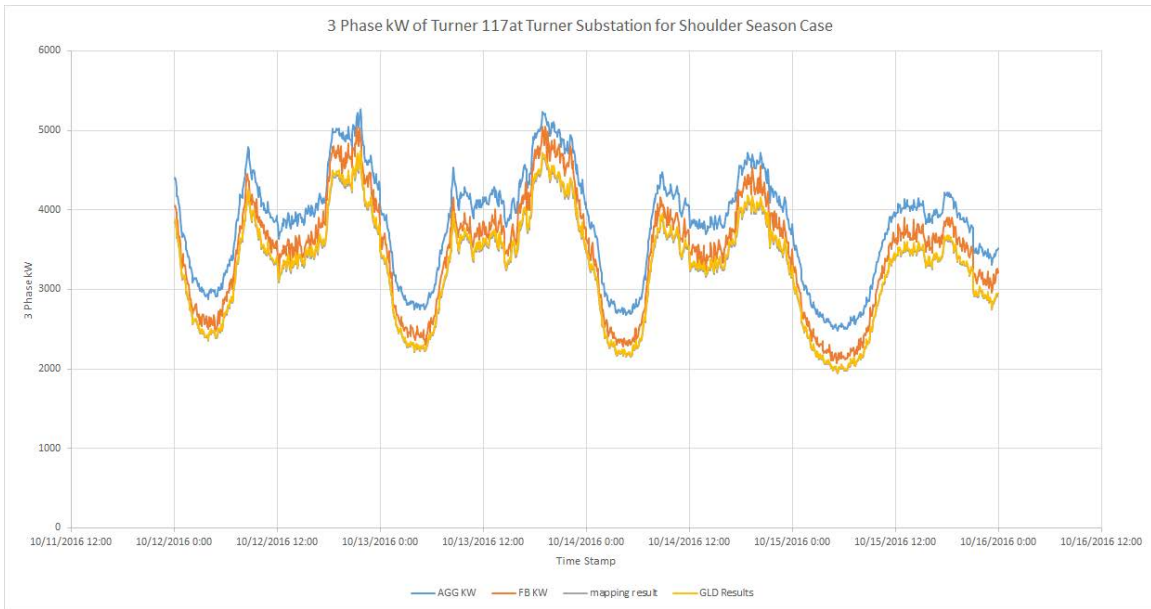


Figure 9. Fall Data MW Output

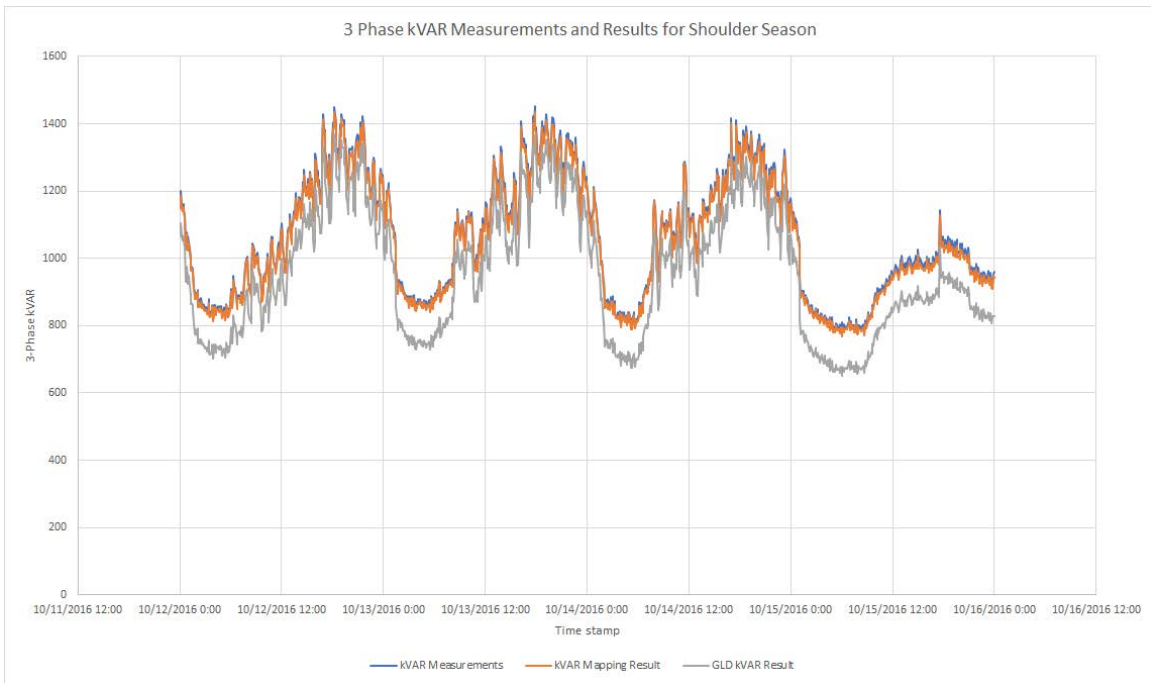


Figure 10. Fall Data Mega Volt Amps (reactive) (MVAR) Output

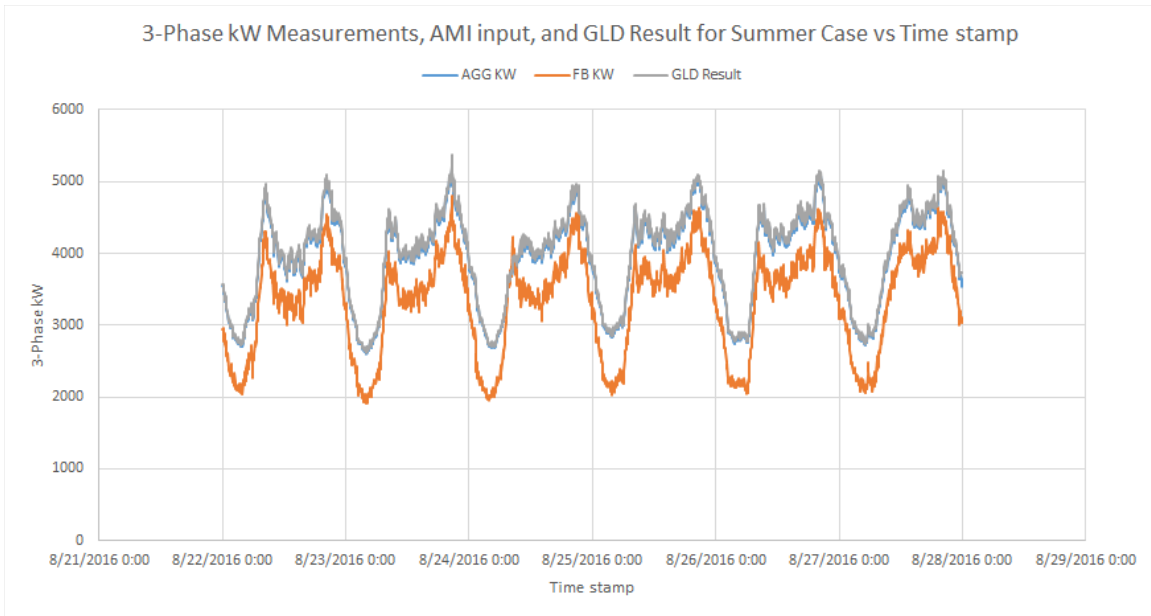


Figure 11. Summer Data MW Output

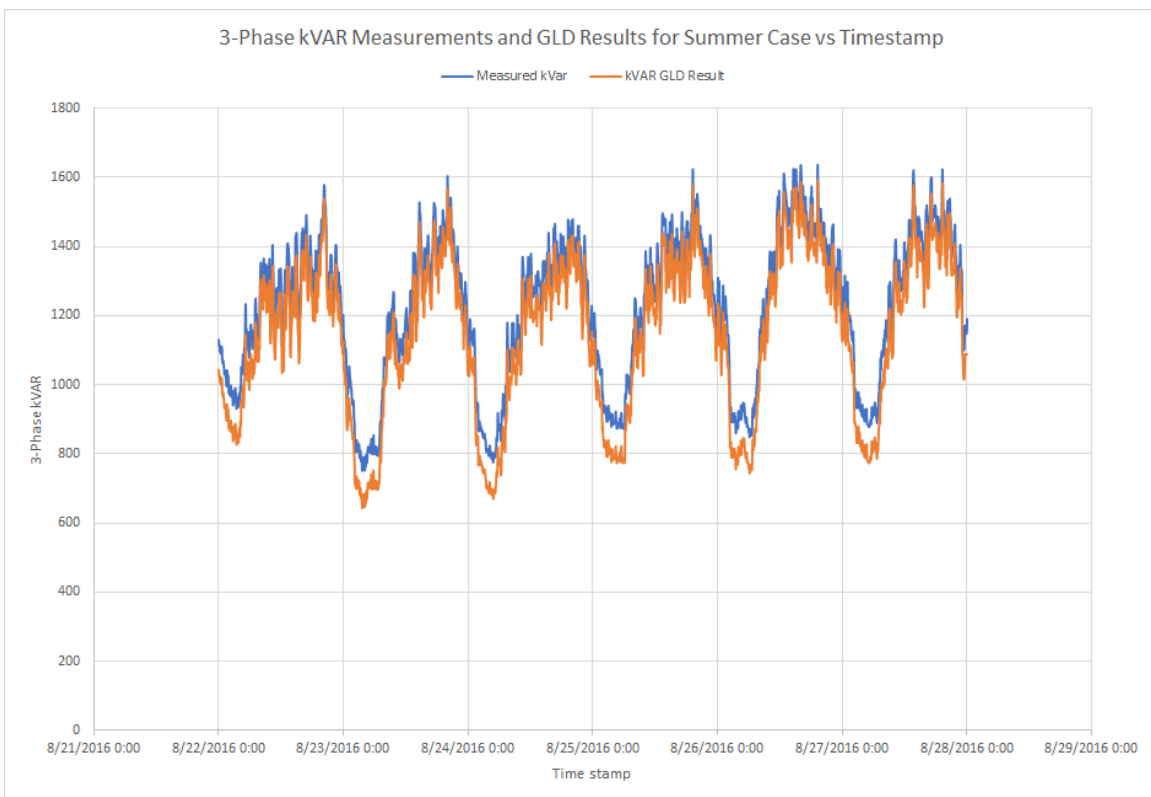


Figure 12. Summer Data MVAR Output

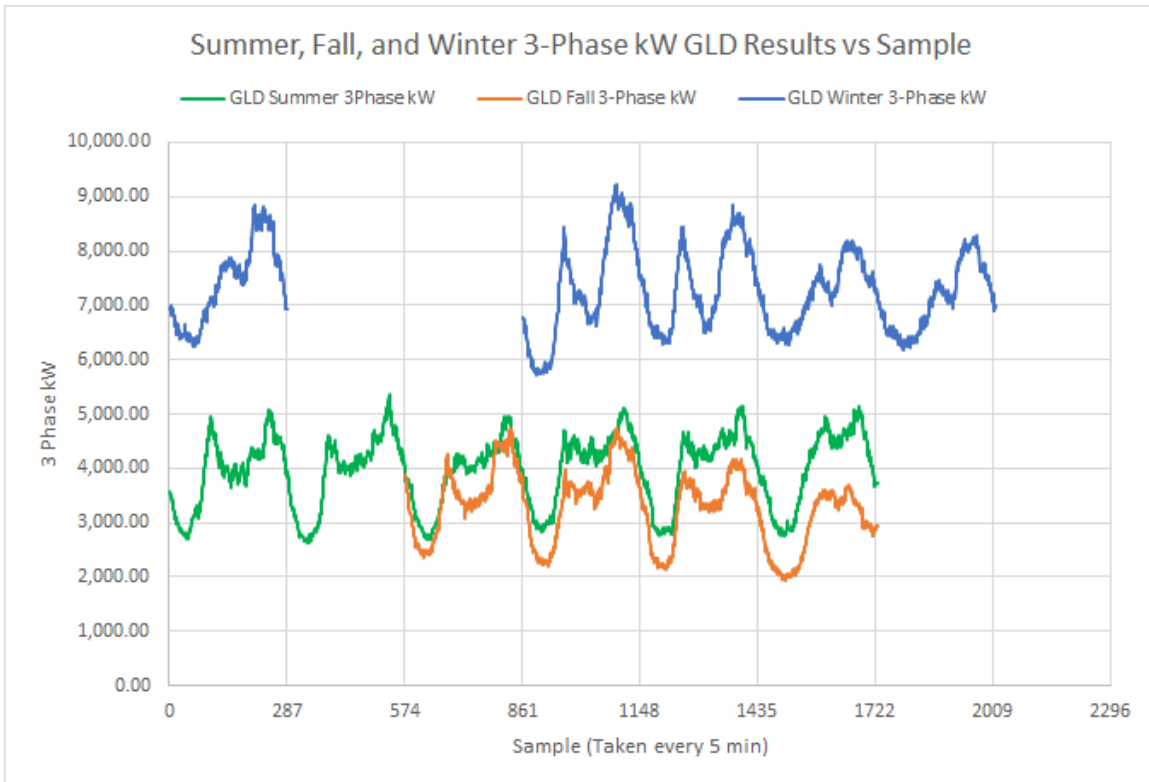


Figure 13. MW Seasonal Comparison

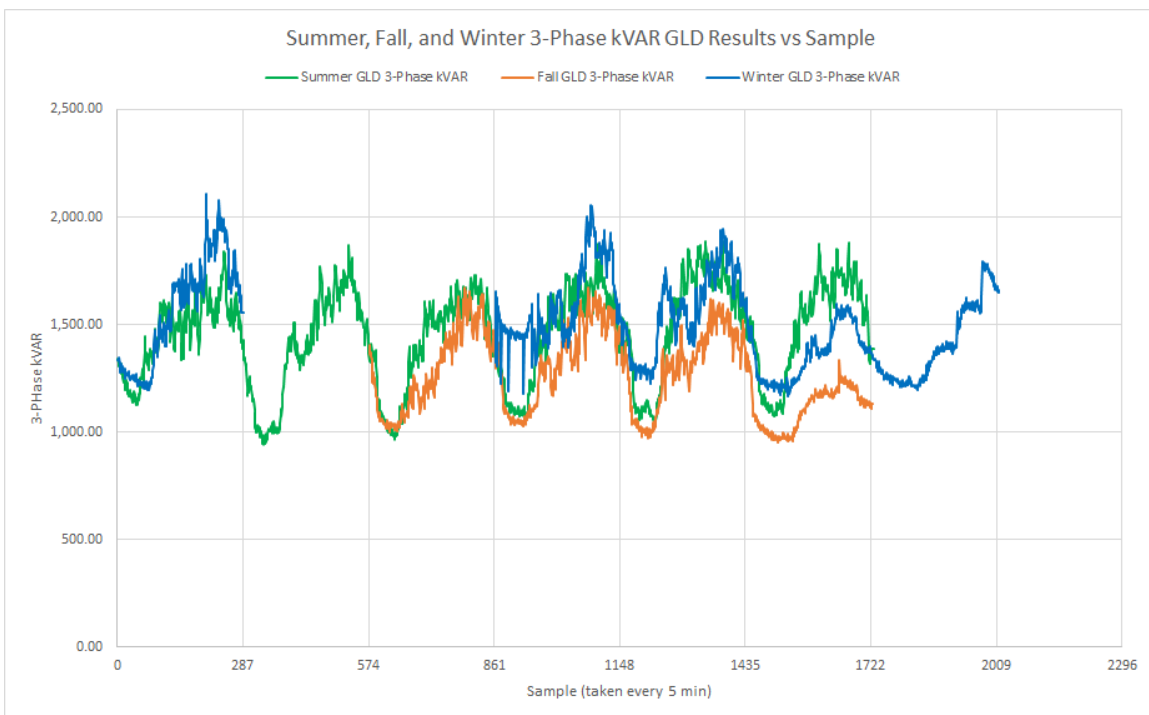


Figure 14. MVAR Seasonal Comparison

7.9 Conclusion

The conversion program developed by WSU successfully converts Synergi Electric feeder model data in the form of an Access database into “.glm” files for use in GridLAB-D. The presented conversion program uses a systematic method to accurately transfer a feeder model in Synergi to GridLAB-D, which preserves the feeder topology but also adheres to the constraints of both software packages. This report presents evidence of the conversion program’s validity by comparing steady-state Synergi load-flow results with GridLAB-D steady-state load flow results.

The Smart Meter Mapping and Load Allocation program, developed by WSU, is also examined in this report. The Euclidean Distance method is explained and justified given the available data and the load allocation method follows power system logic. The validity of the mapping and allocation package is shown in the time-series load comparisons for the winter case.

Together, these two software packages allow for near seamless transition from Synergi Electric to GridLAB-D and provide the basis for much of the project results.

8.0 ESS Real Power Control Strategy for Frequency Support

This section discusses the effect a BESS with different ACE signal distributions has on the Avista system during load-ramping and load-step increases for a 120-second simulation. The BESS size is first set to +/- 10 MW, and the system is subjected to a 20-MW load step increase at $t=20$ seconds. The BESS size is then set to +1.31 MVA/-1.21 kilovolt amps (kVA), and the system is subjected to a 20-MW load step increase at $t=20$ seconds. Finally, the system is subjected to a 3.33-MW load ramp from $t=20$ to $t=80$ seconds. The capability of the BESS to regulate the local frequency under an islanded condition is briefly discussed at the end of this report. The initial conditions for the Avista system are: a maximum generation capacity of 2,000 MW, an initial load of 1,380 MW, a governor time-constant of 0.2 seconds, a turbine time-constant of 0.3 seconds, a prime-mover change delay of 5 seconds, an inertia constant of 228.14 on a 100 MVA base, an equivalent droop of 1.25 percent, the starting output of the BESS is 0 kW, and that the SOC is greater than or equal to 70 percent.

8.1 Motivation

Avista Utilities seeks to understand the most effective method for utilizing their 1.2-MW/3-MWh BESS for regulation services, load-following services, and for real-world flexibility operation. The BESS can be used to offset sudden changes in load or generation due to its quick response time and ability to switch charging and discharging modes nearly instantaneously. An AGC program is used to analyze the performance of the Avista system to a 20-MW load step increase with and without the BESS. The first set of simulations use a 10-MW BESS to dramatize the effect a BESS would have on the single-area system. The second set of simulations use the 1.2-MW/3-MWh BESS. The final simulation analyzes the performance of the 1.2-MW/3-MWh BESS during a 3.33-MW load ramp increase for a duration of 60 seconds. Four different ACE signal distribution strategies are implemented in order to analyze which one gives the lowest magnitude ACE and frequency error and which one returns the ACE and frequency to their nominal operating values the quickest. The four distribution strategies are Static Distribution of AGC, Proportionality-based Dynamic Distribution of AGC, Priority-based Dynamic Distribution of AGC, and the Independent Distribution of AGC. The mathematical representation of these signal distribution strategies is shown in the following section.

8.2 AGC Signal Distribution Strategies

The ACE signal distributions listed in Figures 15 through 20, below, are developed and discussed in (Yunzhi et al., 2014). "DAA" is the dynamic available energy of the BESS, which is dependent on the SOC. The change in SOC is calculated on a per-hour interval. Since these simulations only last 2 minutes, it is assumed that the SOC of the BESS is greater than or equal to the minimum SOC of 70 percent for an output of 1,310 kW. "AA" represents the available reserve generation of the equivalent system generator, which is 620 MW, initially.

$$\begin{aligned}
 & \textit{Static} \\
 & ACE_{s_{bi}} := 0.3 \cdot ACE_{s_i} \\
 & ACE_{s_{gi}} := 0.7 \cdot ACE_{s_i}
 \end{aligned}$$

Figure 15. Static AGC Signal Distribution (SDA)

$$\begin{aligned}
 & \textit{Proportionality} \\
 & ACE_{s_{bi}} := ACE_{s_i} \cdot \frac{DAA_{bi}}{DAA_{bi} + AA_{gi}} \\
 & ACE_{s_{gi}} := ACE_{s_i} - ACE_{s_{bi}}
 \end{aligned}$$

Figure 16. Proportional AGC Signal Distribution (ProDD)

$$\begin{aligned}
 & \textit{Priority} \\
 & ACE_{s_{bi}} := ACE_{s_i} \textit{ if } |ACE_{s_i}| \leq |DAA_{bi}| \\
 & ACE_{s_{bi}} := DAA_{bi} \textit{ if } |ACE_{s_i}| > |DAA_{bi}| \\
 & ACE_{s_{gi}} := ACE_{s_i} - ACE_{s_{bi}}
 \end{aligned}$$

Figure 17. Priority AGC Signal Distribution (PriDD)

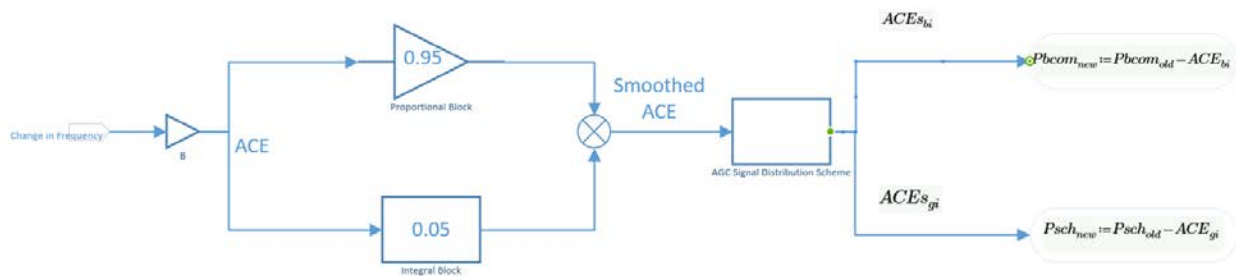


Figure 18. AGC Signal Distribution Block Diagram for SDA, ProDD, and PriDD

$$\begin{aligned}
 &IDA \\
 ACE_{bi} &:= ACE_i \cdot \frac{DAA_{bi}}{DAA_{bi} + AA_{gi}} \\
 ACE_{gi} &:= ACE_i - ACE_{bi}
 \end{aligned}$$

Figure 19. Independent AGC Signal Distribution (IDA)

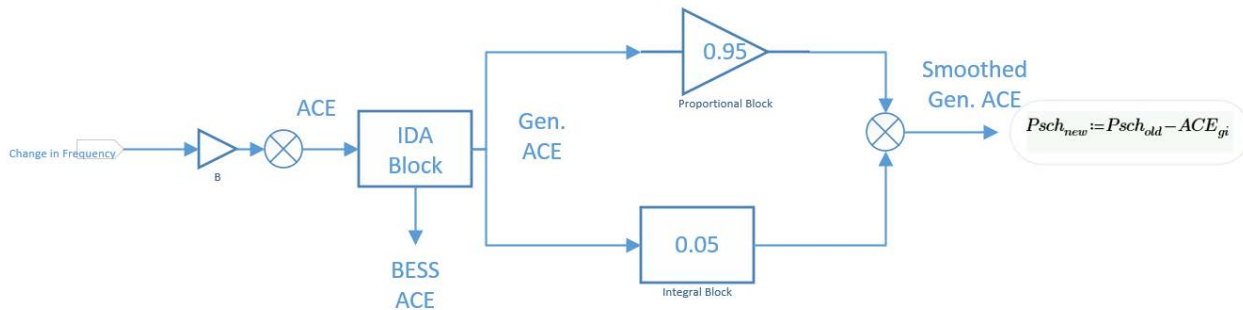


Figure 20. AGC Signal Distribution Block Diagram for IDA

8.3 Analysis

8.3.1 Single Area Program

The Avista system is reduced to a single bus with an equivalent generator rated at 2,000 MW and an equivalent load of 1,380 MW. The time constants for the equivalent generator’s governor and turbine are 200 millisecond (ms) and 300 ms, respectively. There is a 5-second time-delay in the prime mover response. The equivalent generator’s inertia constant, H, is 228.14 in watt-seconds at rated speed in radians per second divided by 100 MVA. The BESS is rated at 10 MW and has a time constant of 1.5 ms. The equivalent generator’s droop, R, is 1.25 percent, and the bias constant, B, is 81. The ACE is calculated every 4 seconds and altered using a Proportional Integral (PI) controller. The proportional constant of the PI controller is 0.99, the integral constant is 0.01, and the interval of integration is the current sample plus the previous 30 samples. The simulation is run using the Euler Method for numerical integration using a step-size of 10 μs over a simulation time frame of 2 minutes. Five different simulations are run in parallel: a simulation without a BESS and four simulations with a BESS using different AGC signal distribution strategies. Figure 21 and Figure 22, below, are images of the block diagrams for the single area program.

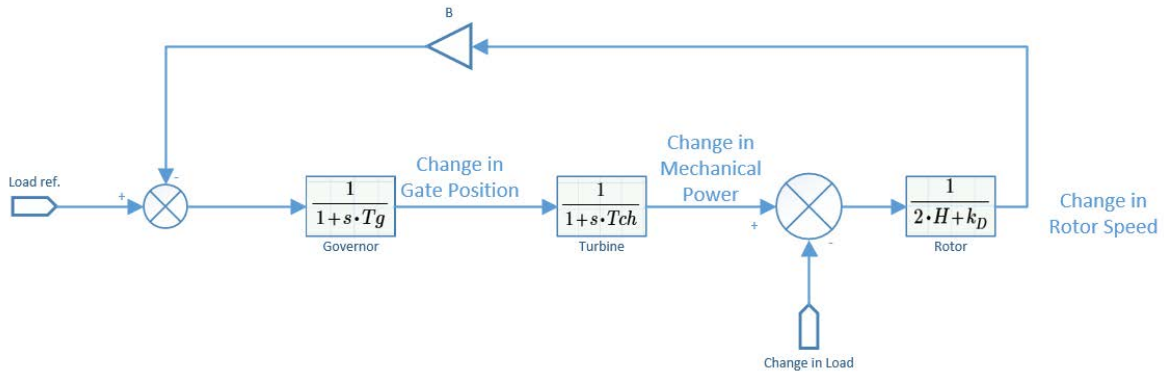


Figure 21. Single Area Block Diagram without BESS

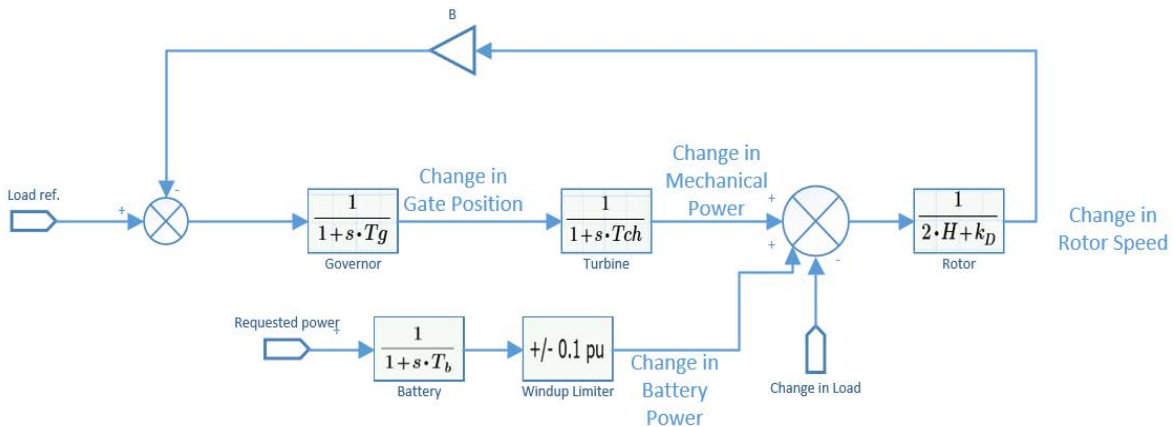


Figure 22. Single Area Block Diagram with BESS

8.4 Results

8.4.1 Avista System with 10-MW BESS Subjected to a 20-MW Load Step Increase

The 10-MW BESS results indicate that the AGC signal distribution strategy that reduces the largest magnitude smoothed ACE is the IDA strategy. The IDA strategy assigns the BESS a portion of the unfiltered ACE burden before it passes through the PI controller, which causes a discrepancy in the smoothed ACE measurement and the frequency measurement. If the ACE is analyzed before the PI controller, it is clear that all the signal distribution strategies give the same performance. In terms of frequency deviation, the PriDD strategy gives the lowest magnitude. Since the PriDD strategy does not use the power divider method, the maximum capability of both the BESS and the conventional generation sources is realized sooner than in the other signal distribution cases. Besides a difference in the largest smoothed ACE magnitude deviation, all of the signal distribution strategies give similar results in terms of time required to return the smoothed ACE to zero. The IDA distribution returns to zero slightly before the remaining distributions, but only due to the BESS removing a portion of ACE before the PI controller. In terms of the frequency response performance, the PriDD distribution gives the lowest magnitude frequency deviation during both the below and above zero swings. The PriDD

implementation also brings the system back to steady-state conditions quicker than the other signal distributions. Graphs of the ACE, BESS power output, system frequency, and equivalent generator output are shown in Figures 23 through 30, below.

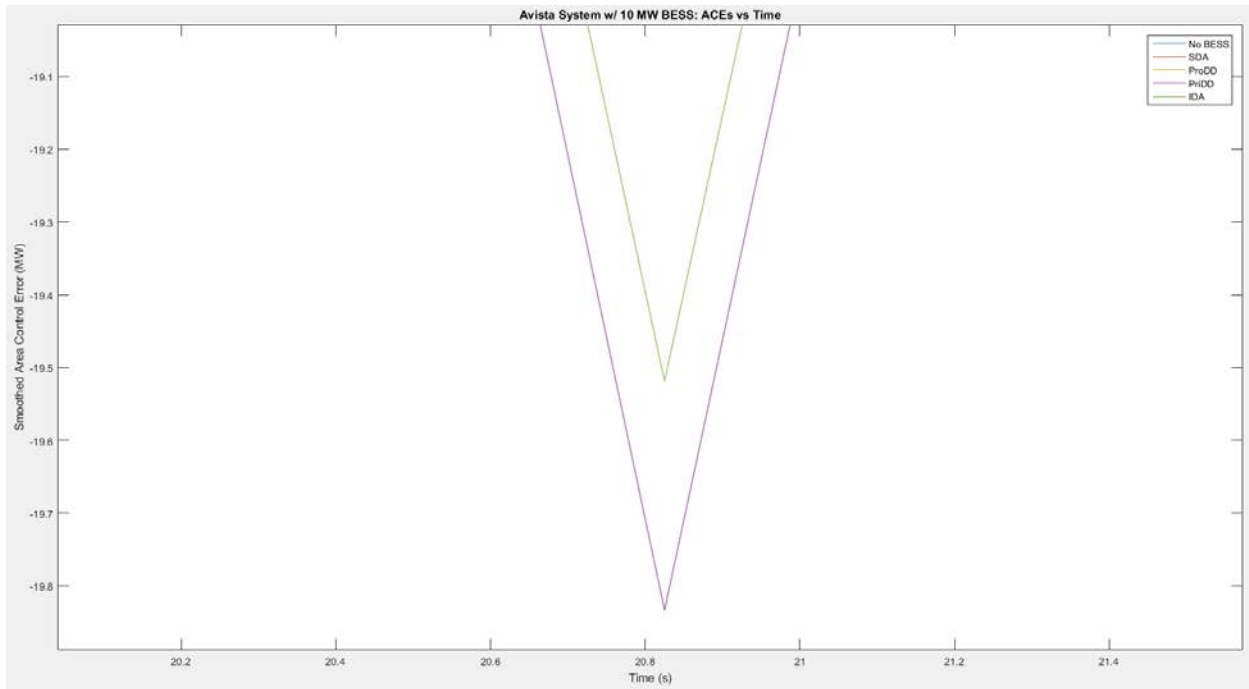


Figure 23. Smoothed ACE (close up on largest magnitude ACEs) in MW vs. Seconds

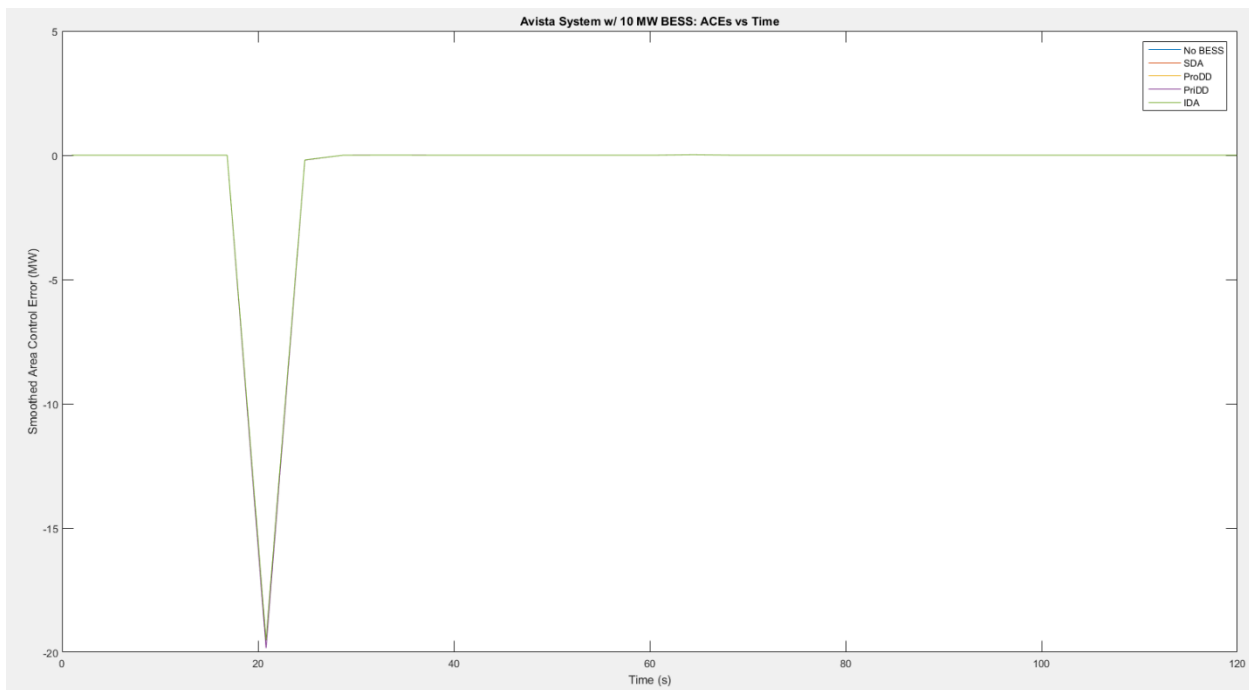


Figure 24. Smoothed ACE (over whole simulation time) in MW vs. Seconds

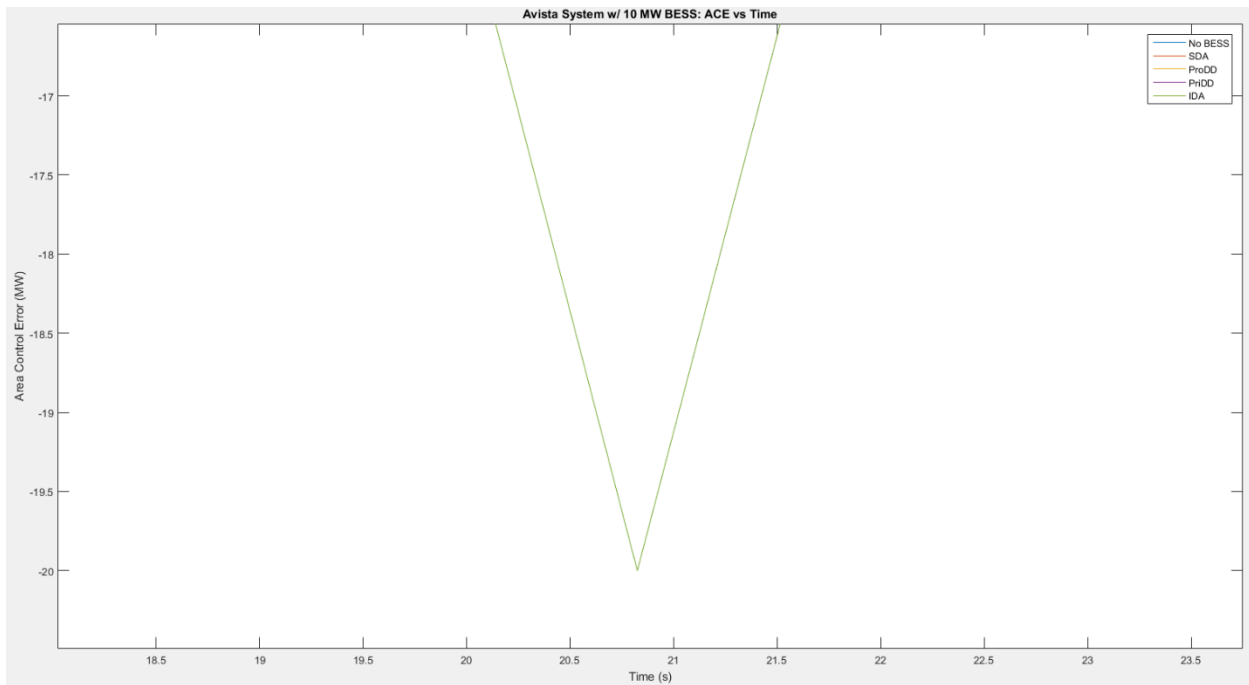


Figure 25. ACE (close up on largest magnitude ACE) in MW vs. Seconds

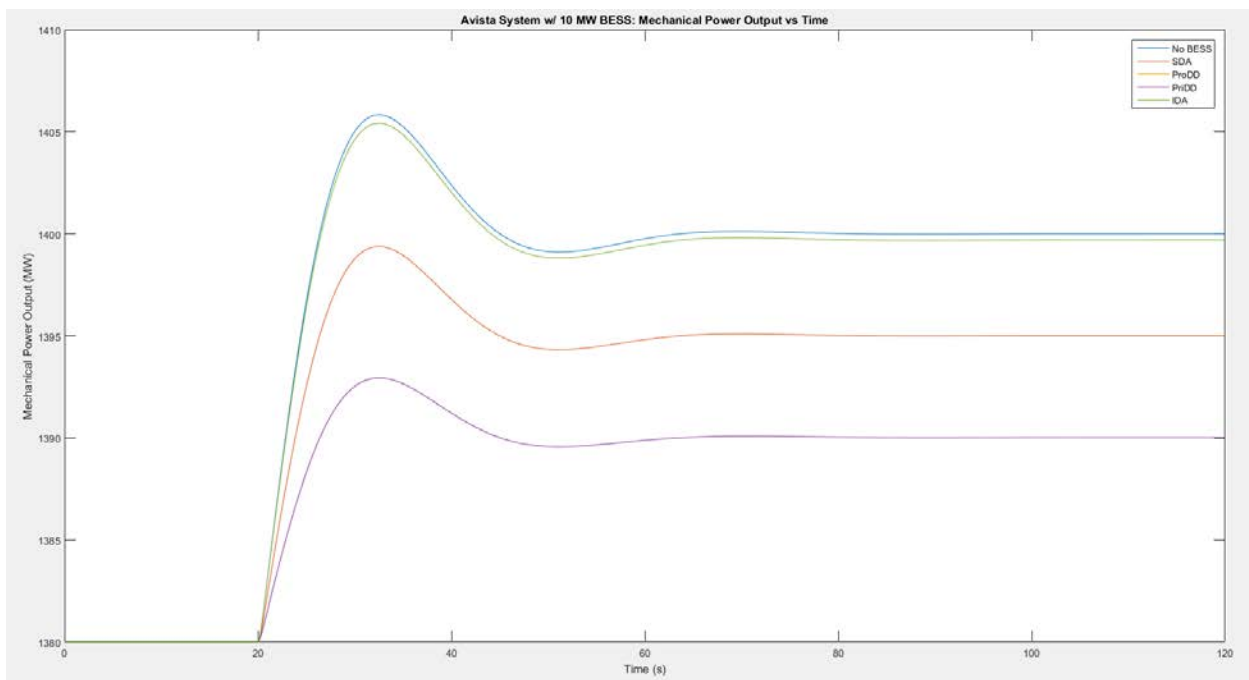


Figure 26. Mechanical Power Output of Equivalent Generator in MW vs. Seconds

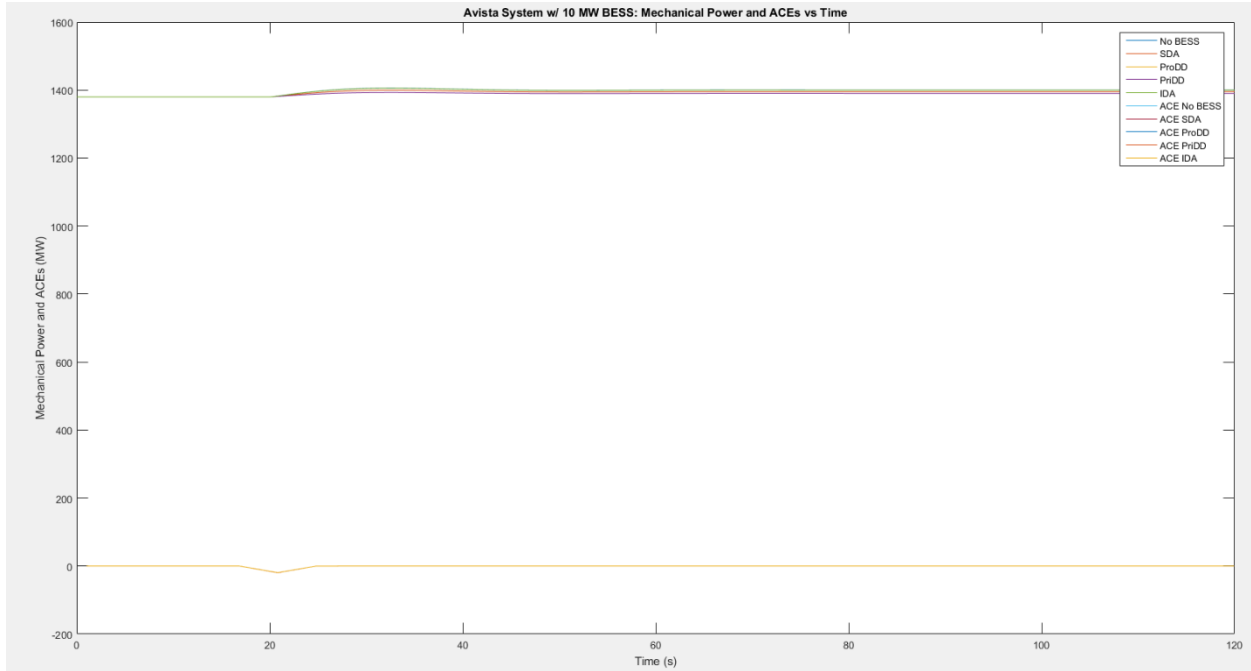


Figure 27. Mechanical Power Output of Equivalent Generator and Smoothed ACE in MW vs. Seconds

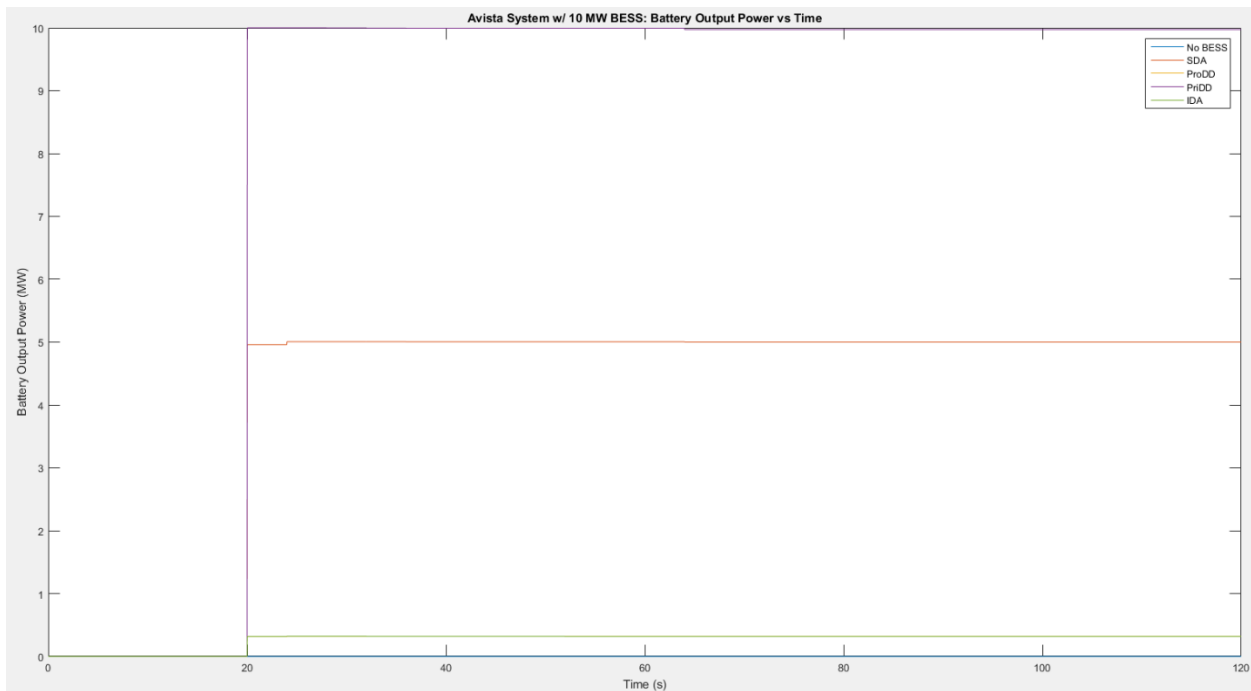


Figure 28. BESS Power Output in MW vs. Seconds

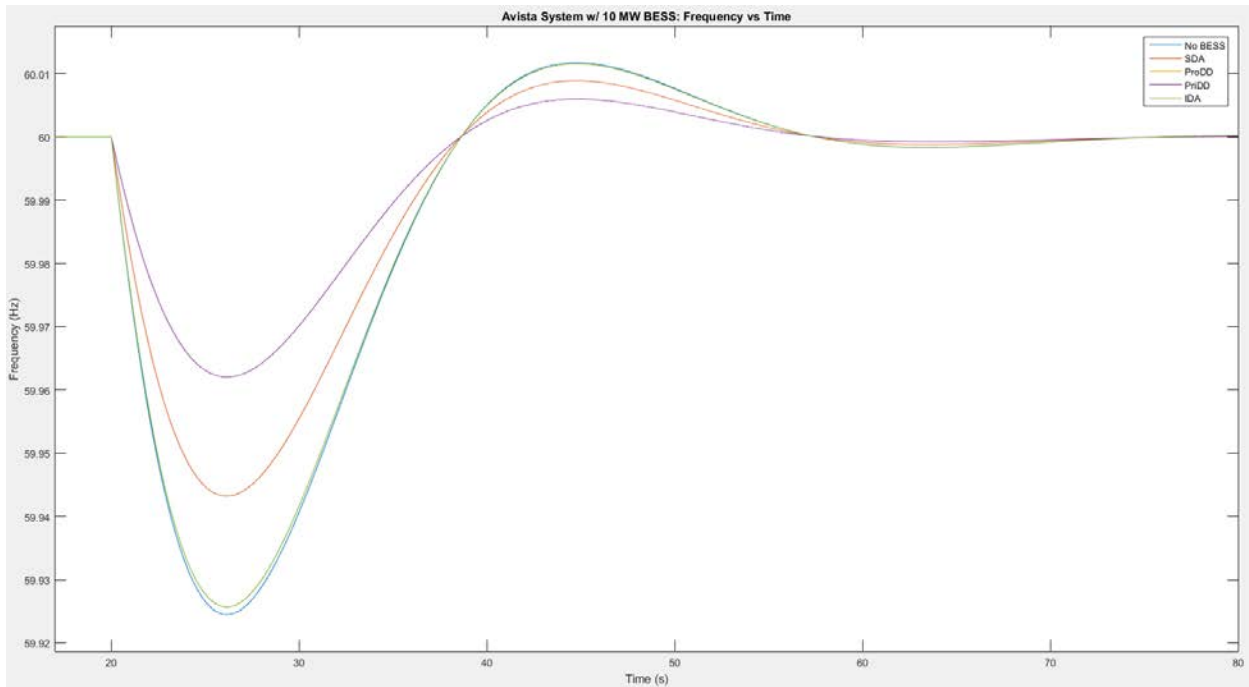


Figure 29. System Frequency Close Up in Hertz (Hz) vs. Seconds

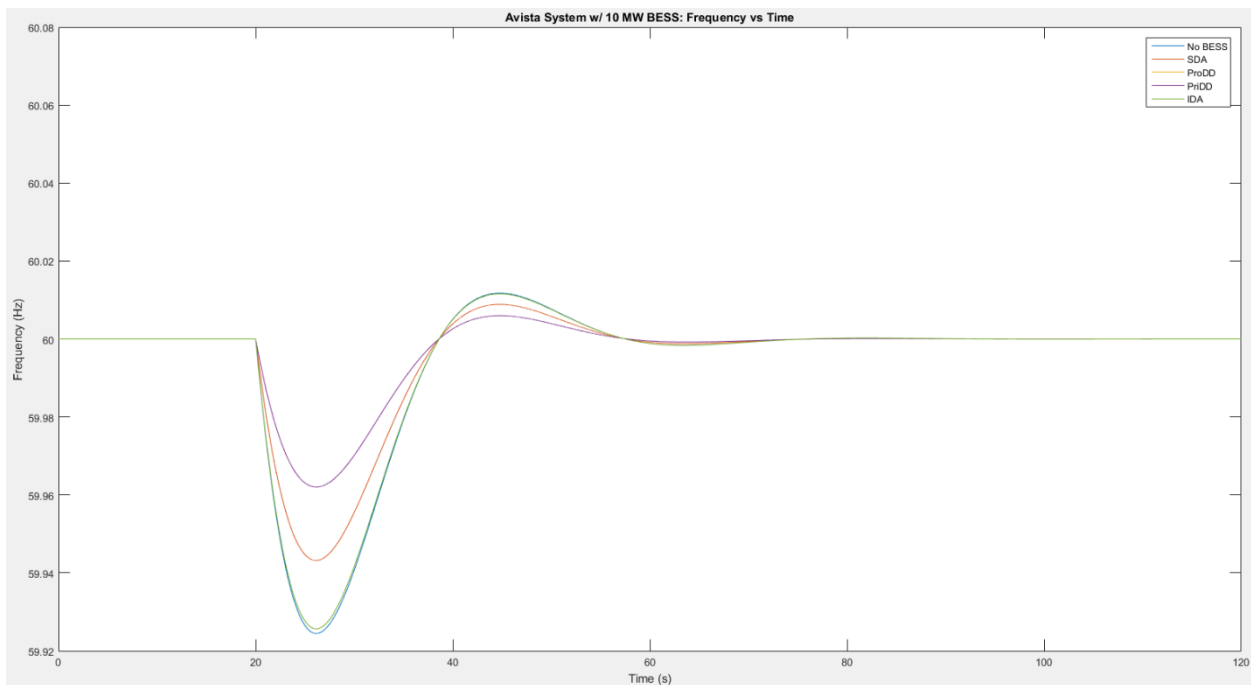


Figure 30. System Frequency in Hz vs. Seconds

8.5 Avista System with 1.31-MW BESS Subjected to a 20-MW Load Step Increase

The 1.3-MW BESS results indicate that the AGC signal distribution strategy that reduces the largest magnitude smoothed ACE error is IDA strategy. The IDA strategy assigns the BESS a portion of the unfiltered ACE burden before it passes through the PI controller, which causes a discrepancy in the smoothed ACE measurement and the frequency measurement. If the ACE is analyzed before the PI controller, it is clear that the IDA, ProDD, and PriDD strategies return the ACE to zero at the same time: at t=29 seconds. In terms of frequency deviation, the PriDD strategy gives the lowest magnitude frequency deviation. Since the PriDD strategy does not use the power divider method, the maximum capability of both the BESS and the conventional generation sources is realized sooner than in the other signal distribution cases. The PriDD and ProDD strategies give similar results in terms of time required to return the smoothed ACE to zero: slightly behind the IDA strategy and distinctly ahead of the SDA strategy. The SDA strategy does not make a zero crossing on the smoothed ACE measurement until 44 seconds have passed. The IDA distribution returns to zero slightly before the remaining distributions, but only due to the BESS removing a portion of ACE before the PI controller. In terms of the frequency response performance, the PriDD distribution gives the lowest magnitude frequency deviation, and it is the quickest to return the frequency deviation to zero. Graphs of the ACE, BESS power output, system frequency, and equivalent generator output are shown in Figures 31 through 38, below.

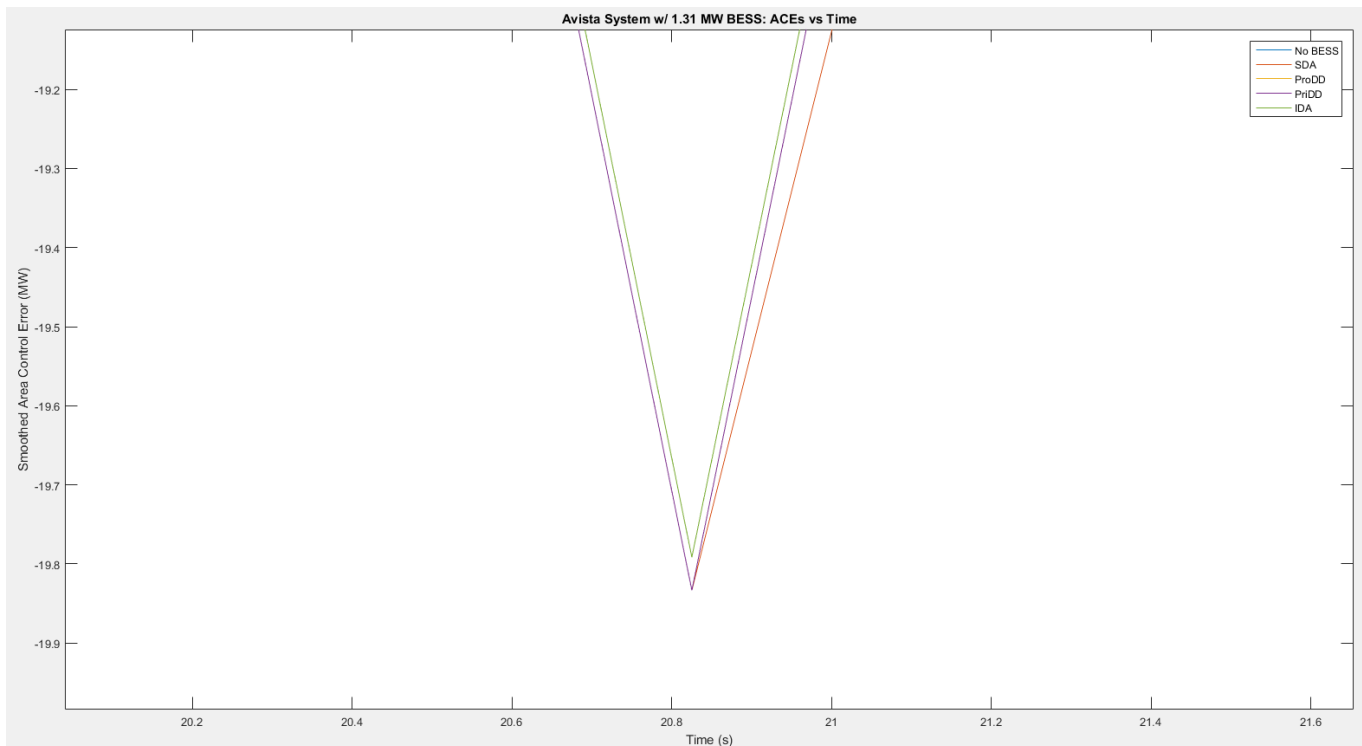


Figure 31. Smoothed ACE (close up on largest magnitude ACE) in MW vs. Seconds

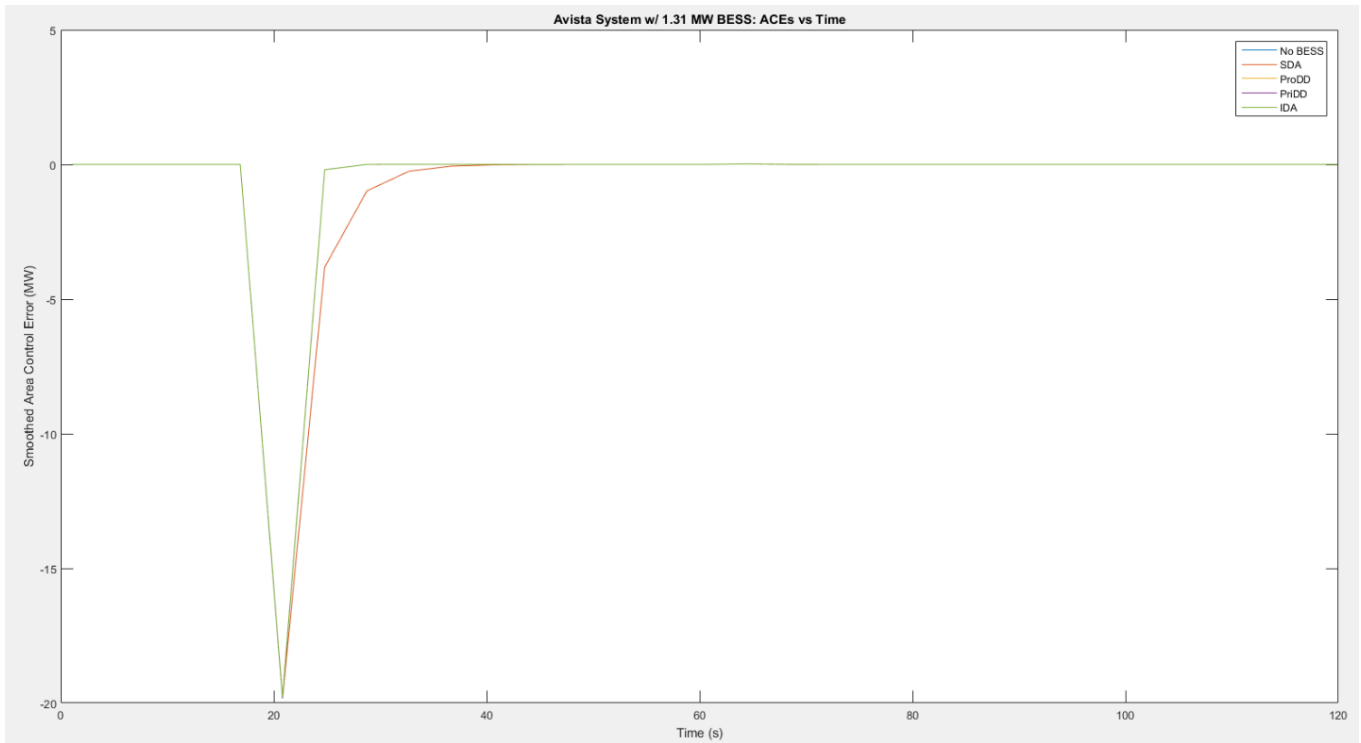


Figure 32. Smoothed ACE (over whole simulation time) in MW vs. Seconds

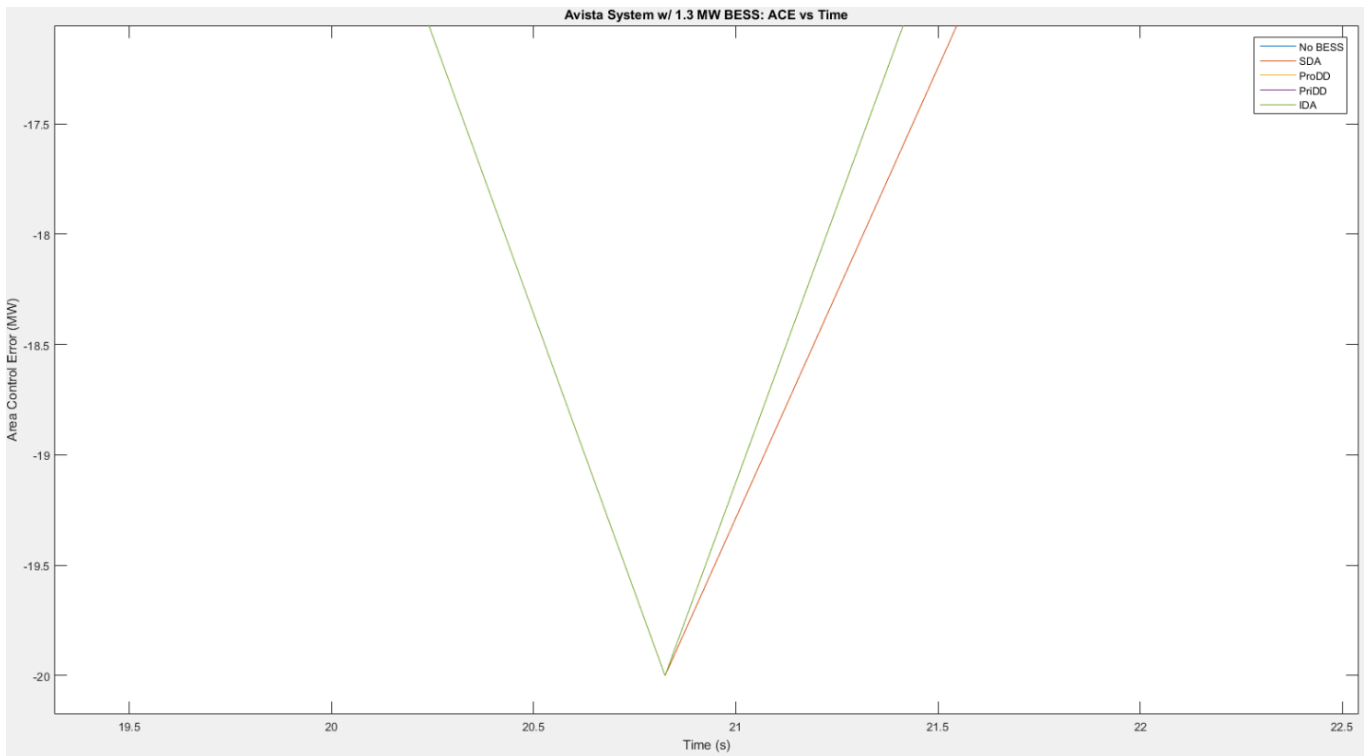


Figure 33. ACE (close up on largest magnitude ACE) in MW vs. Seconds

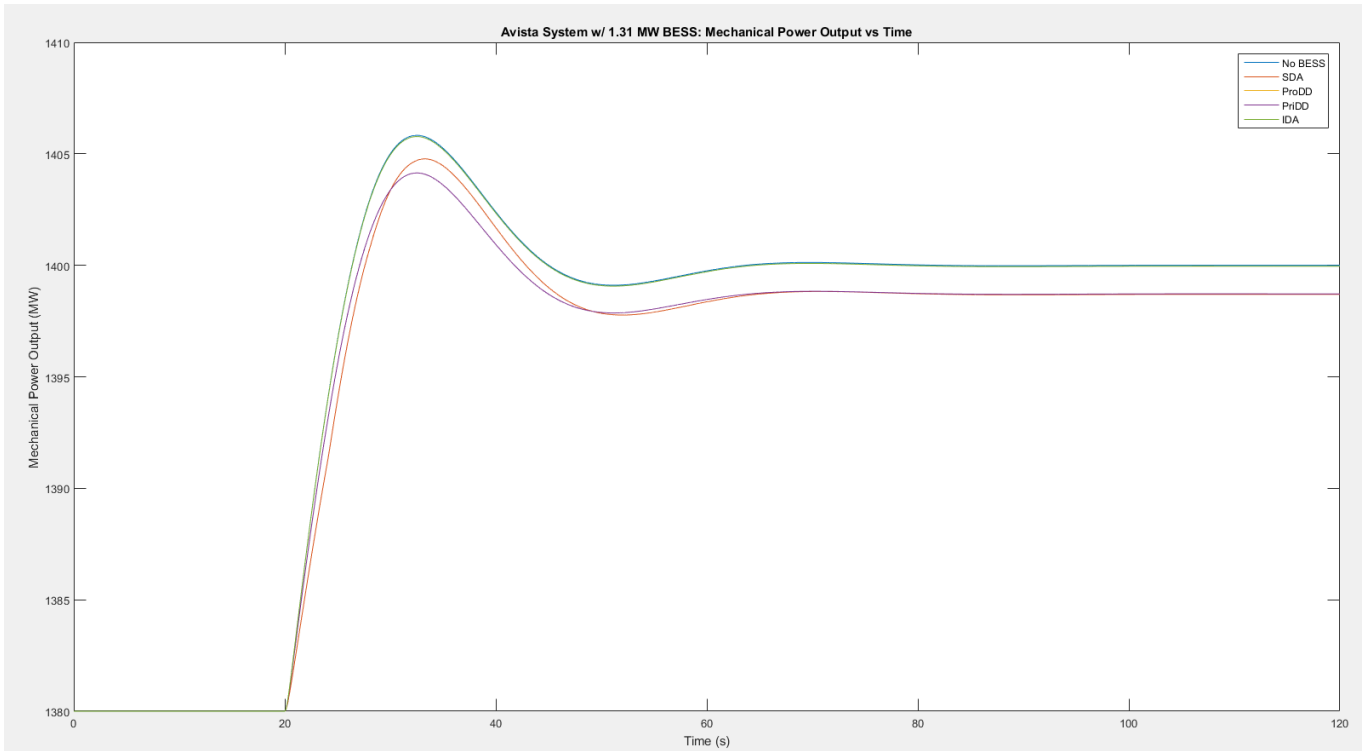


Figure 34. Mechanical Power Output of Equivalent Generator in MW vs. Seconds

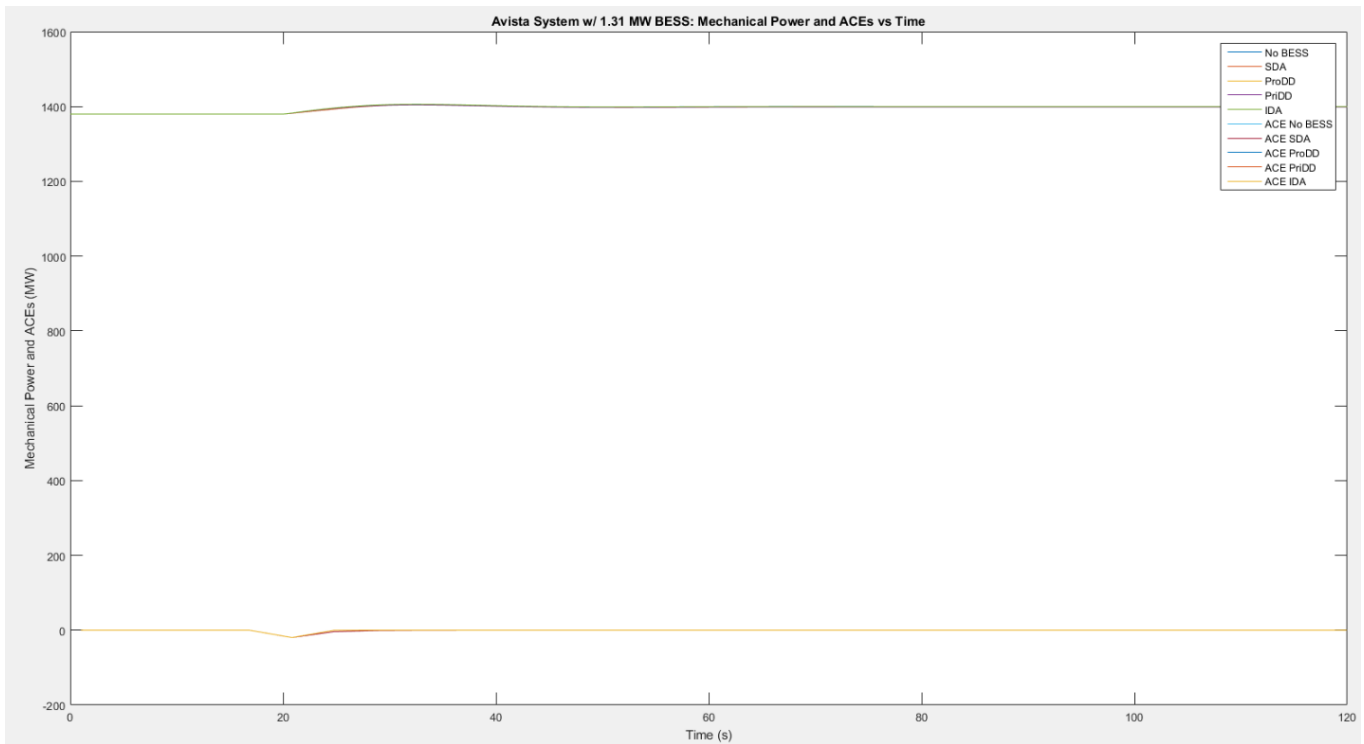


Figure 35. Mechanical Power Output of Equivalent Generator and ACE in MW vs. Seconds

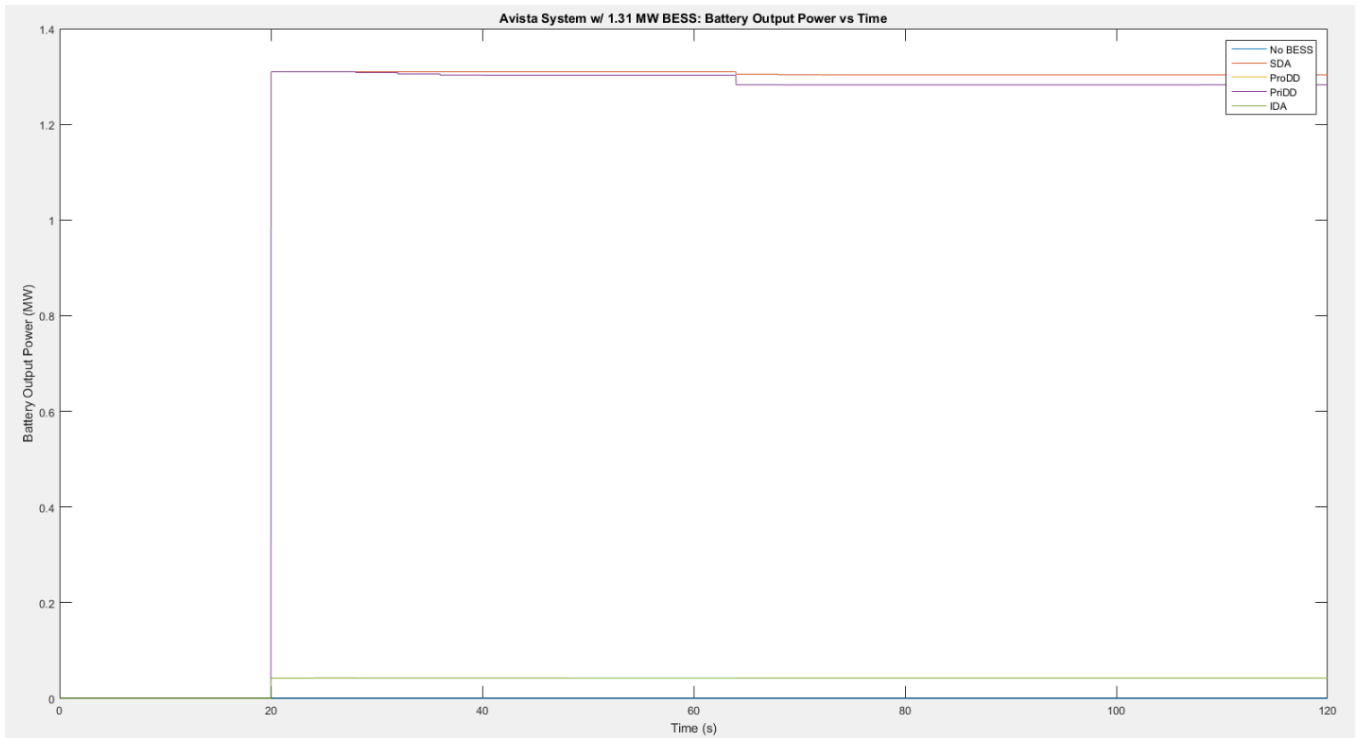


Figure 36. BESS Power Output in MW vs. Seconds

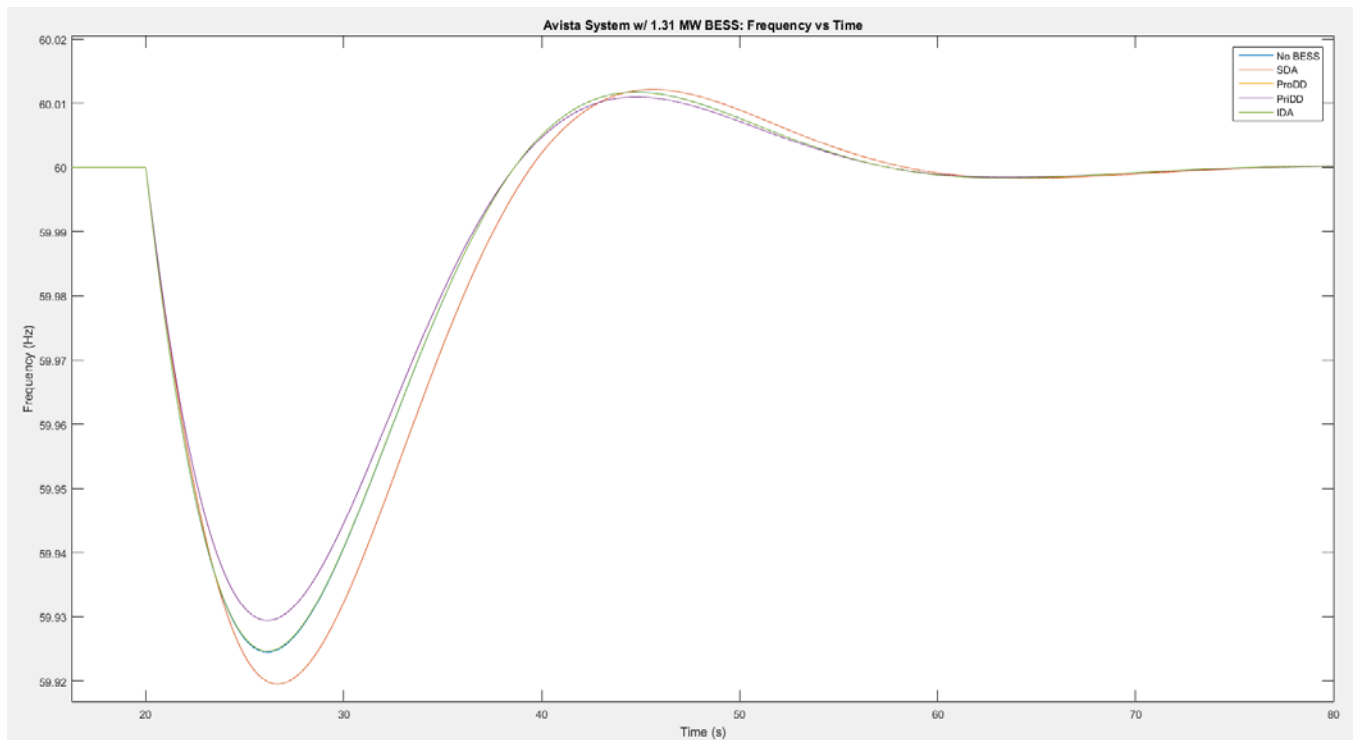


Figure 37. System Frequency close up in Hz vs. Seconds

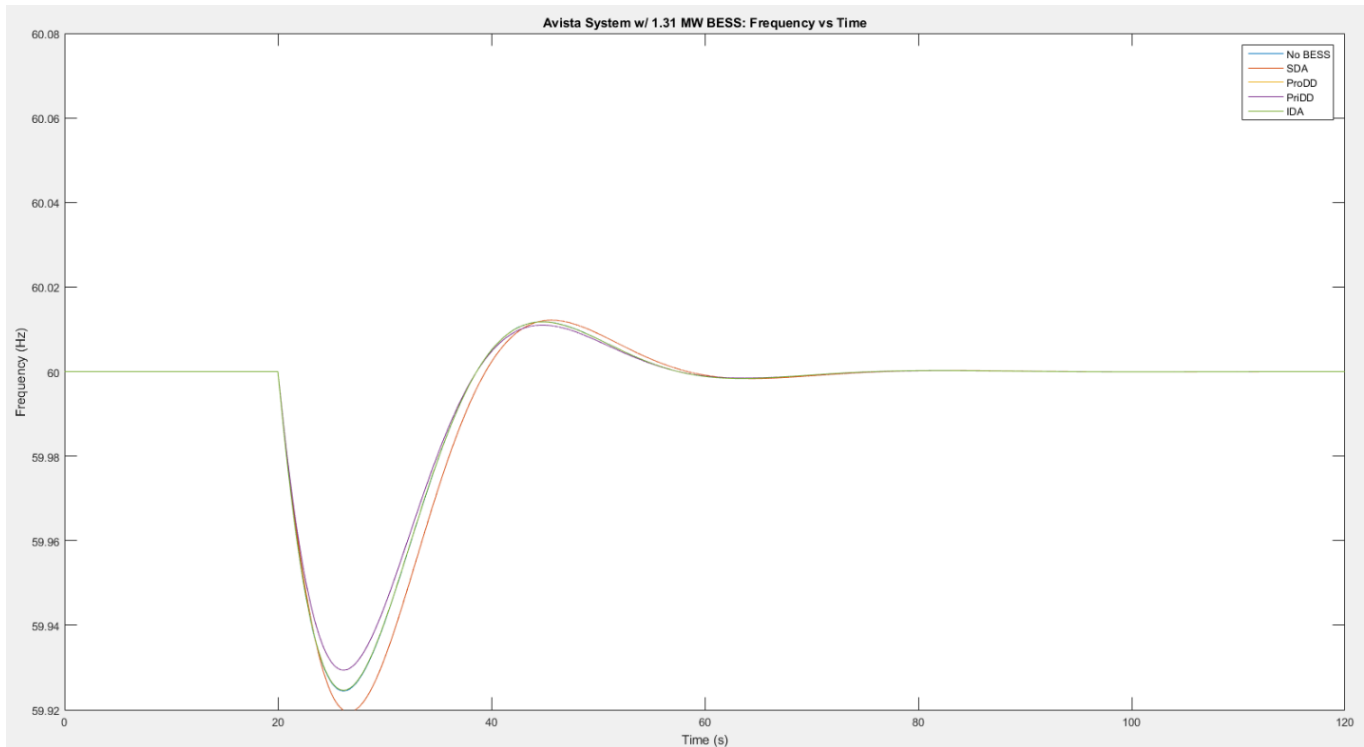


Figure 38. System Frequency in Hz vs. Seconds

8.6 Avista System with 1.31-MW BESS Subjected to a 3.33-MW Load Ramp Increase

The performance of the Avista system with a 1.3-MW BESS when subjected to a load ramp increase of 3.33 MW per second for 60 seconds is in this section. The ProDD, PriDD, and IDA strategies give similar performances in terms of minimizing the magnitude of smoothed ACE error, settling at -1.34 MW during the ramp period. The SDA strategy produces the worst smoothed ACE performance, settling at -1.8 MW during the ramp period. The ProDD, PriDD, and IDA strategies give identical performances in terms of minimizing the magnitude frequency deviation, oscillating at about the 59.985-Hz mark during the ramping period. The SDA strategy gives the worst performance over the ramping timeframe, oscillating at about the 59.98 Hz mark. The IDA, ProDD, and PriDD strategies cross the 60-Hz mark about 10 seconds after the ramp has stopped, and the SDA strategy crosses the 60-Hz mark 13 seconds after the ramp has stopped. Graphs of the ACE, BESS power output, system frequency, and equivalent generator output are shown in Figures 39 through 44, below. The performance of the BESS during the ramp increase versus the step increase is displayed on the last graph in Figure 45.

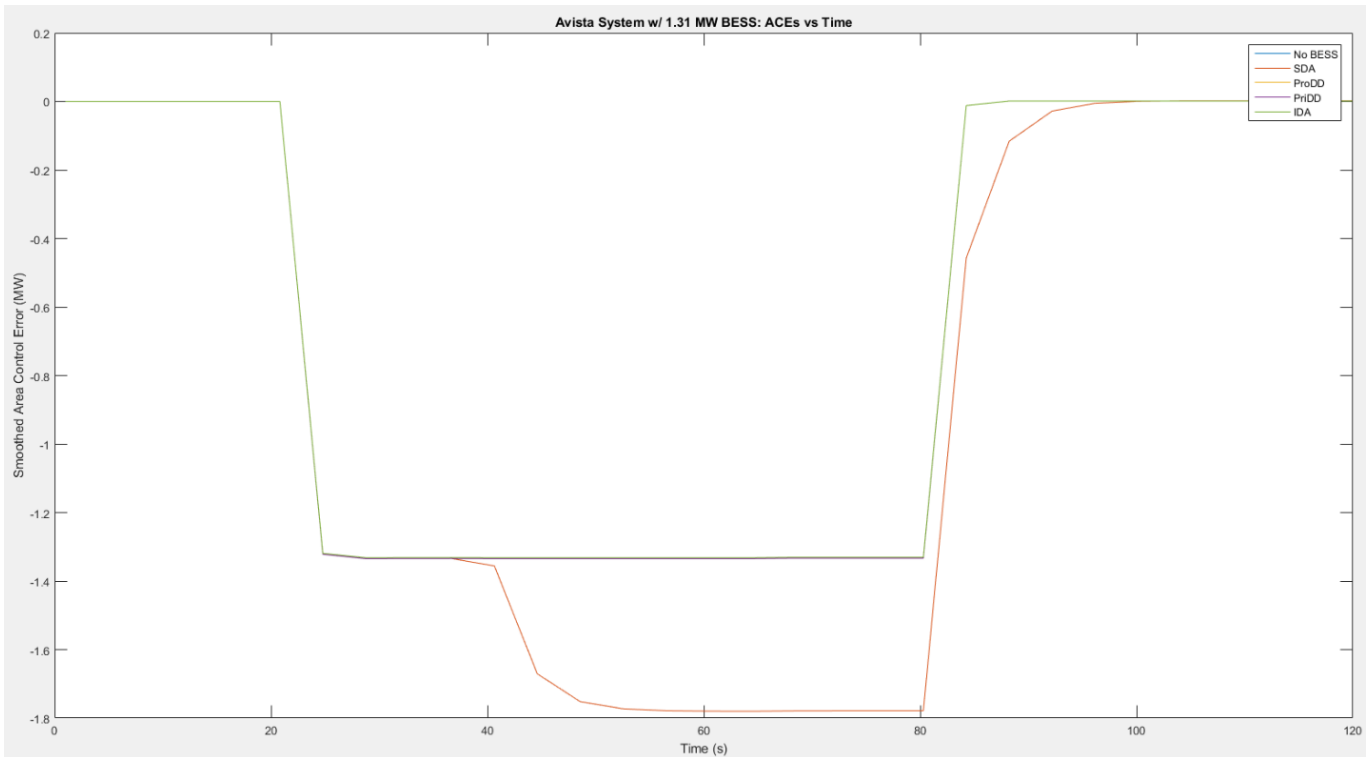


Figure 39. Smoothed ACE (over whole simulation time) in MW vs. Seconds

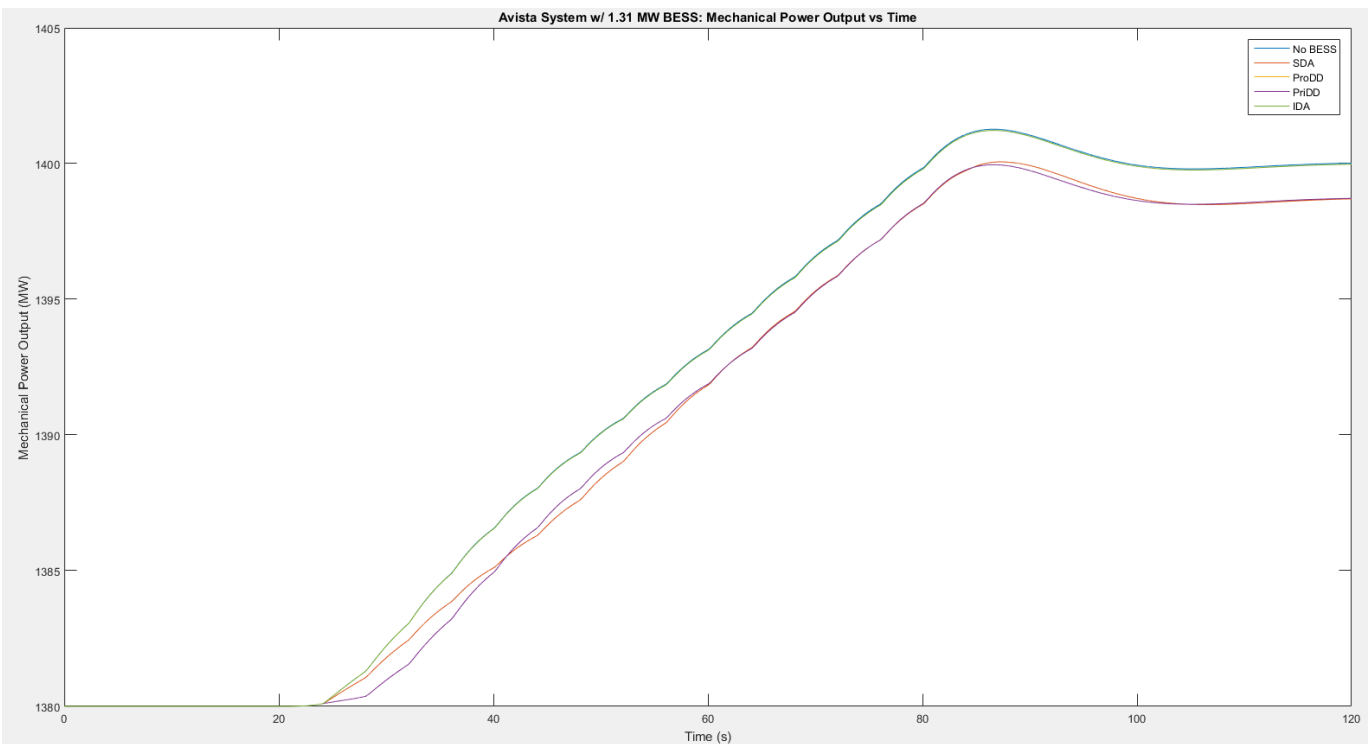


Figure 40. Mechanical Power Output of Equivalent Generator in MW vs. Seconds

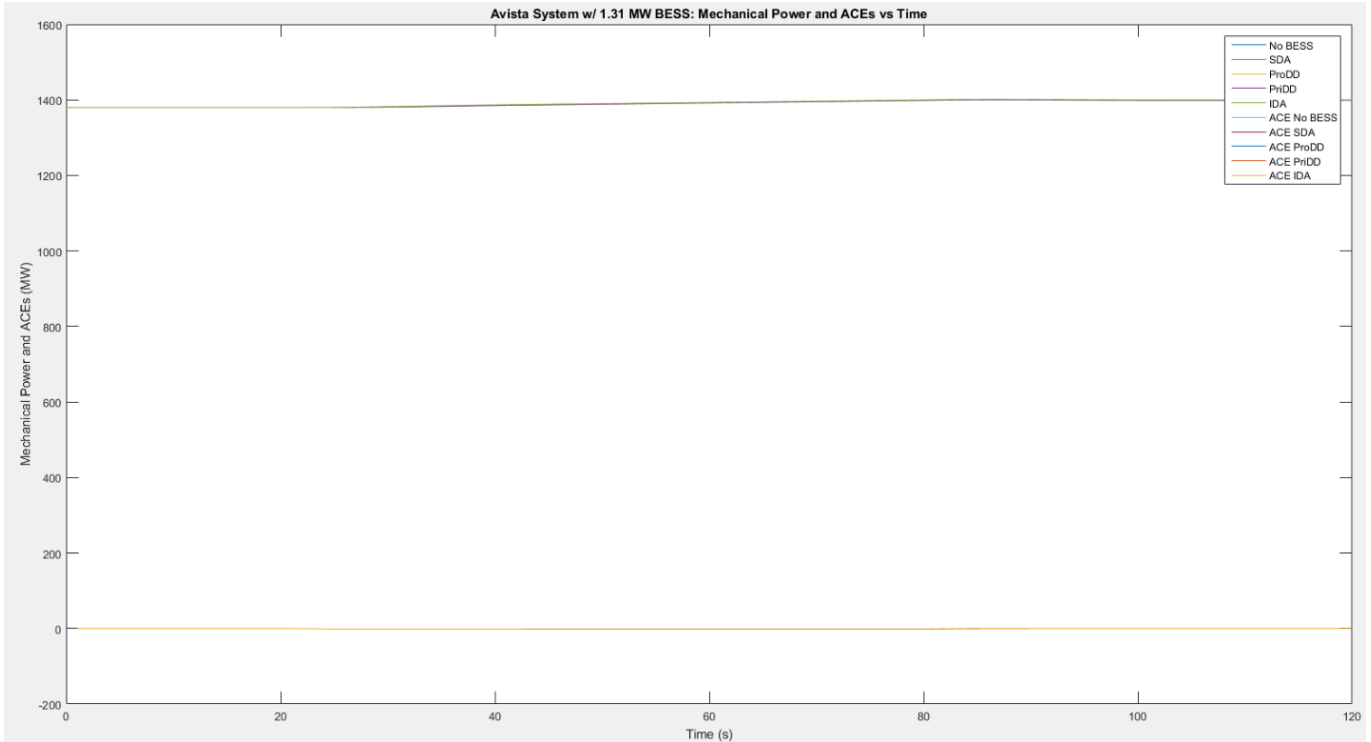


Figure 41. Mechanical Power Output of Equivalent Generator and ACE in MW vs. Seconds

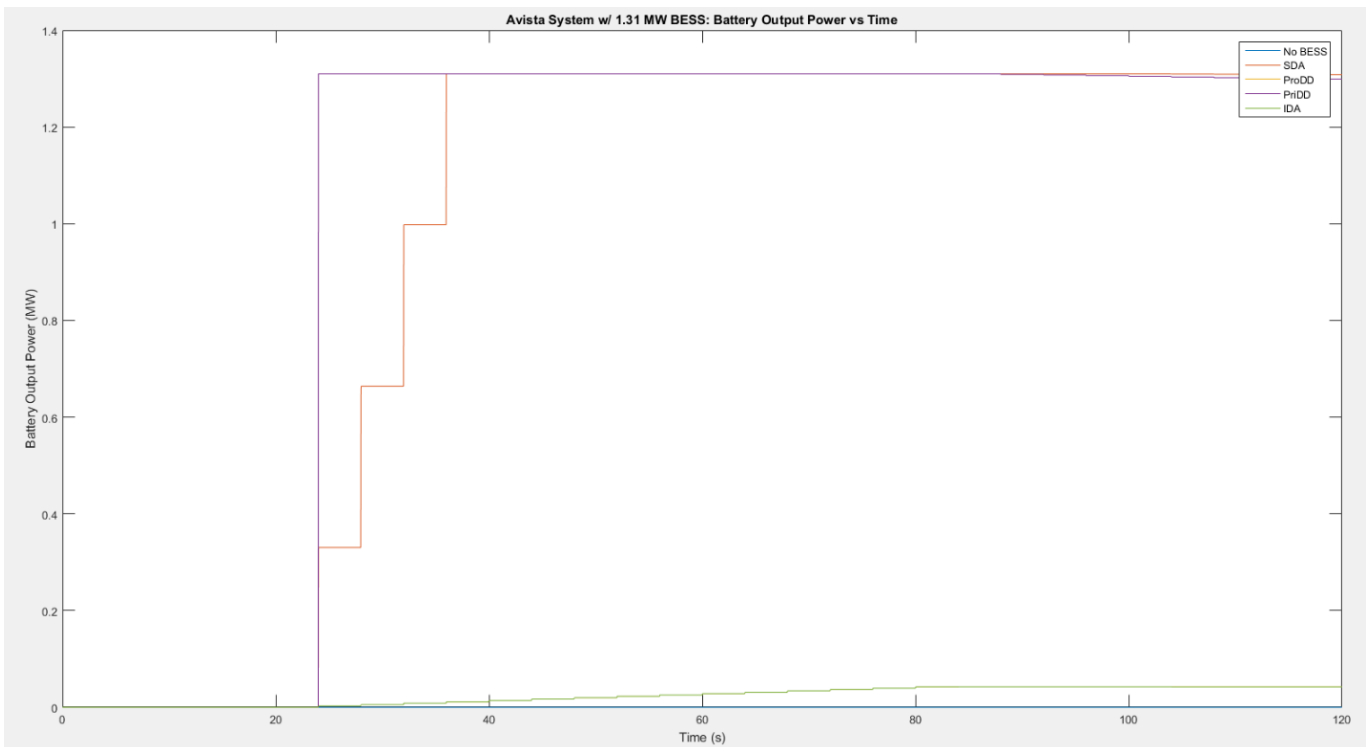


Figure 42. BESS Power Output in MW vs. Seconds

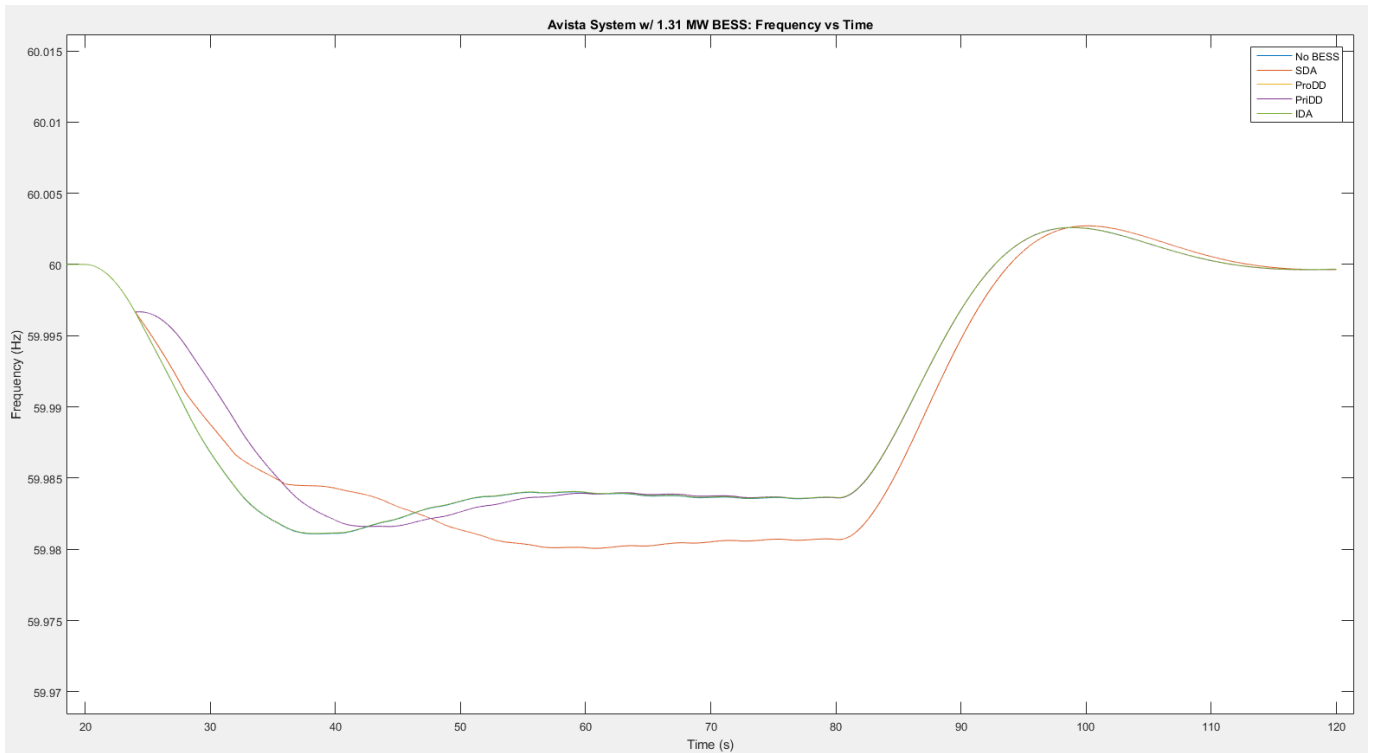


Figure 43. System Frequency Close Up on Ramp Settling Frequency in Hz vs. Seconds

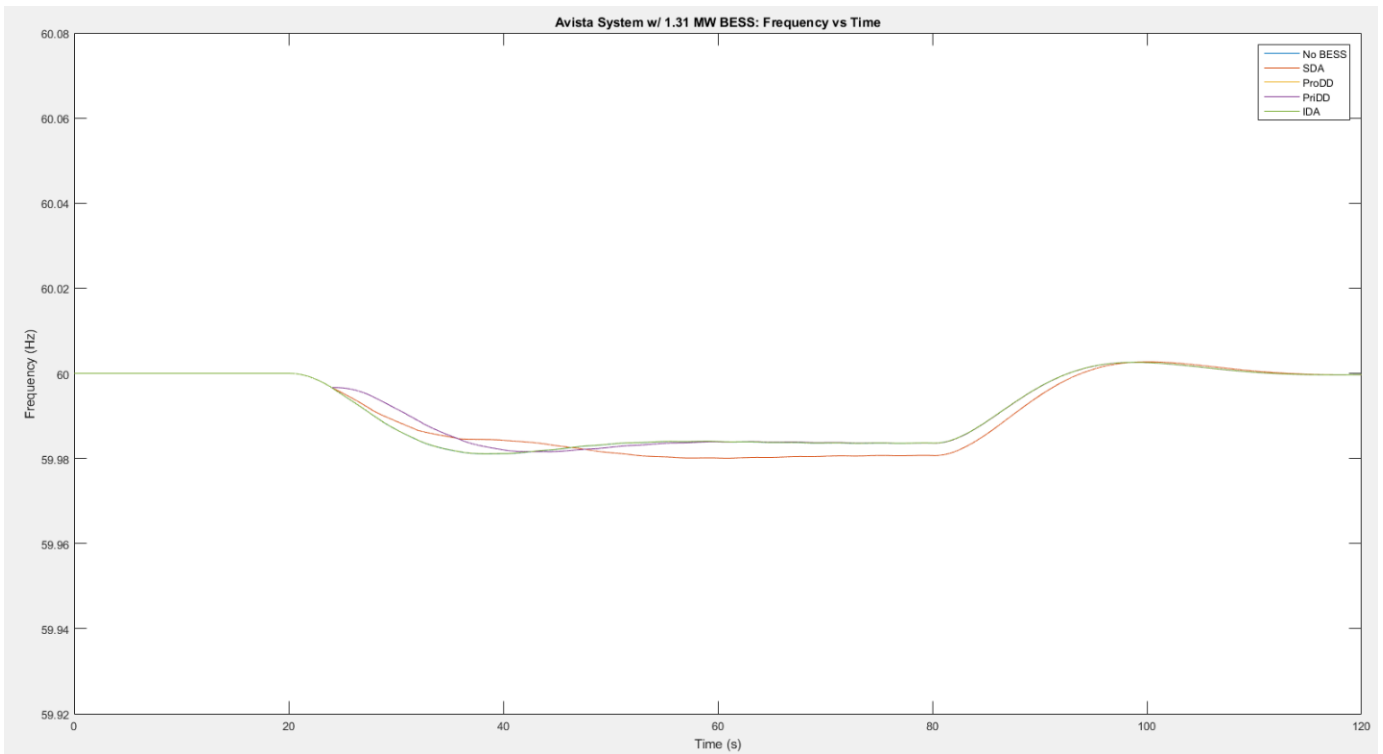


Figure 44. System Frequency in Hz vs. Seconds

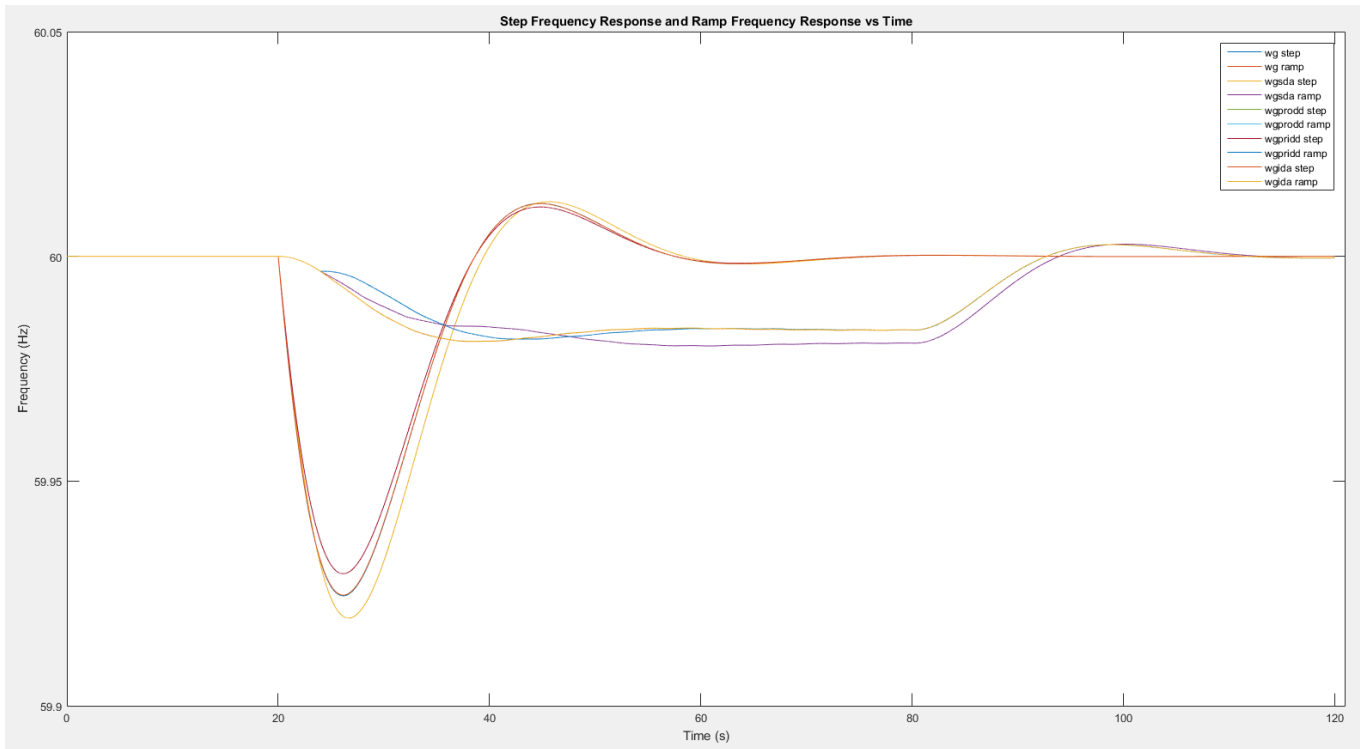


Figure 45. System Frequency Comparison Between Load Step Increase and Load Ramp in Hz vs. Seconds

8.7 BESS Performance When Operating in Island Mode

The BESS’s new inverter has the capability to operate as a standalone generation unit during an islanded condition. The capability of the inverter to maintain acceptable voltage levels during the islanded condition is not known. Assuming that the inverter can maintain an acceptable voltage level during the island condition, the BESS has the capability to supply power to portions of the Turner 116 feeder or the Turner 117 feeder, but not both. Based on the SynerGEE model, and assuming an initial SOC of 100 percent, the BESS can supply a 427-kW portion of Turner 117 (screenshot shown below in Figure 46) for 8 hours without the SOC falling below 10 percent. Based on the SynerGEE model, and assuming an initial SOC of 100 percent, the BESS can supply a 200 kW of Turner 116 (screenshot shown below in Figure 47) for 18 hours without the SOC falling below 10 percent.

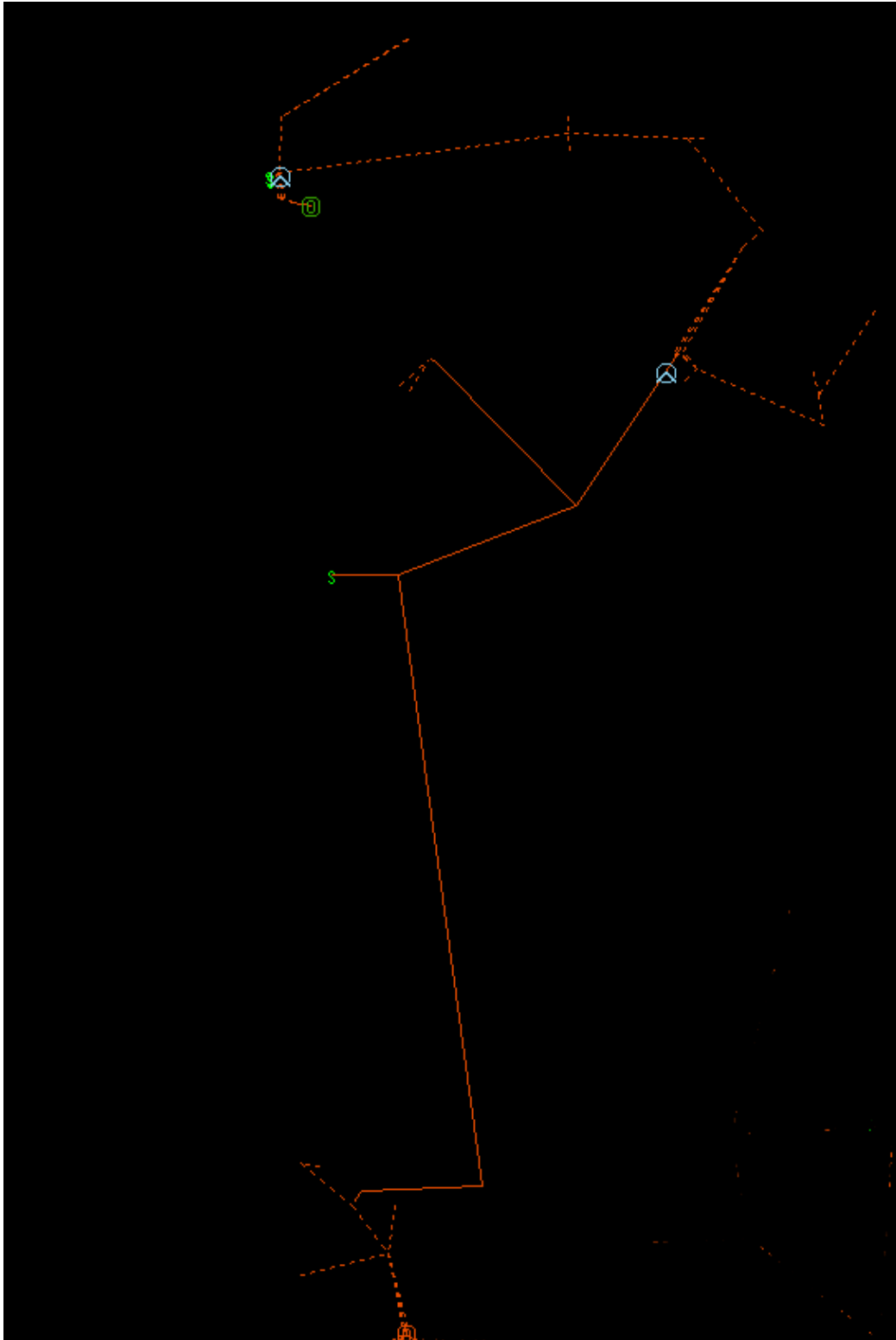


Figure 46. Turner 117 Screenshot

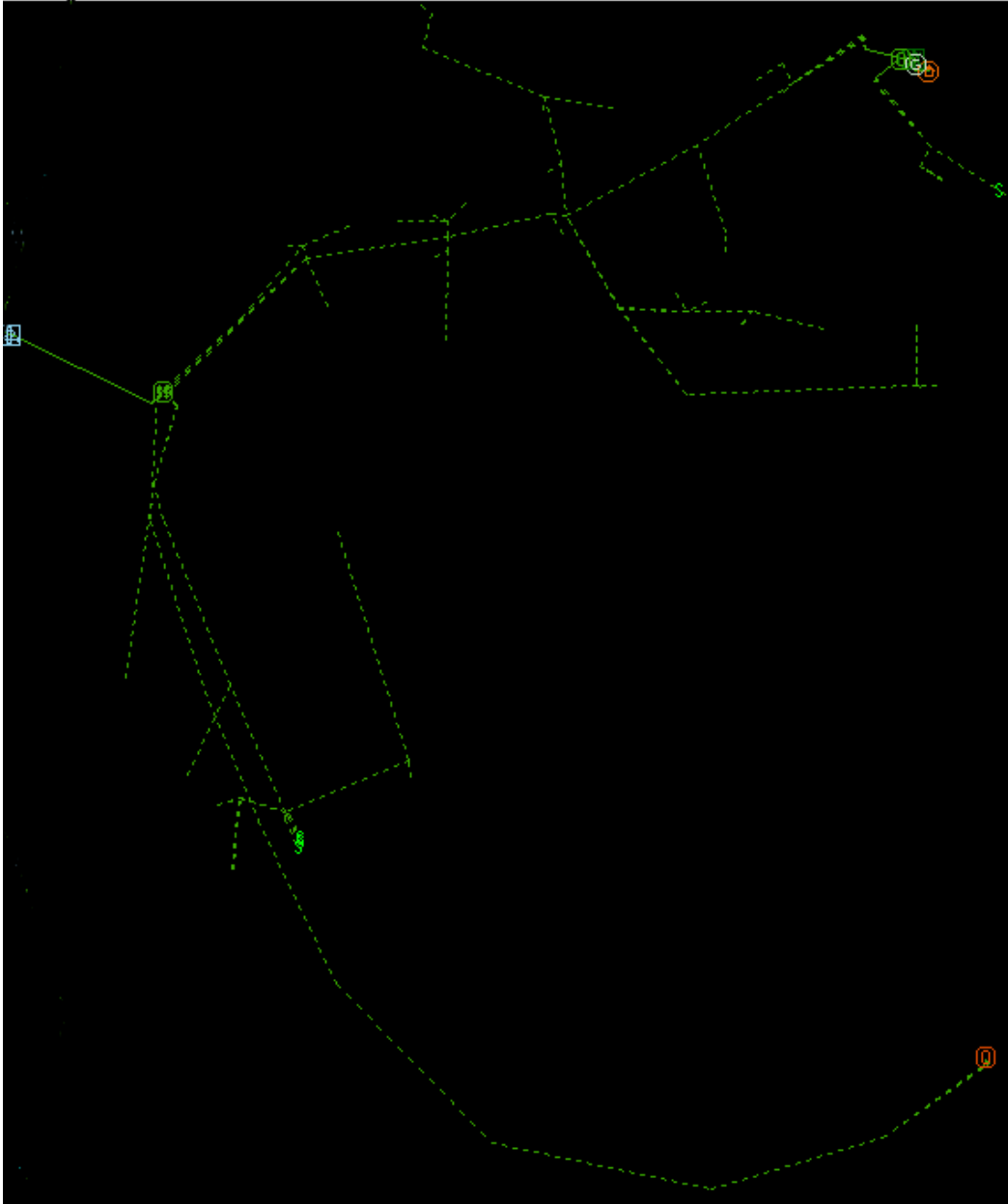


Figure 47. Turner 116 Screenshot

8.8 Conclusions

Based on the results of the 20-MW load step increase and the 3.33-MW per second load ramp increase, the best AGC signal distribution strategy for the Avista system using a 1.2-MW/3-MWh BESS is the PriDD strategy. The PriDD strategy minimizes the step change magnitude frequency error the most, matches the performance of the IDA and ProDD strategies during the ramping period, and returns the frequency to a steady-state 60-Hz frequency the quickest. The worst-performing strategy in both simulations is the SDA strategy and should be avoided. For the island condition, the BESS can feed a 200-kVA portion of Turner 116 for 18 hours and a 427-kVA portion of Turner 117 for 8 hours, assuming an initial SOC of 100 percent and a minimum SOC threshold of 10 percent.

9.0 ESS Reactive Power Control Strategy for Voltage Support

9.1 Introduction

9.1.1 Abstract

Voltage control in the distribution system is becoming very challenging due to the enhanced number of control variables and with the increasing penetration of distribution generations (e.g., photo-voltaic arrays). There is a need for new voltage control strategy considering fast control and four-quadrant operation of ESS in presence of the traditional voltage control devices like capacitor banks and transformer tap changers. In this project, a sensitivity-based voltage control strategy is developed for the ESS and validated using feeder Turner 117. As demonstrated through the simulation results, the proposed control strategy contributes to the voltage profile improvement with varying load conditions and various levels of PV penetration.

9.2 Methodology Description

9.2.1 Voltage Sensitivity Analysis

The fundamental theory behind the proposed ESS voltage control strategy is based on voltage sensitivity analysis. This section will provide description for this analysis method, and the actual implementation of it in ESS controller will be explained in next section. For a specific time, the standard power flow equations can be expressed as follows:

$$P_k = \sum_{n=1}^N |V_k| \cdot |V_n| \cdot |Y_{kn}| \cdot \cos(\theta_{kn} + \delta_n - \delta_k) \quad (4)$$

$$Q_k = \sum_{n=1}^N |V_k| \cdot |V_n| \cdot |Y_{kn}| \cdot \sin(\theta_{kn} + \delta_n - \delta_k) \quad (5)$$

where P_k and Q_k are the injected active and reactive powers at bus k; V_k and V_n are the voltage magnitude for bus k and n. δ_k , δ_n are the voltage angle for bus k and n. $Y_{kn} \angle \theta_{kn}$ represents the admittance between bus k and n. For a nominal operation point, the standard power flow equations can be linearized as:

$$\begin{bmatrix} \Delta P \\ \Delta Q \end{bmatrix} = \begin{bmatrix} \frac{\partial P}{\partial \delta} & \frac{\partial P}{\partial V} \\ \frac{\partial Q}{\partial \delta} & \frac{\partial Q}{\partial V} \end{bmatrix} \cdot \begin{bmatrix} \Delta \delta \\ \Delta V \end{bmatrix} \quad (6)$$

Taking inverse of the Jacobian matrix yield the sensitivities of the bus angles and voltages to the active and reactive powers:

$$\begin{bmatrix} \Delta \delta \\ \Delta V \end{bmatrix} = \begin{bmatrix} S_{\delta p} & S_{\delta q} \\ S_{vp} & S_{vq} \end{bmatrix} \cdot \begin{bmatrix} \Delta P \\ \Delta Q \end{bmatrix} \quad (7)$$

where $S_{\delta p}$ is the sensitivity matrix between bus angle and active power, $S_{\delta q}$ is the sensitivity matrix between bus angle and reactive power, S_{vp} is the sensitivity matrix between bus voltage magnitude and active power, and S_{vq} is the sensitivity matrix between bus voltage magnitude

and reactive power. Given an operational point, the voltage deviation at each bus can be estimated using the battery reactive power schedule. Suppose the battery is connected at bus k , if the reactive power output of battery is adjusted by ΔQ_B . The voltage at an arbitrary bus is changed by:

$$\Delta V_i = S_{vq}(i, k) \cdot \Delta Q_B \quad (8)$$

The positive values of ΔQ_B indicate increase in reactive power generation, while negative values indicate decrease in reactive power generation. Since the proposed control strategy is voltage/Var control, ΔP_B is zero and $S_{vp}(i, k)$ is neglected. The sensitivity factor is defined as:

$$K \stackrel{\text{def}}{=} 1/S_{vq}(k, k) \quad (9)$$

Noting that for any $i \neq k$, $S_{vq}(i, k) \leq S_{vq}(k, k)$, the reactive compensation affects the local voltage most effectively ($|\Delta V_i| \leq |\Delta V_k|$) (Synergi Electric, n.d.).

9.3 Reactive Compensation Strategy of Battery

Objective: Determine the reactive compensation (ΔQ_B) using only local measurements, i.e., voltage at the battery bus (V_B), and the active and reactive power generated by the battery (P_B and Q_B).

Theory: According to the voltage sensitivity analysis, to achieve a target voltage V_{target} at the battery bus, the reactive compensation can be estimated by

$$\Delta Q_B = \frac{(V_{\text{target}} - V_B)}{S_{vq}(k, k)} = K \cdot (V_{\text{target}} - V_B) \quad (10)$$

where

$$K \stackrel{\text{def}}{=} 1/S_{vq}(k, k) \quad (11)$$

Solution: The heuristic reactive compensation strategy can be obtained by the following steps:

- Define the ranges of V_B in per unit (i.e., [0.93, 0.94], [0.94, 0.95], etc.) and assume that the K value for each range is constant.
- Run the GridLAB-D time-serial simulation with $\Delta Q_B = 0$ (base case) and $\Delta Q_B = 100 \text{ kVar}$ (after reactive compensations) and obtain voltage data.
- Estimate K for each range of V_B and set the target voltages. A strategy table that uses only local measurements is then obtained.

9.4 Simulation Guide

Step 1: Run GridLAB-D model for the target day without any battery output.

Step 2: Run Initial_Result_Save.m to save the initial result.

- If the regulator is disabled, set `disable_regulator=true`. The result will be saved at `result_wo_battery_wo_regulator.mat`.

- If the regulator is enabled, set `disable_regulator= false`. The result will be saved at `result_wo_battery_w_regulator.mat`.

Step 3: Adjust `Q_Out` as 100 kVar in the `Battery_inverter.glm` and run GridLAB-D model again.

Step 4: Run “Control_Table_Generator.m” to generate both the voltage control table in `k_value.mat` and the BESS reactive power schedule player file “`batterysch.player`.”

Step 5: Run GridLAB-D model with “`batterysch.player`” for `Q_out` again.

Step 6: Run `Voltage_scenarios_analysis.m` to get the simulation results.

9.5 Initial Test on Turner 117 Model on September 14, 2016

9.5.1 Basic Information of Feeder Turner 117

The topology for feeder Turner 117 is shown in Figure 48. During this initial test, since the aggregate smart meter data does not match the DMS data at the substation, three lumped loads are added to the model so that the total load matches the DMS measurements. The deviation between DMS measurement and aggregated smart meters’ measurement at three different phases is shown in Figure 49. Since this case is a very light case study, the voltage drop along the feeder is very small. Therefore, for voltage regulation study purpose, this model extends the length of the distribution line after the regulator from 190.295719 feet to 20190.295719 feet.

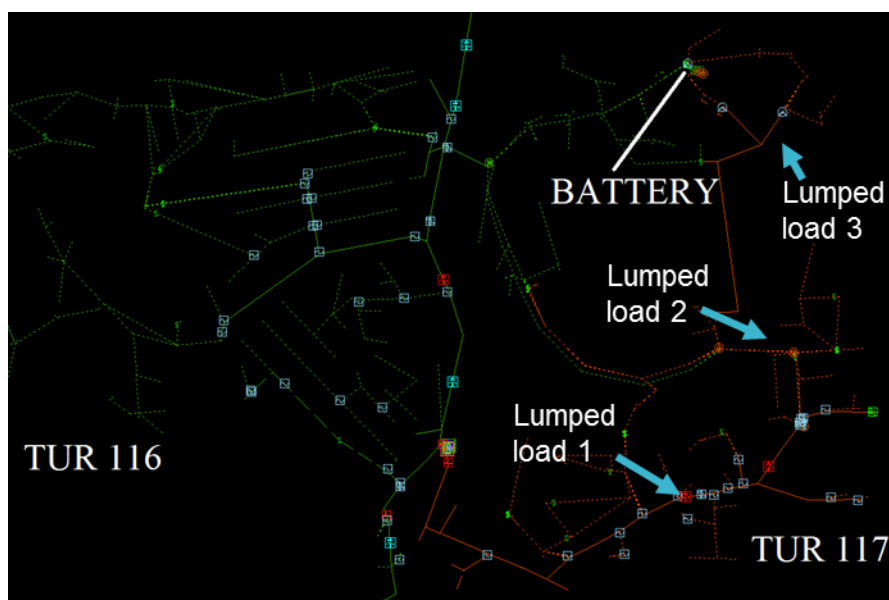


Figure 48. Topology of Feeder Turner 117

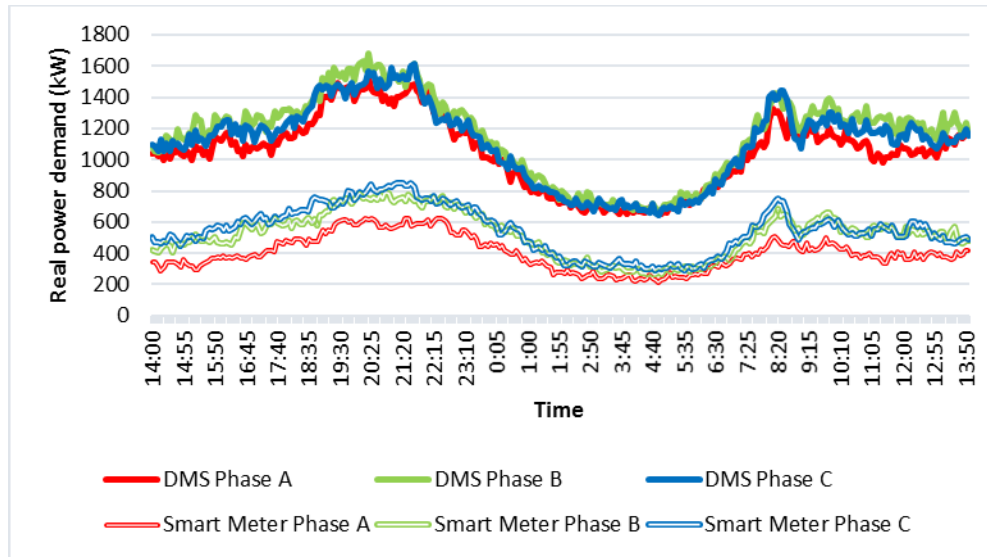


Figure 49. The Deviation Between DMS Measurement and Aggregated Smart Meters Measurement

9.5.2 Voltage Profile of Feeder Turner 117

The voltage profile along the feeder at a relative heavy-load time (09/14/2016 21:00) is plotted in Figure 50. Seen from this figure, bus with the lowest voltage is ND 391-280208, the voltage is lower than 0.96 at phase B. Noting that the sharp voltage drop at the beginning of the feeder is resulting from line length extension.

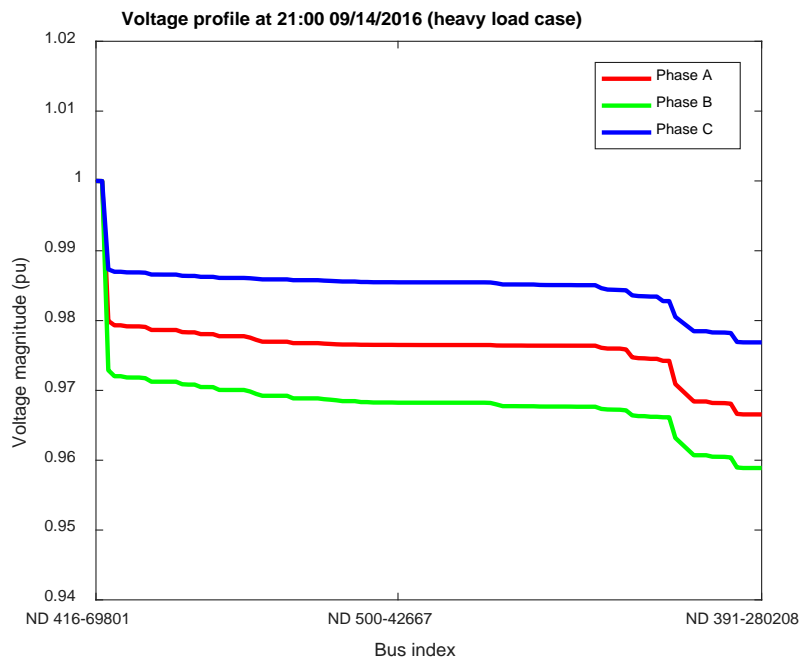


Figure 50. The Voltage Profile Along the Feeder at a Relative Heavy-Load Time

9.5.3 Voltage Sensitive to Reactive Power

Following the simulation guide in section 7.7, time-series power flow calculations are performed with GridLAB-D for two scenarios:

Scenario 1: Without reactive power from battery ($Q_{B1} = 0$).

Scenario 2: Battery injecting 100 kVar of reactive power ($Q_{B2} = 100$ kVar).

For each snapshot, a value of K (inverse of sensitivity) can be calculated by

$$K = \frac{\Delta Q_B}{\Delta V_B} = \frac{Q_{B2} - Q_{B1}}{V_{B2} - V_{B1}} = \frac{100}{V_{B2} - V_{B1}} \text{ kVar/p. u.} \quad (12)$$

where, the average voltage (average value of *abc*-phase voltages) at the battery bus for the scenarios 1 and 2 are denoted by V_{B1} and V_{B2} , respectively. In Table 3, the 288 K values are divided into several groups according to the range of V_{B1} . For each group, the average value of K is computed. The sensitivity K table for this simulation case is shown in Table 3.

Table 3. The Sensitivity Table for September 16, 2016 Case

Voltage at battery bus (p. u.)	Inverse of sensitivity K (kVar/p. u.)
[0.96 0.965]	54203
[0.965 0.97]	54808
[0.97 0.975]	55192
[0.975 0.98]	55527
[0.98 0.985]	55929
[0.985 0.99]	56409

9.6 Volt-Var Control Strategy with Battery

Based on the sensitivity table, a Volt-Var control strategy of battery using only local measurements is obtained. The reactive power incensement can be determined by:

$$\Delta Q_B = K \cdot (V_{\text{target}} - V_B) \quad (13)$$

$$V_{\text{target}} = 0.99 \text{ p. u.} \quad (14)$$

Note that the total apparent power of battery cannot exceed its kVA capacity (1.2 MW). Applying the strategy to Turner 117, the schedule of reactive power of battery for September 14, 2016 is given in Figure 51.

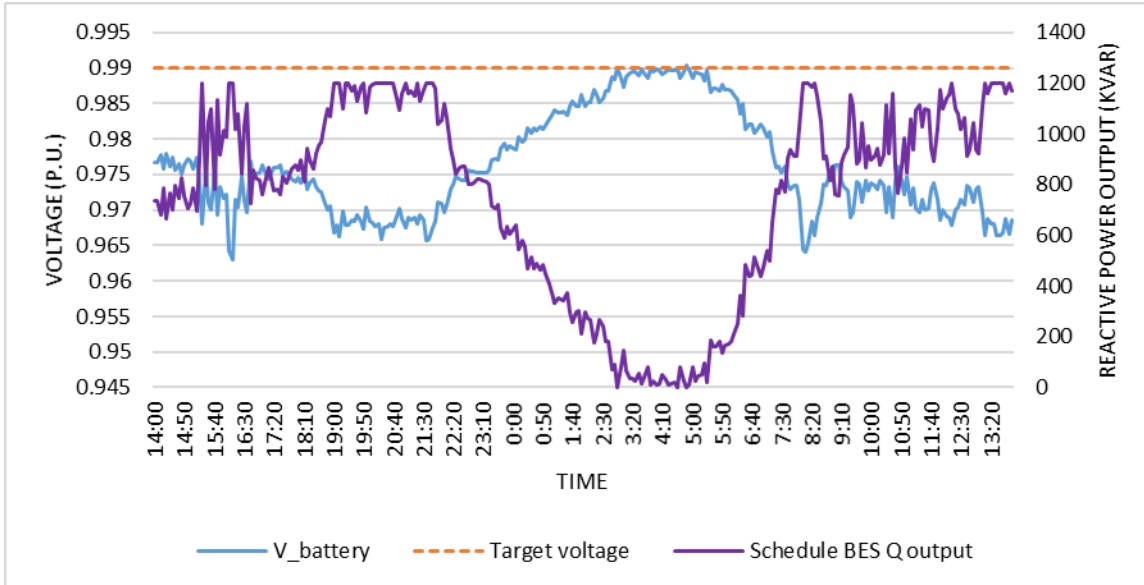


Figure 51. The Schedule of Reactive Power of Battery, Average Battery Voltage Before Reactive Power Control and Target Voltage Value for the Target Day

9.7 Performance of the Proposed Strategy

The voltage profile along the feeder before and after BESS control is shown in Figure 52. Seen from this figure, the BESS control strategy boosts the voltage along the feeder. For example, the voltage of phase B at node 391-280209 is boosted from 0.96 p.u to 0.98 p.u.

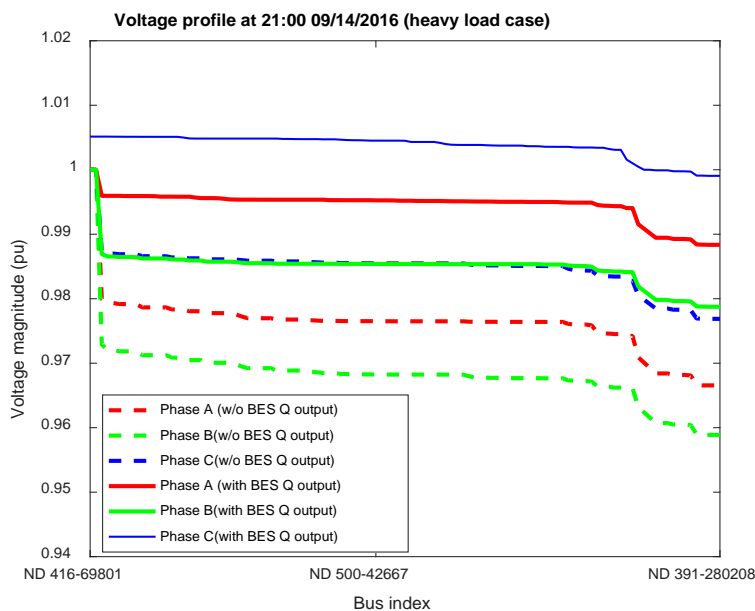


Figure 52. Voltage Profile Comparison Between Cases with and without BES Control

The average voltage at battery bus before and after BESS control is shown in Figure 53. It is clearly that the average voltage after the BESS control is very close to 0.99 p.u. Since it is very close to our setting point, this figure proves the correctness of the proposed BESS control strategy.

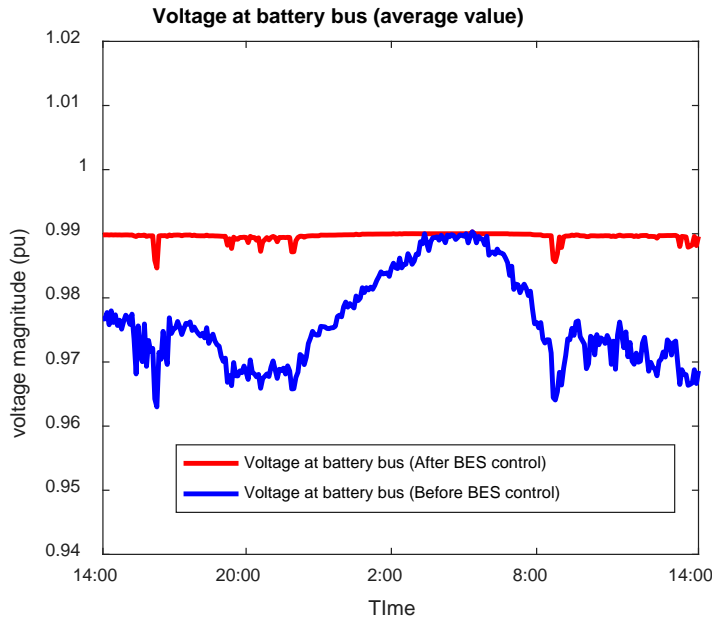


Figure 53. Average Voltage at Battery Bus Before and After BESS Control

The three phases voltages at the node in feeder end is shown in Figure 54. After the BESS support, this bus’s voltage during the day is boosted. Therefore, it shows the BESS effect on the bus suffering from voltage issues the most. It is clearly that BESS could provide a good voltage support.

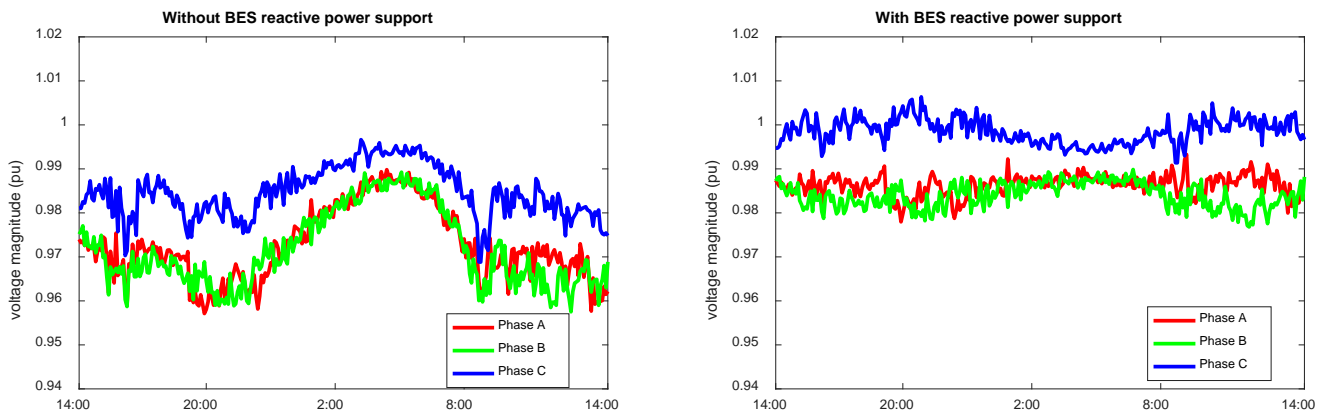


Figure 54. Voltage of Three Phases at the Bus with Lowest Voltage with and without BESS Control

9.8 Simulation Results for Clear Data without PV – Winter Data Testing on Turner 117

9.8.1 Simulation Results for January 12, 2017

The sensitivity table for the January 12, 2017 case is shown in Table 4. The average battery voltage before and after BESS control and the scheduled BESS reactive power output is plotted in Figure 55. The results about voltage profile comparison between cases with and without BESS control are plotted in Figure 56.

Table 4. The Sensitivity Table for January 12, 2017 Case

Voltage at battery bus (<i>p. u.</i>)	Inverse of sensitivity <i>K</i> (<i>kVar/p. u.</i>)
[0.975 0.98]	187750
[0.98 0.985]	188700
[0.985 0.99]	190020

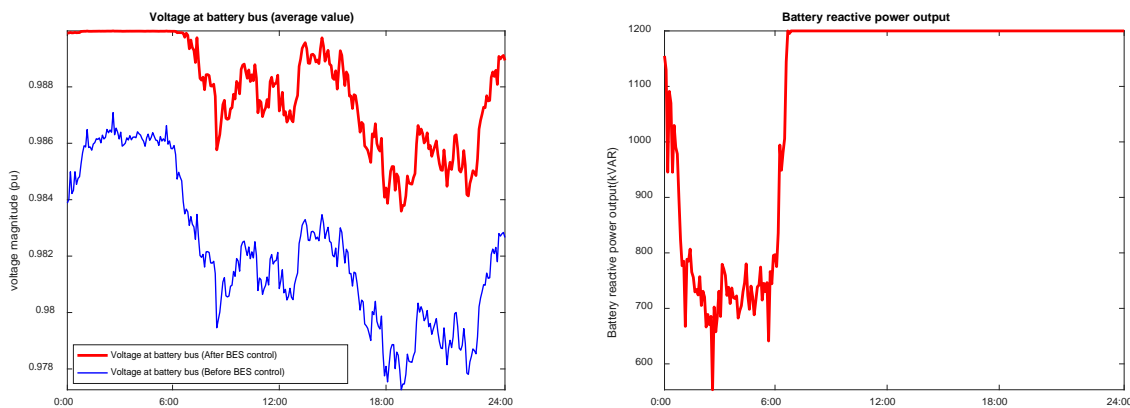


Figure 55. Average Battery Voltage Before and After Reactive Power Control (left) and the Schedule of Reactive Power of Battery for January 12, 2017 (right)

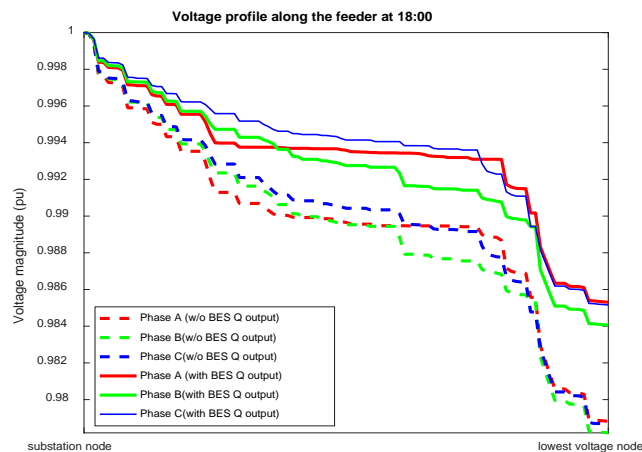


Figure 56. Voltage Profile Comparison Between Case with and without BESS Control for January 12, 2017

9.8.2 Simulation Results for January 13, 2017

The sensitivity table for the January 13, 2017 case is shown in Table 5. The average battery voltage before and after BESS control and the scheduled BESS reactive power output is plotted in Figure 57. The results about voltage profile comparison between cases with and without BESS control are plotted in Figure 58.

Table 5. The Sensitivity Table for January 13, 2017 Case

Voltage at battery bus (<i>p.u.</i>)	Inverse of sensitivity <i>K</i> (<i>kVar/p.u.</i>)
[0.975 0.98]	187880
[0.98 0.985]	188590
[0.985 0.99]	189720

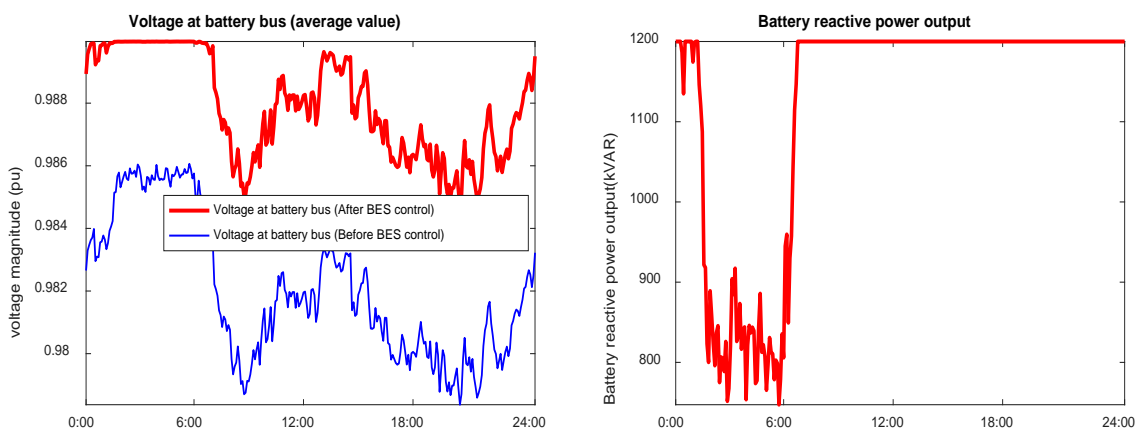


Figure 57. Average Battery Voltage Before and After Reactive Power Control (left) and the Schedule of Reactive Power of Battery for January 13, 2017 (right)

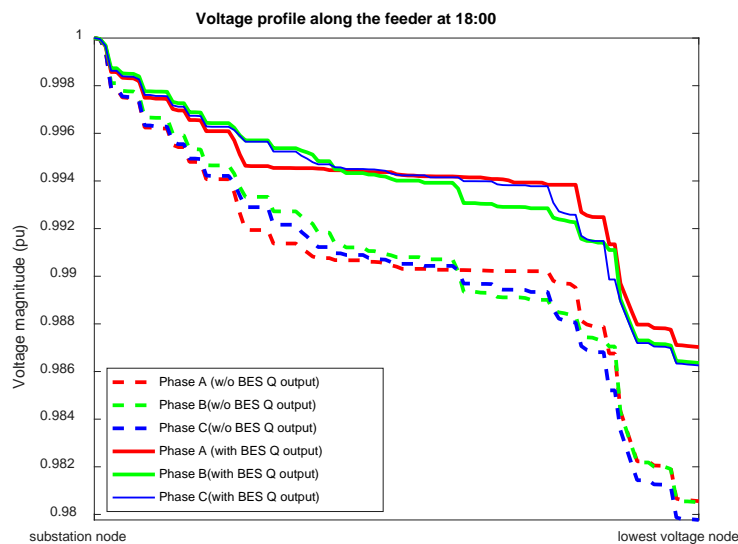


Figure 58. Voltage Profile Comparison Between Case with and without BESS Control for January 13, 2017

9.8.3 Simulation Results for January 14, 2017

The sensitivity table for the January 14, 2017 case is shown in Table 6. The average battery voltage before and after BESS control and the scheduled BESS reactive power output is plotted in Figure 59. The results about voltage profile comparison between cases with and without BESS control are plotted in Figure 60.

Table 6. The Sensitivity Table for January 14, 2017 Case

Voltage at battery bus (<i>p. u.</i>)	Inverse of sensitivity <i>K</i> (<i>kVar/p. u.</i>)
[0.98 0.985]	189500
[0.985 0.99]	189950

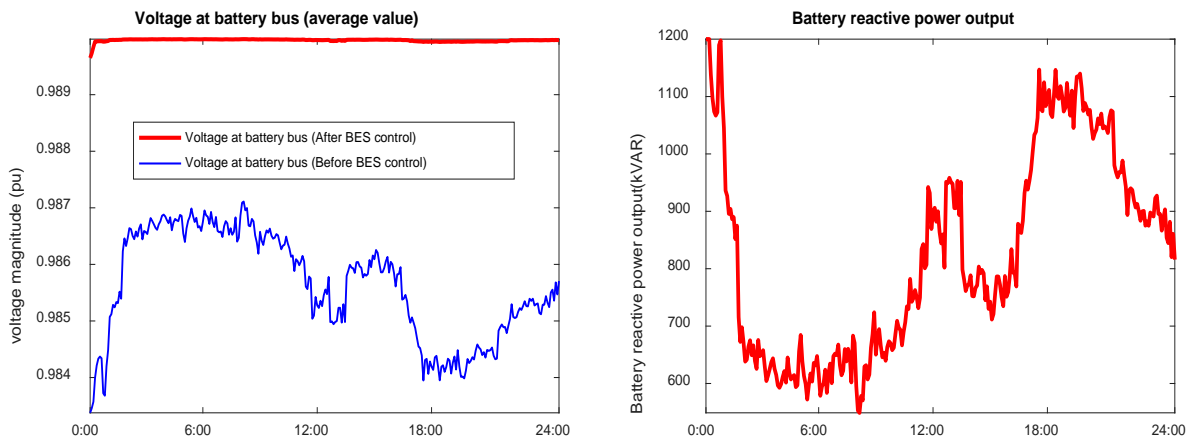


Figure 59. Average Battery Voltage Before and After Reactive Power Control (left) and the Schedule of Reactive Power of Battery for January 14, 2017 (right)

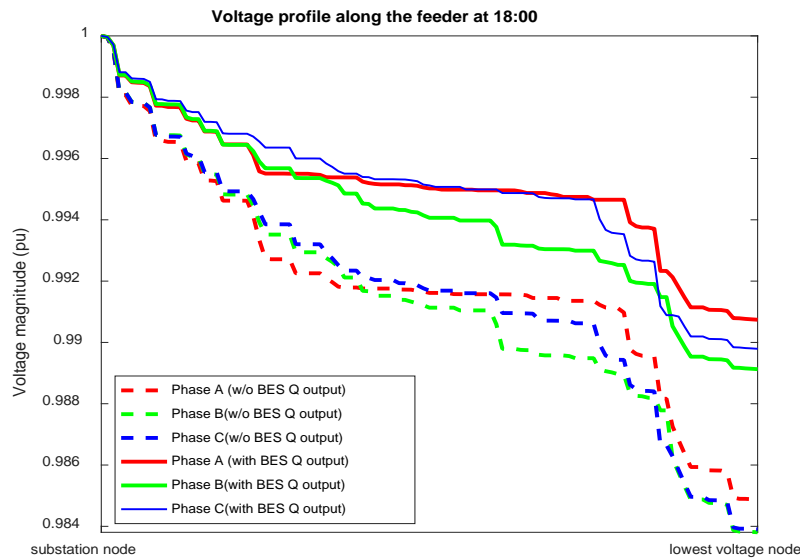


Figure 60. Voltage Profile Comparison Between Case with and without BESS Control for January 14, 2017

9.8.4 Simulation Results for January 15, 2017

The sensitivity table for the January 15, 2017 case is shown in Table 7. The average battery voltage before and after BESS control and the scheduled BESS reactive power output is plotted in Figure 61. The results about voltage profile comparison between cases with and without BESS control are plotted in Figure 62.

Table 7. The Sensitivity Table for January 15, 2017 Case

Voltage at battery bus (<i>p. u.</i>)	Inverse of sensitivity <i>K</i> (<i>kVar/p. u.</i>)
[0.98 0.985]	189500
[0.985 0.99]	190040

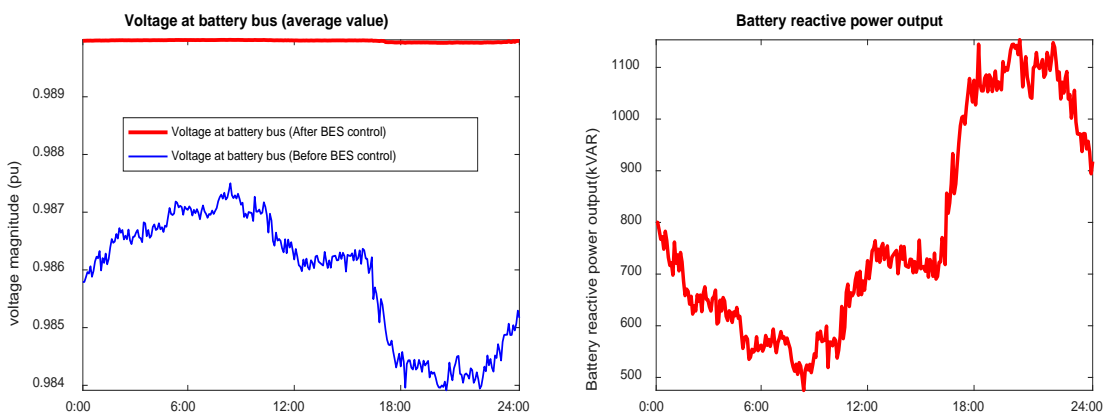


Figure 61. Average Battery Voltage Before and After Reactive Power Control (left) and the Schedule of Reactive Power of Battery for January 15, 2017 (right)

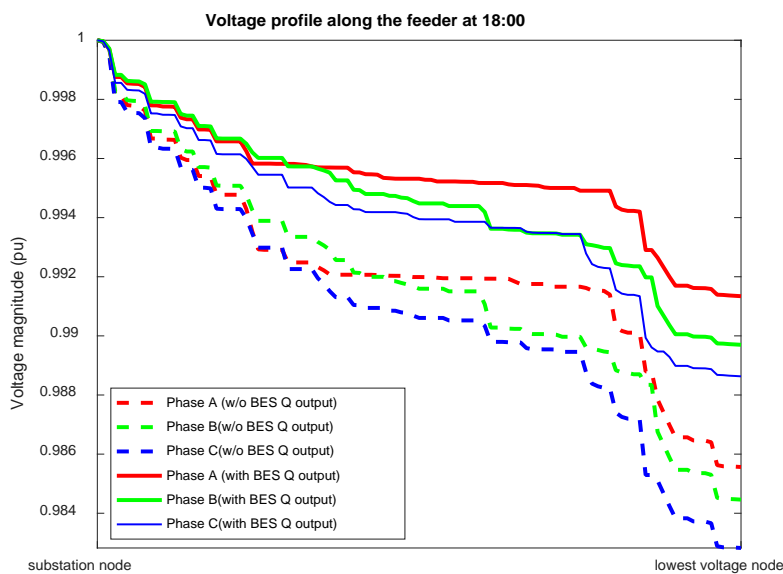


Figure 62. Voltage Profile Comparison Between Case with and without BESS Control for January 15, 2017

9.8.5 Simulation Results for January 16, 2017

The sensitivity table for the January 16, 2017 case is shown in Table 8. The average battery voltage before and after BESS control and the scheduled BESS reactive power output is plotted in Figure 63. The results about voltage profile comparison between cases with and without BESS control are plotted in Figure 64.

Table 8. The Sensitivity Table for January 16, 2017 Case

Voltage at battery bus (<i>p.u.</i>)	Inverse of sensitivity <i>K</i> (<i>kVar/p.u.</i>)
[0.975 0.98]	187880
[0.98 0.985]	188550
[0.985 0.99]	190050

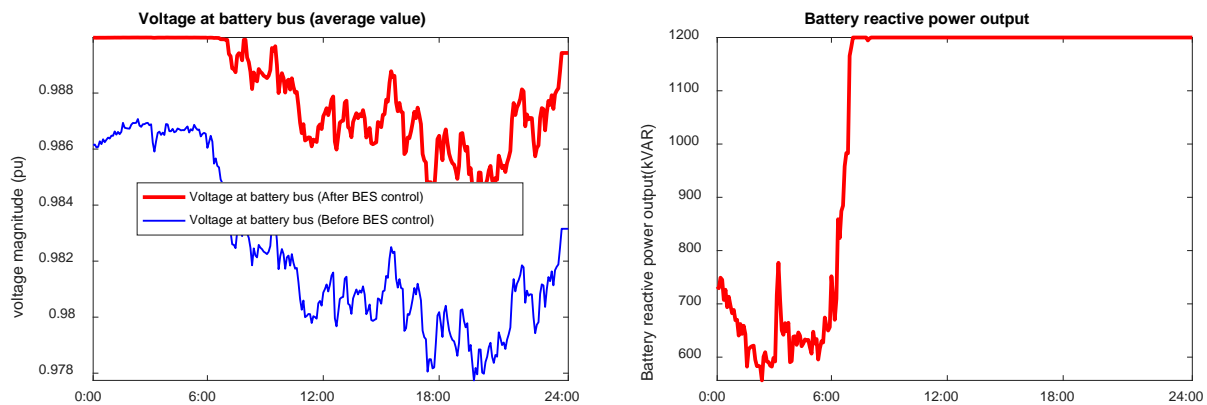


Figure 63. Average Battery Voltage Before and After Reactive Power Control (left) and the Schedule of Reactive Power of Battery for January 16, 2017 (right)

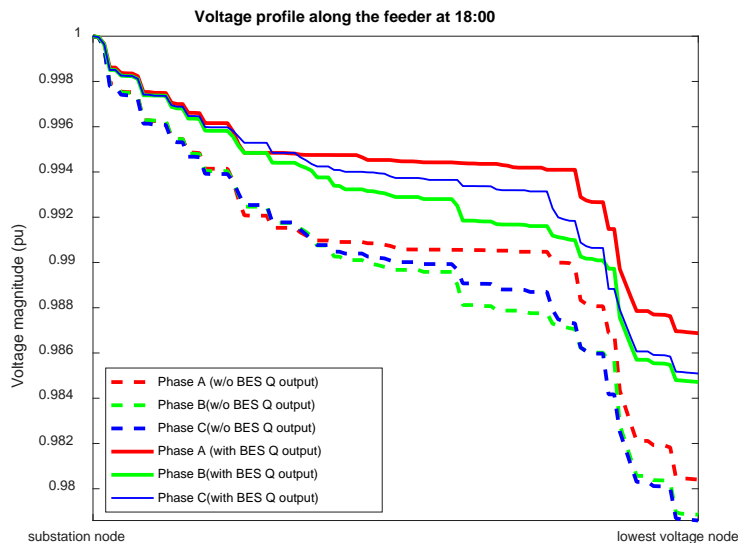


Figure 64. Voltage Profile Comparison Between Case with and without BESS Control for January 16, 2017

9.9 Simulation Results for Clear Data without PV – Summer Data Testing on Turner 117

9.9.1 Simulation Results for August 22, 2017

The sensitivity table for the August 22, 2017 case is shown in Table 9. The average battery voltage before and after BESS control and the scheduled BESS reactive power output is plotted in Figure 65. The results about voltage profile comparison between cases with and without BESS control are plotted in Figure 66.

Table 9. The Sensitivity Table for August 22, 2017 Case

Voltage at battery bus (p. u.)	Inverse of sensitivity K (kVar/p. u.)
[0.975 0.98]	187709
[0.98 0.985]	188688
[0.985 0.99]	189902

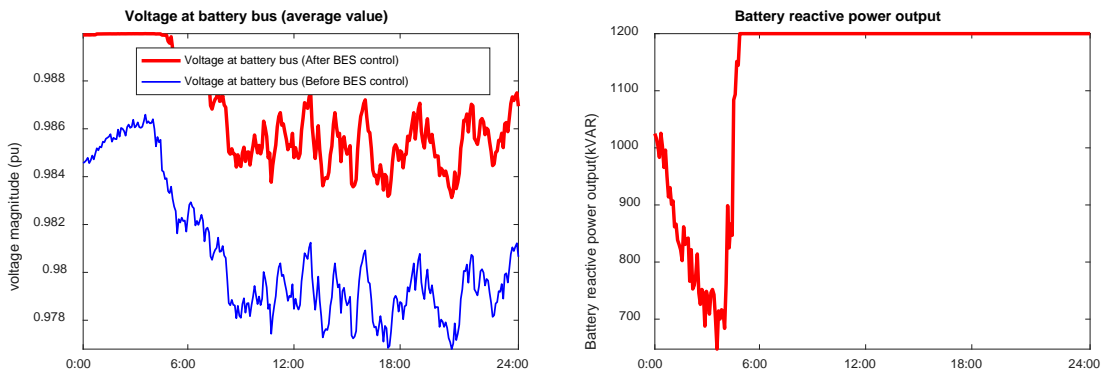


Figure 65. Average Battery Voltage Before and After Reactive Power Control (left) and the Schedule of Reactive Power of Battery for August 22, 2017 (right)

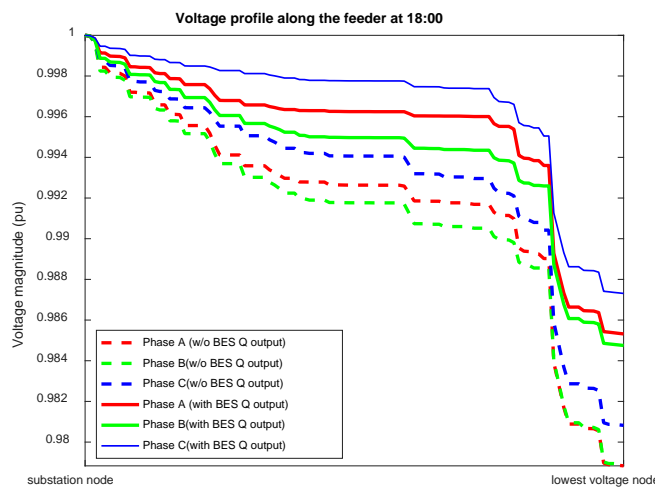


Figure 66. Voltage Profile Comparison Between Cases with and without BESS Control for August 22, 2017

9.9.2 Simulation Results for August 23, 2017

The sensitivity table for the August 23, 2017 case is shown in Table 10. The average battery voltage before and after BESS control and the scheduled BESS reactive power output is plotted in Figure 67. The results about voltage profile comparison between cases with and without BESS control are plotted in Figure 68.

Table 10. The Sensitivity Table for August 23, 2017 Case

Voltage at battery bus (<i>p.u.</i>)	Inverse of sensitivity <i>K</i> (<i>kVar/p.u.</i>)
[0.975 0.98]	187640
[0.98 0.985]	188810
[0.985 0.99]	190188

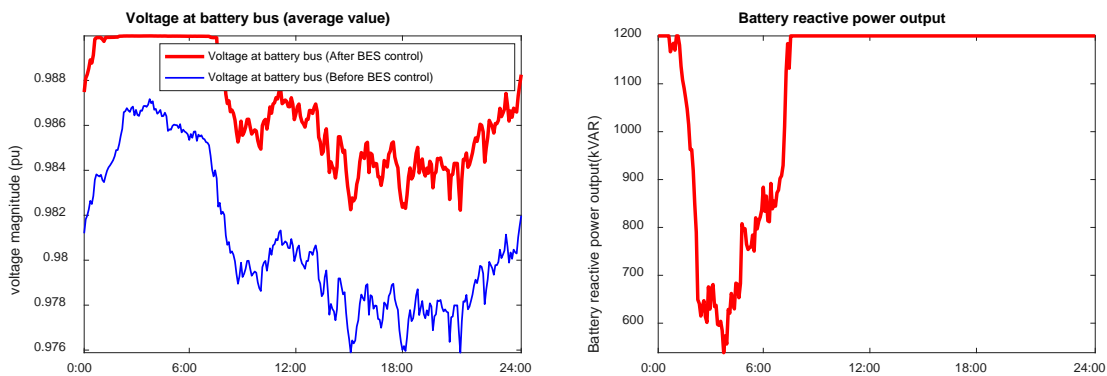


Figure 67. The Average Battery Voltage Before and After Reactive Power Control (left) and the Schedule of Reactive Power of Battery for August 23, 2017 (right)

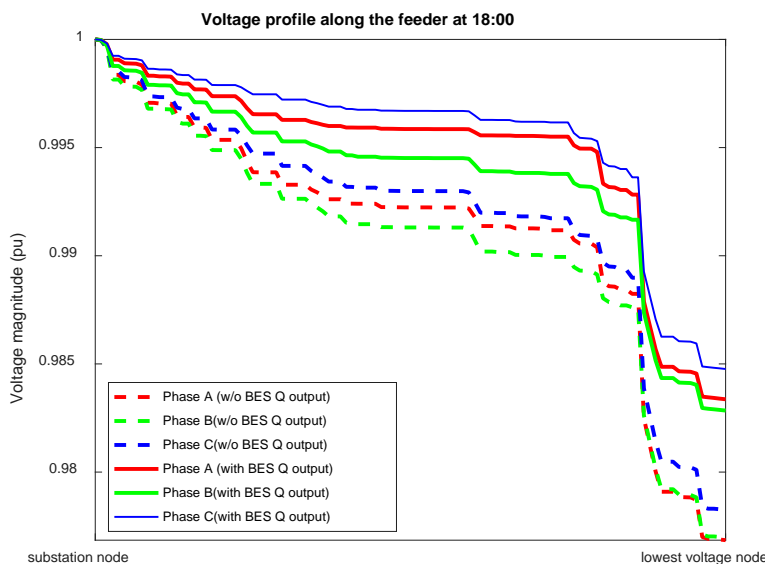


Figure 68. Voltage Profile Comparison Between Cases with and without BESS Control for August 23, 2017

9.9.3 Simulation Results for August 24, 2017

The sensitivity table for the August 24, 2017 case is shown in Table 11. The average battery voltage before and after BESS control and the scheduled BESS reactive power output is plotted in Figure 69. The results about voltage profile comparison between cases with and without BESS control are plotted in Figure 70.

Table 11. The Sensitivity Table for August 24, 2017 Case

Voltage at battery bus (<i>p. u.</i>)	Inverse of sensitivity <i>K</i> (<i>kVar/p. u.</i>)
[0.975 0.98]	187625
[0.98 0.985]	188856
[0.985 0.99]	190178

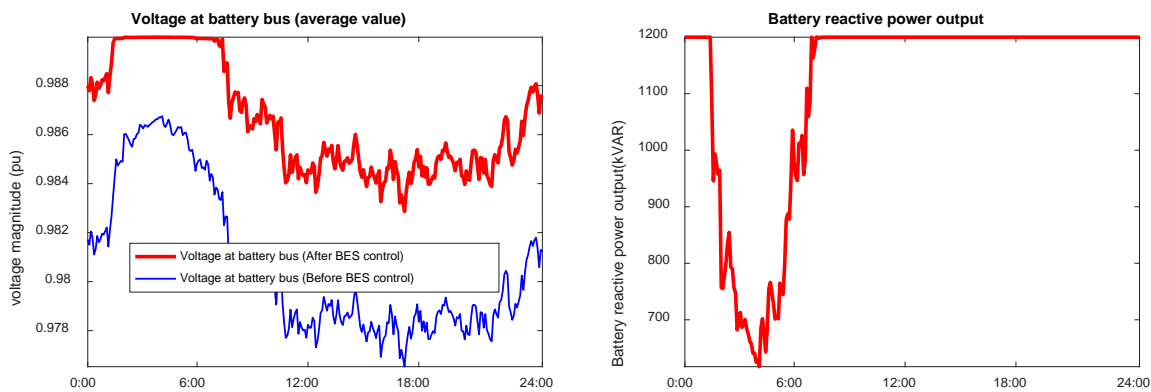


Figure 69. Average Battery Voltage Before and After Reactive Power Control (left) and the Schedule of Reactive Power of Battery for August 24, 2017 (right)

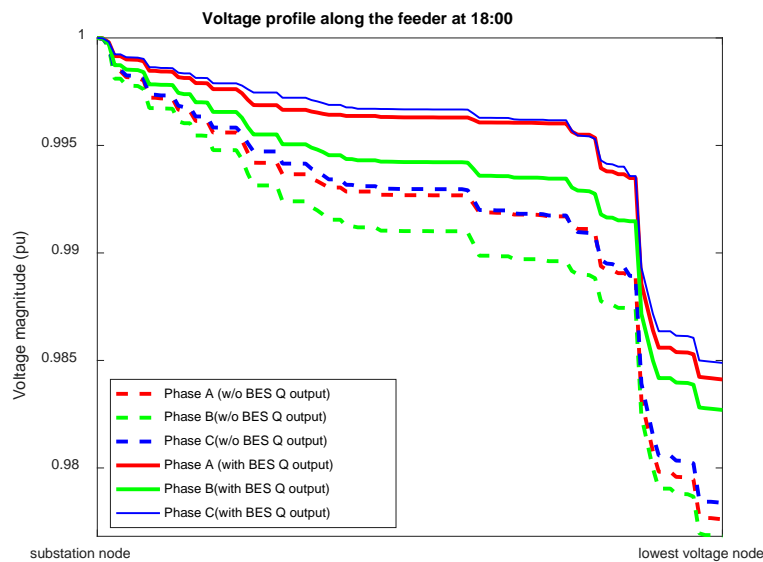


Figure 70. Voltage Profile Comparison Between Cases with and without BESS Control for August 24, 2017

9.9.4 Simulation Results for August 25, 2017

The sensitivity table for the August 25, 2017 case is shown in Table 12. The average battery voltage before and after BESS control and the scheduled BESS reactive power output is plotted in Figure 71. The results about voltage profile comparison between cases with and without BESS control are plotted in Figure 72.

Table 12. The Sensitivity Table for August 25, 2017 Case

Voltage at battery bus (<i>p. u.</i>)	Inverse of sensitivity <i>K</i> (<i>kVar/p. u.</i>)
[0.975 0.98]	187536
[0.98 0.985]	189107
[0.985 0.99]	189886

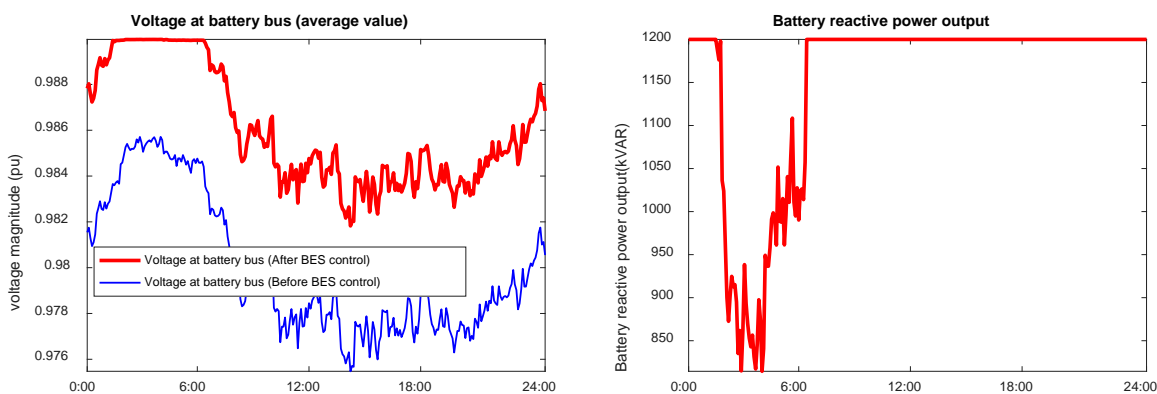


Figure 71. Average Battery Voltage Before and After Reactive Power Control (left) and the Schedule of Reactive Power of Battery for August 25, 2017 (right)

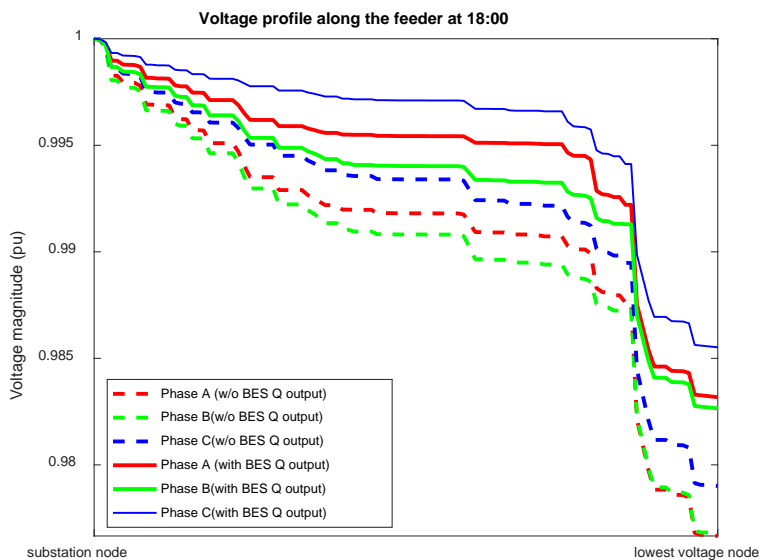


Figure 72. Voltage Profile Comparison Between Cases with and without BESS Control for August 25, 2017

9.10 Simulation Results for Clear Data without PV – Autumn Data Testing on Turner 117

9.10.1 Simulation Results for October 12, 2017

The sensitivity table for the October 12, 2017 case is shown in Table 13. The average battery voltage before and after BESS control and the scheduled BESS reactive power output is plotted in Figure 73. The results about voltage profile comparison between cases with and without BESS control are plotted in Figure 74.

Table 13. The Sensitivity Table for October 12, 2017 Case

Voltage at battery bus (p. u.)	Inverse of sensitivity K (kVar/p. u.)
[0.98 0.985]	189029
[0.985 0.99]	190283

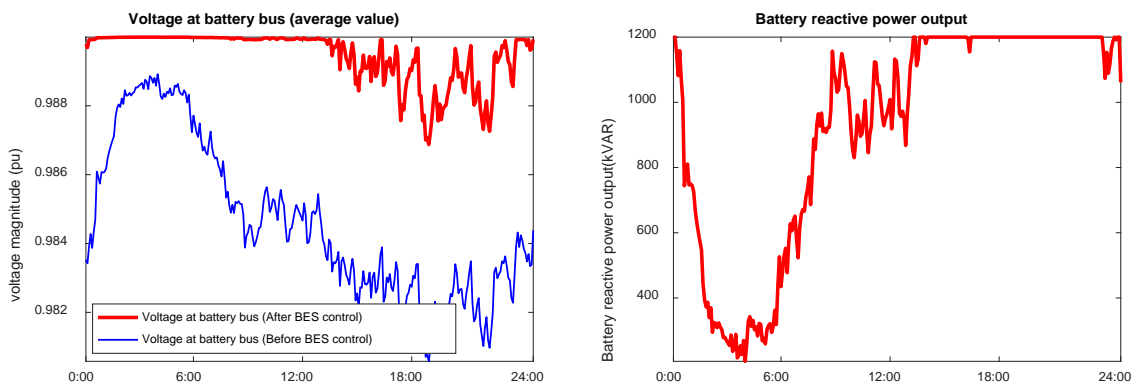


Figure 73. Average Battery Voltage Before and After Reactive Power Control (left) and the Schedule of Reactive Power of Battery for October 12, 2017 (right)

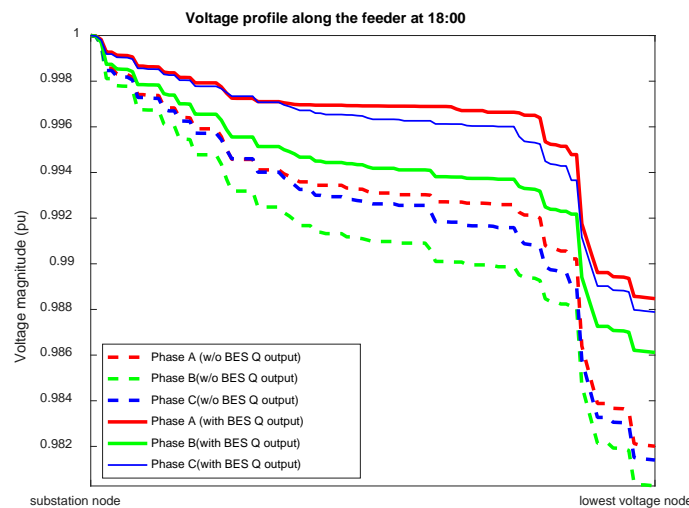


Figure 74. Voltage Profile Comparison Between Cases with and without BESS Control for October 12, 2017

9.10.2 Simulation Results for October 13, 2017

The sensitivity table for the October 13, 2017 case is shown in Table 14. The average battery voltage before and after BESS control and the scheduled BESS reactive power output is plotted in Figure 75. The results about voltage profile comparison between cases with and without BESS control are plotted in Figure 76.

Table 14. The Sensitivity Table for October 13, 2017 Case

Voltage at battery bus (<i>p. u.</i>)	Inverse of sensitivity <i>K</i> (<i>kVar/p. u.</i>)
[0.98 0.985]	188920
[0.985 0.99]	190299

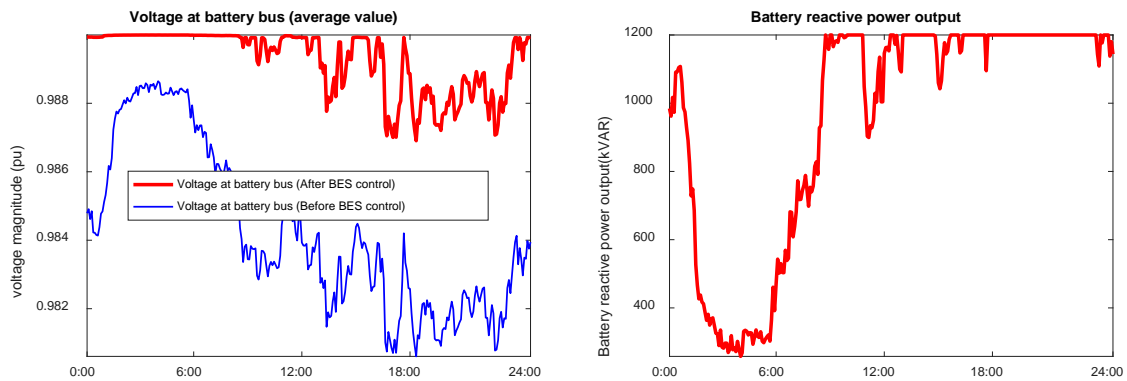


Figure 75. The Average Battery Voltage Before and After Reactive Power Control (left) and the Schedule of Reactive Power of Battery for October 13, 2017 (right)

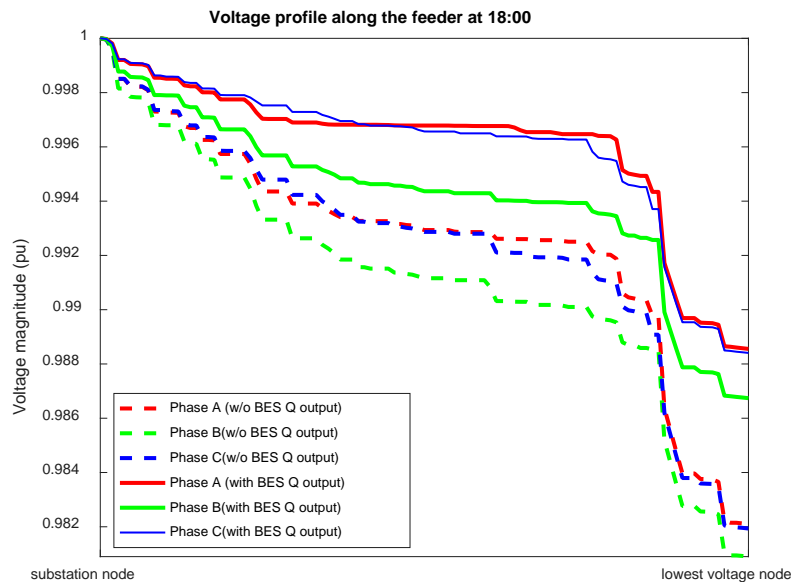


Figure 76. Voltage Profile Comparison Between Cases with and without BESS Control for October 13, 2017

9.10.3 Simulation Results for October 14, 2017

The sensitivity table for the October 14, 2017 case is shown in Table 15. The average battery voltage before and after BESS control and the scheduled BESS reactive power output is plotted in Figure 77. The results about voltage profile comparison between cases with and without BESS control are plotted in Figure 78.

Table 15. The Sensitivity Table for October 14, 2017 Case

Voltage at battery bus (<i>p.u.</i>)	Inverse of sensitivity <i>K</i> (<i>kVar/p.u.</i>)
[0.98 0.985]	189049
[0.985 0.99]	190399

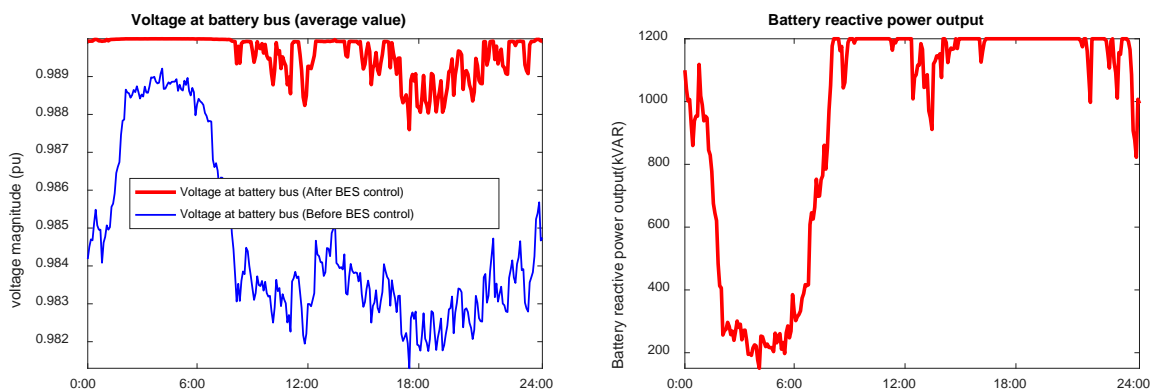


Figure 77. Average Battery Voltage Before and After Reactive Power Control (left) and the Schedule of Reactive Power of Battery for October 14, 2017 (right)

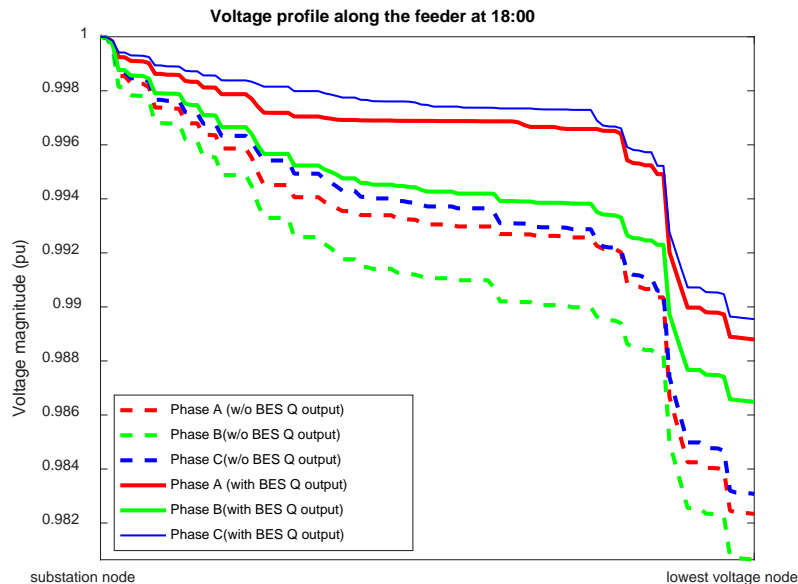


Figure 78. Voltage Profile Comparison Between Cases with and without BESS Control for October 14, 2017

9.10.4 Simulation Results for October 15, 2017

The sensitivity table for the October 15, 2017 case is shown in Table 16. The average battery voltage before and after BESS control and the scheduled BESS reactive power output is plotted in Figure 79. The results about voltage profile comparison between cases with and without BESS control are plotted in Figure 80.

Table 16. The Sensitivity Table for October 15, 2017 Case

Voltage at battery bus (<i>p. u.</i>)	Inverse of sensitivity <i>K</i> (<i>kVar/p. u.</i>)
[0.985 0.99]	190648

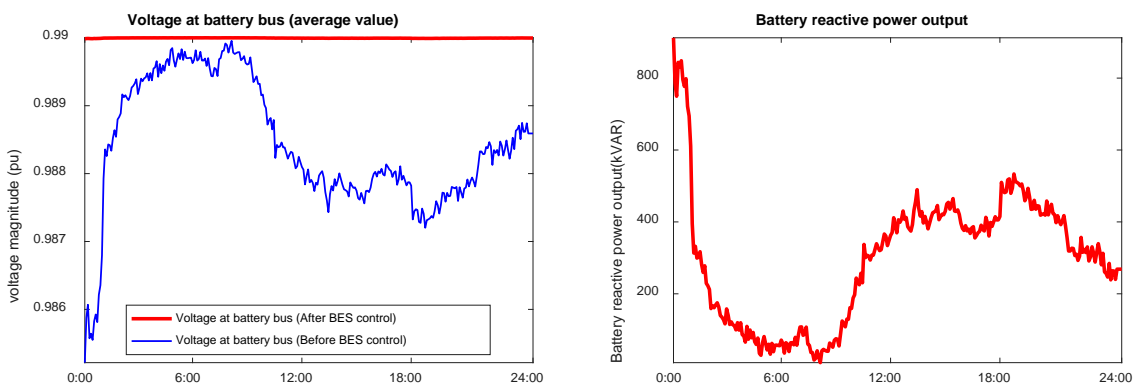


Figure 79. Average Battery Voltage Before and After Reactive Power Control (left) and the Schedule of Reactive Power of Battery for October 15, 2017 (right)

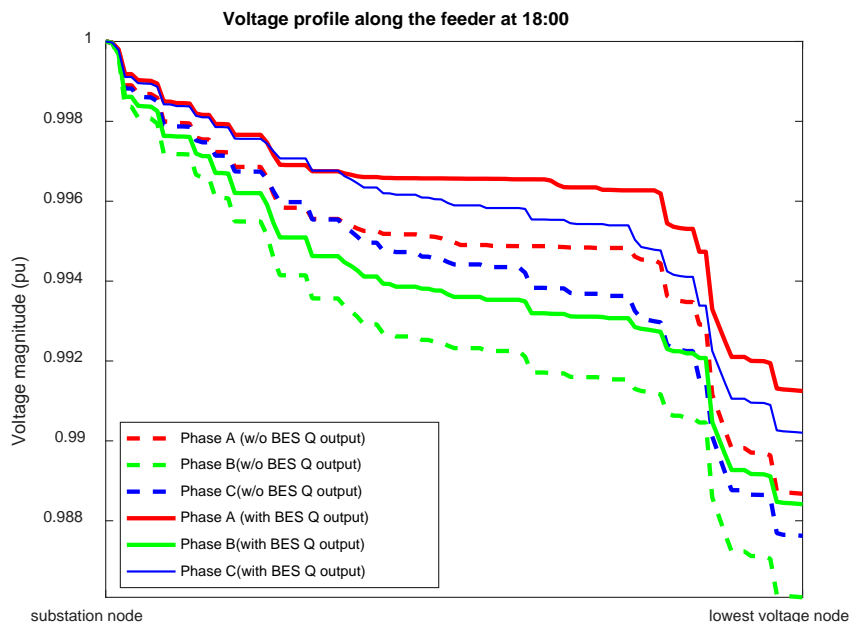


Figure 80. Voltage Profile Comparison Between Cases with and without BESS Control for October 15, 2017

9.11 Statistical Analysis of ESS Controller

In this section, the statistical analysis for the impact of ESS controller for all testing days is presented based on power factor correction. As seen from Figure 81, ESS helps to increase the power factor during the simulation and the improvement is relatively low during morning and high during the rest of the time. To quantify the improvement for all the tests, the maximum, minimum, and average power factor with/without ESS controller are listed in Table 17.

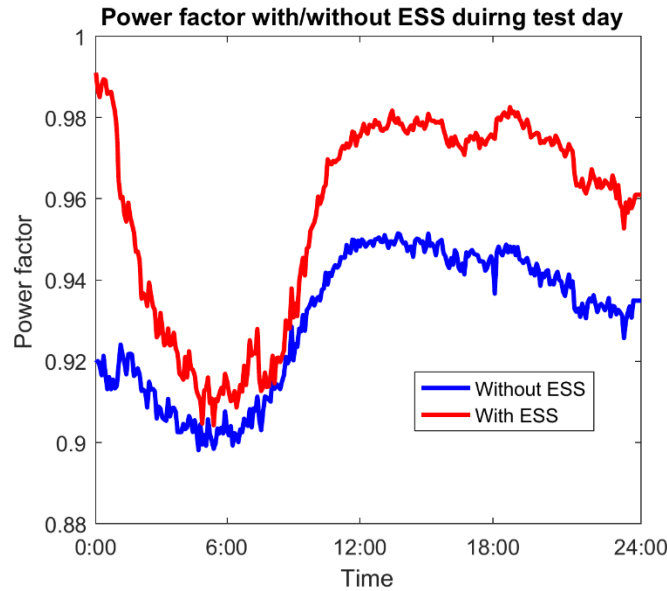


Figure 81. Power Factor Improvement for October 15, 2016

Table 17. Power Factor Improvement from ESS Controller for All Test Cases

Season	Date	Minimum Power Factor		Maximum Power Factor		Average Power Factor	
		No ESS	With ESS	No ESS	With ESS	No ESS	With ESS
Summer	Aug 22,2016	0.903	0.983	0.952	1.000	0.929	0.996
	Aug 23,2016	0.916	0.987	0.958	1.000	0.937	0.997
	Aug 24,2016	0.924	0.989	0.948	1.000	0.934	0.997
	Aug 25,2016	0.922	0.990	0.956	1.000	0.935	0.997
Autumn	Oct 12,2016	0.916	0.949	0.965	1.000	0.938	0.990
	Oct 13,2016	0.907	0.945	0.952	1.000	0.933	0.989
	Oct 14,2016	0.907	0.937	0.957	1.000	0.929	0.988
	Oct 15,2016	0.898	0.904	0.951	0.991	0.930	0.956

Season	Date	Minimum Power Factor		Maximum Power Factor		Average Power Factor	
		No ESS	With ESS	No ESS	With ESS	No ESS	With ESS
Winter	Jan 12,2017	0.987	0.997	0.996	1.000	0.991	0.999
	Jan 13,2017	0.988	0.997	0.995	1.000	0.992	0.999
	Jan 14,2017	0.992	0.999	0.997	1.000	0.995	1.000
	Jan 15,2017	0.988	1.000	0.996	1.000	0.994	1.000
	Jan 16,2017	0.985	0.997	0.996	1.000	0.992	1.000

The installed ESS can increase the average power factor to close to 1 p.u. in most of the test cases. On some days, like October 15, 2016, the reactive power demand is much higher than the other cases, and the ESS can only improve it to 0.96. After conducting simulation for more cases with varying ESS size and load, a suitable ESS can be determined for a given industrial feeder. Through improving the power factor, ESS will help to reduce the total current flow and free additional feeder capacity. The reduced load could help to extend the life of system devices and enrich switching options during contingency (Yunzhi et al., 2014).

9.12 Validation of a Constant K Value for Winter Season

Utilizing different sensitivity factors for the different voltage ranges may add burden for real-time operation and maintenance; therefore, this section tests the feasibility of using the same sensitivity factor for all the voltage ranges. The sensitivity factor of each voltage range for testing days are presented in Table 18. As shown in this table, the variation of sensitivity factors is very small among different voltage ranges. Moreover, the highest load variation for these simulation days is about 9 percent for the peak demand. In contrast, the sensitivity factor variation is only 0.5 percent. Therefore, using a constant sensitivity factor for all voltage ranges instead of distinct factors for each voltage range is possible.

Table 18. The Sensitivity Table for January 12 to 16, 2017 Cases

Voltage at battery bus	Inverse of sensitivity				
	12-Jan	13-Jan	14-Jan	15-Jan	16-Jan
[0.975 0.98]	187750	187880	N/A	N/A	187880
[0.98 0.985]	188700	188590	189500	189500	188550
[0.985 0.99]	190020	189720	189950	190040	190050

To validate this assumption, the average value of k among the five test cases is calculated first. After that, the performance of using same and different sensitivity factors in BESS control is compared on January 15. The battery reactive output comparison of these two settings are shown in Figure 82. The BESS reactive power output difference is very small. Therefore, using same sensitivity factor for different voltage ranges is possible, and this setting will simplify the design and maintenance of BESS controller in real-time operation at the cost of the small deviation in performance of the BESS controller.

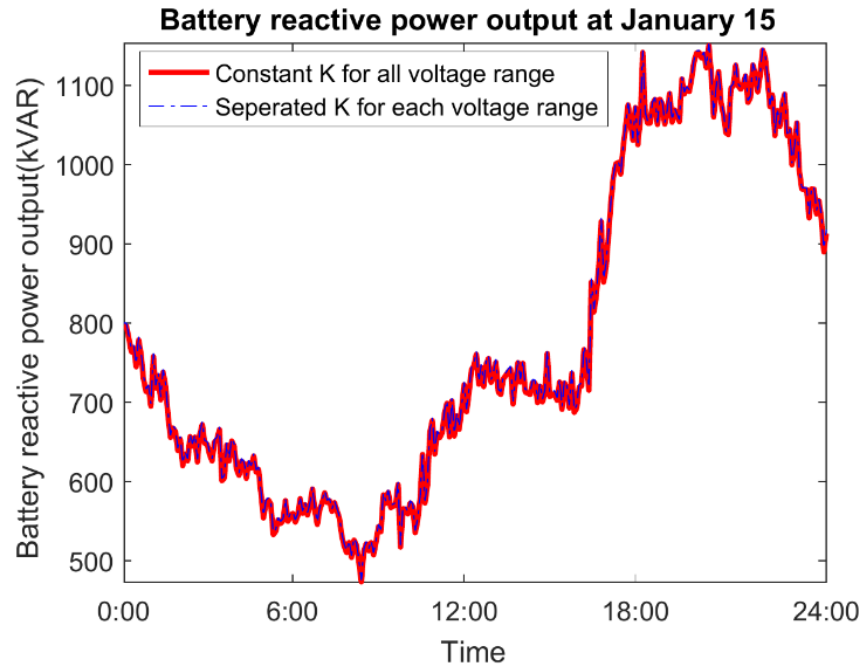


Figure 82. Reactive Power Schedule of BESS Generated by Constant K and Separated K for Each Voltage Range at January 15, 2017

9.13 Simulation Results without PV

9.13.1 PV Installation Location

In this project, a 75kW PV model is added to the feeder model to test the voltage control strategy with different levels of PV penetration. Currently, the PV has not been connected to the grid, but an estimated installed location is available (ND_391-889858), as seen in Figure 83. After testing with weather data (CA-Bakersfield.tmy2), the feeder model with PV component is working, there is no error for the simulation, and there are outputs from PV panels.

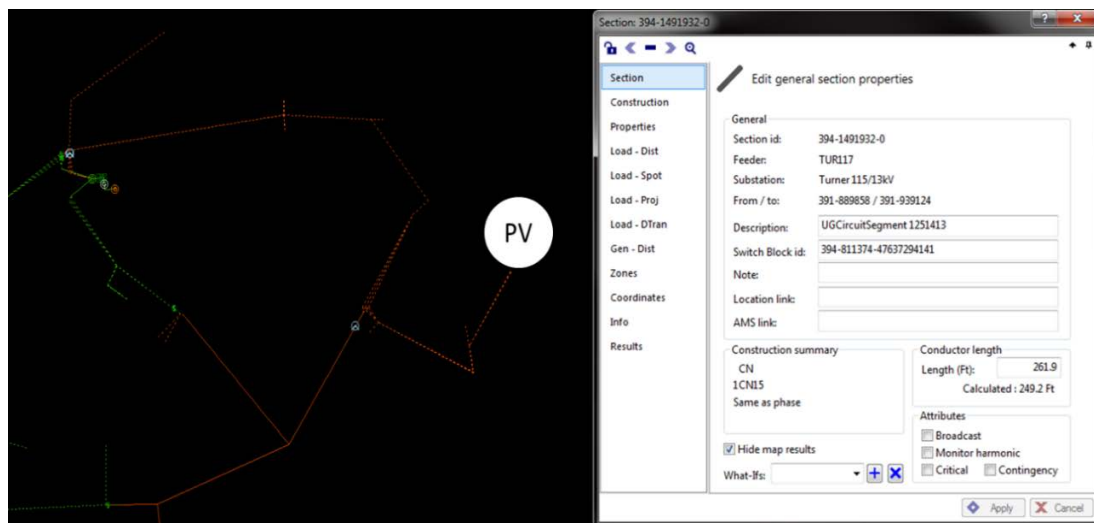


Figure 83. PV Location and Connected Node ID

The output from the PV module from GridLAB-D is recorded by collector in “solar_collector_day.csv.” Since it was connected to phase C only, there is only output from that phase. In the following, two simulation cases are generated to validate the correctness of PV model. The first case is Turner 117 with a 750-kVA PV panel, and the other one is Turner 116 without the PV panel. Comparing the real power demand difference and the recorded PV output from the recorder in Figure 84, it is clearly that the PV model is functioning well.

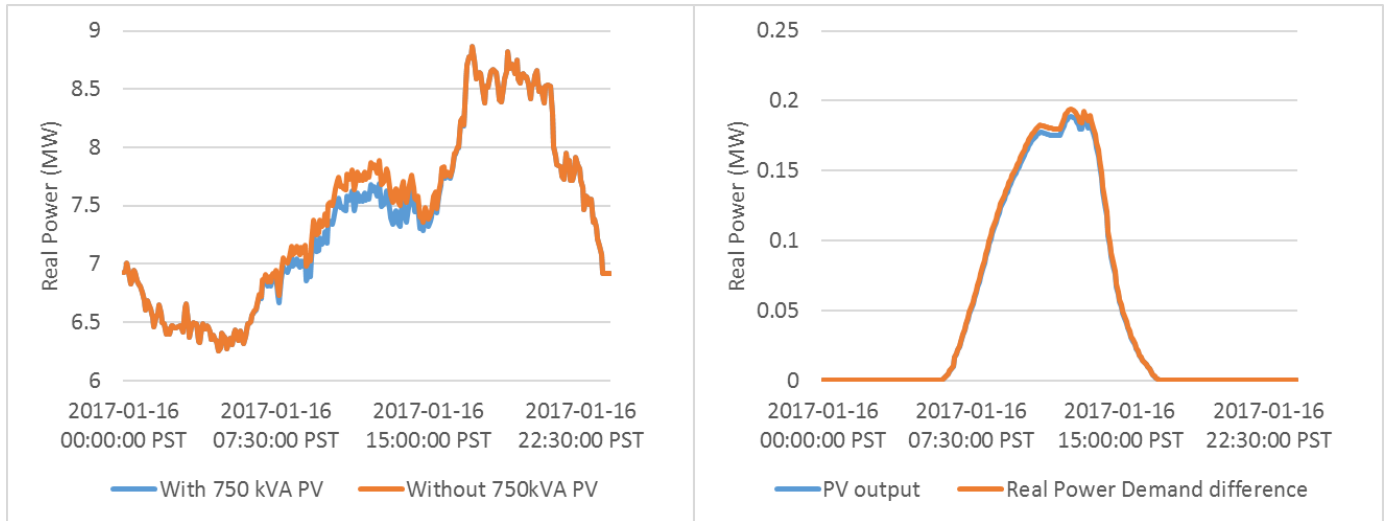


Figure 84. Real Power Demand for January 16 w/wo a 750 kVA PV Panel (left); the PV Output and the Real Power Demand Difference w/wo PV Panel Penetration

9.13.2 Voltage Control Results for Different Levels of PV Penetration

9.13.2.1 Voltage Control Results for 75 KVA PV Penetration

The sensitivity table for the January 16, 2017 case with 75 KVA is shown in Table 19. The average battery voltage before and after BESS control and the scheduled BESS reactive power output is plotted in Figure 85. The results about voltage profile comparison between cases with and without BESS control are plotted in Figure 86.

Table 19. The Sensitivity Table for January 16, 2017 Case with 75 kVA PV

Voltage at battery bus (<i>p. u.</i>)	Inverse of sensitivity <i>K</i> (<i>kVar/p. u.</i>)
[0.975 0.98]	187790
[0.98 0.985]	188540
[0.985 0.99]	190050

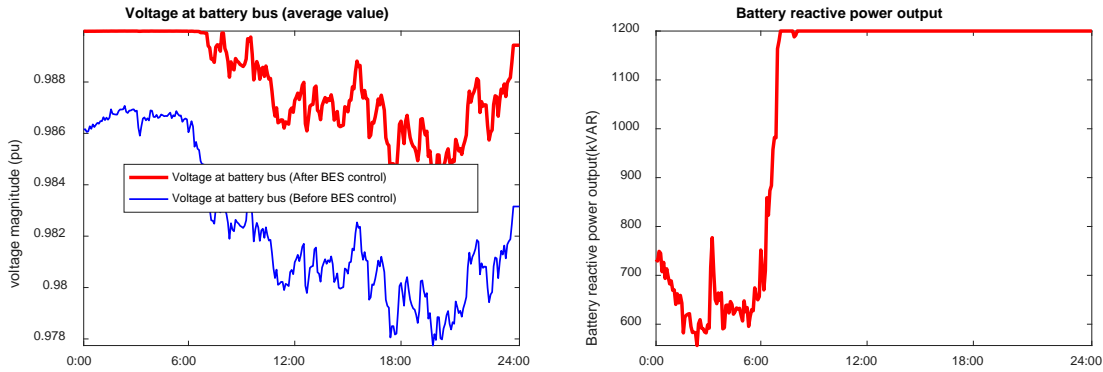


Figure 85. Average Battery Voltage Before and After Reactive Power Control (left) and the Schedule of Reactive Power of Battery for January 16, 2017 with 75 kVA PV (right)

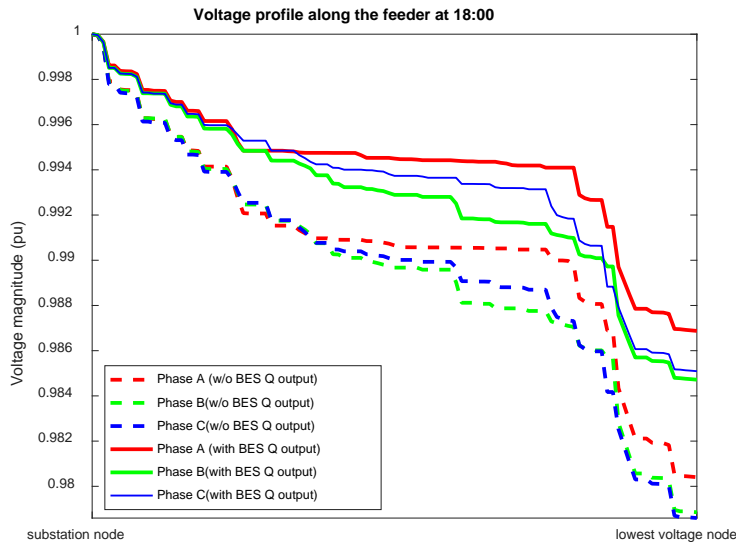


Figure 86. Voltage Profile Comparison Between Case with and without BESS Control for January 16, 2017 with 75 kVA PV

9.13.2.2 Voltage Control Results for 750 kVA PV Penetration

The sensitivity table for the January 16, 2017 case with 750 kVA is shown in Table 20. The average battery voltage before and after BESS control and the scheduled BESS reactive power output is plotted in Figure 87. The results about voltage profile comparison between cases with and without BESS control are plotted in Figure 88.

Table 20. The Sensitivity Table for January 16, 2017 Case with 750 kVA PV

Voltage at battery bus (<i>p. u.</i>)	Inverse of sensitivity <i>K</i> (<i>kVar/p. u.</i>)
[0.975 0.98]	187760
[0.98 0.985]	188610
[0.985 0.99]	190050

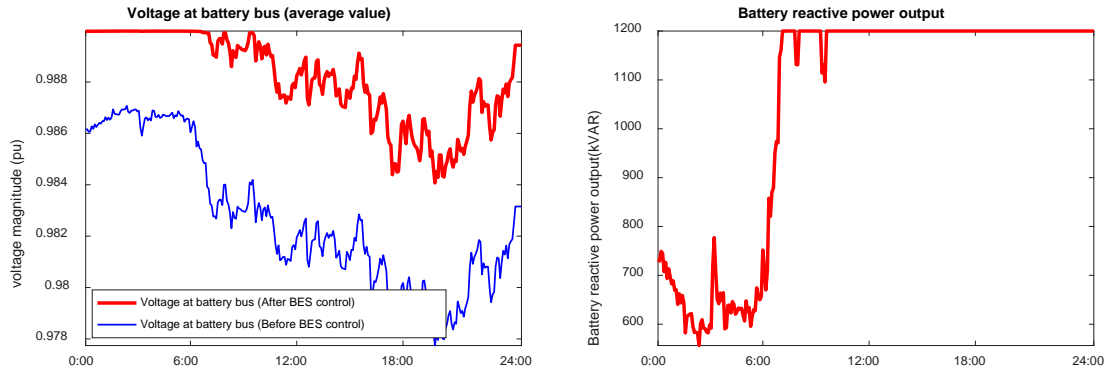


Figure 87. Average Battery Voltage Before and After Reactive Power Control (left) and the Schedule of Reactive Power of Battery for January 16, 2017 with 750 kVA PV (right)

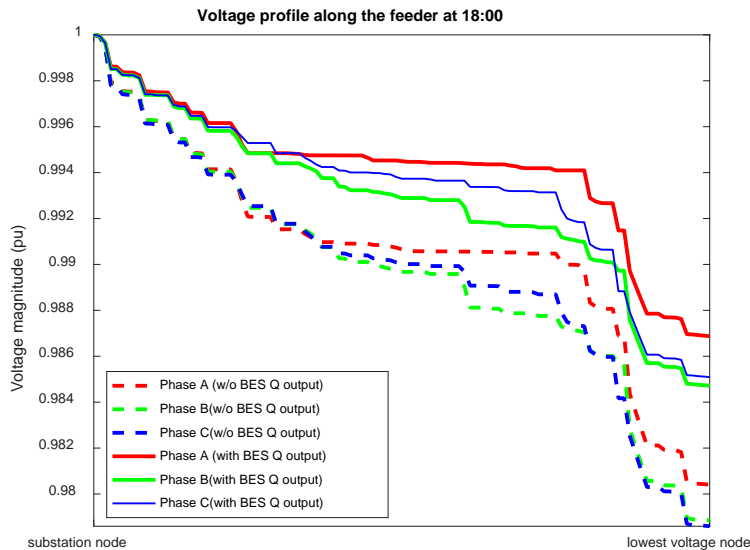


Figure 88. Voltage Profile Comparison Between Case with and without BESS Control for January 16, 2017 with 750 kVA PV

9.13.2.3 Voltage Control Results for 3000 kVA PV Penetration

The sensitivity table for the January 16, 2017 case with 3000 kVA is shown in Table 21. The average battery voltage before and after BESS control and the scheduled BESS reactive power output is plotted in Figure 89. The results about voltage profile comparison between cases with and without BESS control are plotted in Figure 90.

Table 21. The Sensitivity Table for January 16, 2017 Case with 3000 kVA PV

Voltage at battery bus (<i>p. u.</i>)	Inverse of sensitivity <i>K</i> (<i>kVar/p. u.</i>)
[0.975 0.98]	187770
[0.98 0.985]	188740
[0.985 0.99]	189810

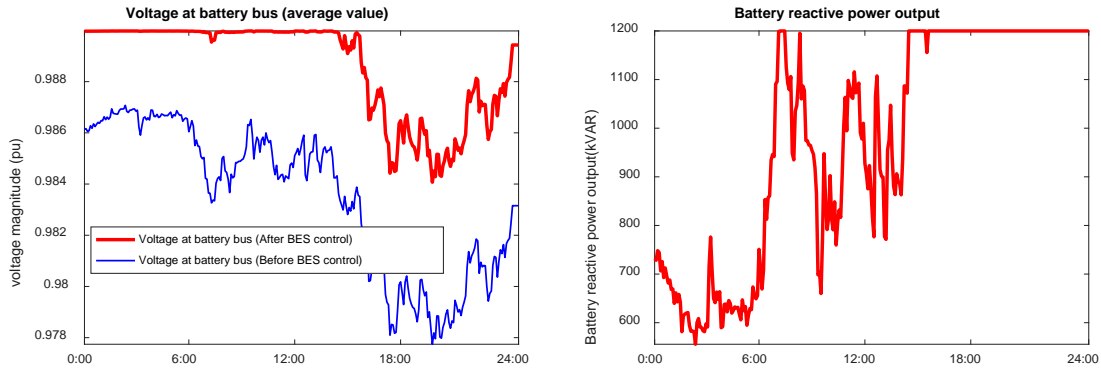


Figure 89. Average Battery Voltage Before and After Reactive Power Control (left) and the Schedule of Reactive Power of Battery for January 16, 2017 with 3000 kVA PV (right)

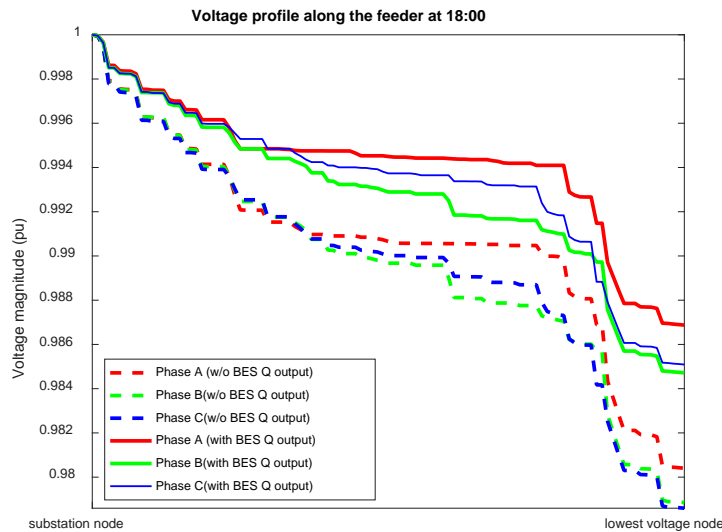


Figure 90. Voltage Profile Comparison Between Case with and without BESS Control for January 16, 2017 with 3000 kVA PV

9.13.2.4 Results Comparison for Different Levels of PV Penetration

The sensitivity table for different levels of PV penetration is listed in Table 22. It is clear that increasing the PV penetration has very limited effect on the sensitivity parameter K. A constant sensitivity value for winter season is still validated.

Table 22. The Sensitivity Table for January 12 to 16, 2017 Cases

Voltage at battery bus	Inverse of sensitivity for Jan. 16			
	No PV	75 kVA PV	750 kVA PV	3000 kVA PV
[0.975 0.98]	187880	187790	187760	187770
[0.98 0.985]	188550	188540	188610	188740
[0.985 0.99]	190050	190050	190050	189810

Since the PV output provides much real power support during noon time, at high PV penetrations like a 3000-kVA installation, the battery output limit is relaxed during noon time. Observing the battery reactive power output profiles w/o PV penetration, it is apparent that the battery output will not cap at 1.2 MVAR during noon time when installing 3000 kVA PV.

However, the PV installation may lead to power unbalance issues since the current PV is only connected to phase. Seen from Figure 91, due to the significant output from PV during noon time, a clear voltage unbalancing phenomenon occurs. Therefore, under high penetration class, a three-phase connection may provide better service.

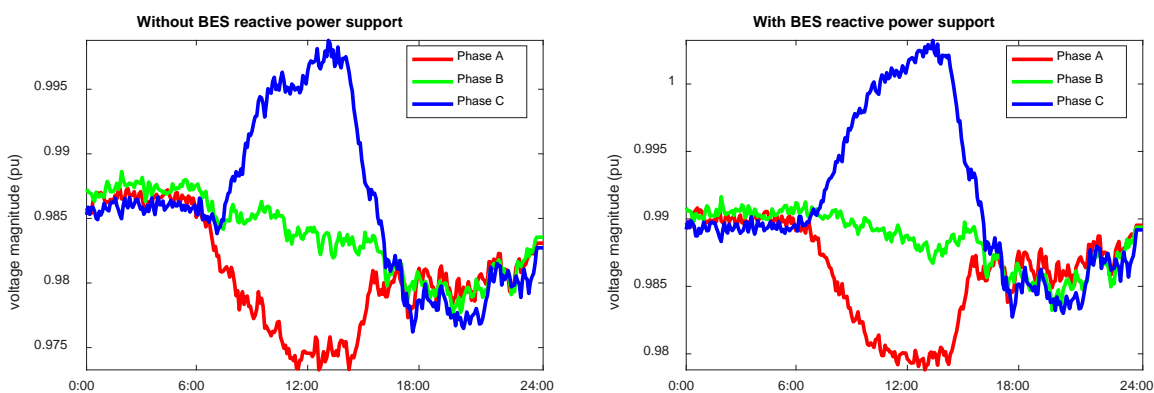


Figure 91. Voltage of Three Phases at the Bus with Lowest Voltage with and without BESS Control for 3000 kVA PV Penetration Case

9.14 Simulations Conclusion

In summary, this section proposed an ESS voltage control strategy based on the voltage sensitivity analysis. For the real-time operation, the proposed controller utilizes only average voltage measured at the ESS bus to determine the control signal. Validation of the proposed control strategy for several test scenarios demonstrates the voltage support along the feeder for all the test cases. Comparison of the measured voltage with and without the ESS control at the ESS bus also demonstrates the accuracy of the proposed method. The performance of the proposed ESS control scheme under a heavy load scenario and system involving PV penetration were tested, as well. For the high load cases, the measured voltage at the ESS bus does not reach the target voltage even after the ESS support for a certain period due to the reactive output limitation of the ESS. This limitation could be released, either by increasing the ESS capacity or lowering the voltage setting point at the ESS bus. Simulation results with PV integration show that PV has very limited influence on the ESS controller at low PV penetration. Under high PV penetration, PV output will have a significant impact on ESS controller. During peak time of PV generation, PV can help to mitigate the load stress and give ESS more room to provide voltage support. Simulation results also demonstrate that a same sensitivity factor for the different voltage range is possible at the cost of minor impact on the performance of the controller. Developed control mechanisms for ESS can be extended for optimal and coordinated control in the future given required infrastructure to implement such a centralized control scheme.

10.0 Conclusion

This report presented the work performed by PNNL and WSU to assist Avista in developing and implementing control strategies for a 1-MW/3.2-MWh ESS project at the Avista Turner substation funded by Washington CEF program. PNNL's work contributed to the conceptual development of control strategies, including capabilities to address the uncertainties in prices and a high-level guideline on deploying the control strategies. WSU's scope was to enable understanding how real and reactive power control by the ESS will benefit Avista in providing various ancillary support for network management, for instance, supporting sudden change in load, load ramping, voltage, etc.

In examining all the potential services the ESS might provide, it is clear that the types of information needed to optimally dispatch each of these services is not uniform. Analysis revealed three types of services that need to be provisioned by the controller as a whole:

- **Market Services** – Services where both the price/value forecast is fully defined, and the optimizer is directly able to fully determine the charge/discharge commands for the ESS. Example: energy arbitrage.
- **Operational Services** – Services where no meaningful price/value forecast is possible, and the exact charge/discharge behavior of the ESS is fully defined by operating conditions at the ESS. Example: outage mitigation.
- **Hybrid Services** – Services where a price/value forecast is available, but the charge/discharge commands cannot be determined by the optimizer. Instead, these commands must be generated based on current electrical system conditions. Example: frequency regulation.

Due to limitations in communication and computation in Avista's system, it is not possible for a single controller to handle all three of these types of services. It is proposed to split the controller into three portions, as summarized below.

- An optimization controller that accepts price/value forecasts as inputs and generates an optimized dispatch schedule. This controller fully provisions all market services and indicates to the real-time controller the timing of the engagement of the hybrid services.
- A real-time controller accepts the optimized dispatch schedule (for market services) and converts commands to offer hybrid services into optimized charge/discharge commands based on current system conditions. This controller completes the provision for all hybrid services.
- A local controller that accepts the optimized charge/discharge commands as input from the real-time controller and executes them as on the ESS proper. In the case of an operational event (such as the beginning of an outage), the local controller will instantaneously override the optimized charge/discharge commands and provide the immediately required service. This controller fully and independently provisions all operational services.

All forecasts contain uncertainty (whether quantified or not), and any optimization that ignores these may produce a mathematically valid optimal schedule that is so sensitive to input conditions that it is practically impossible to achieve that value. It is proposed that the optimization engine at the core of the optimization controller be modified to accept

uncertainty information associated with all of the forecasts it uses in forming its optimized dispatch schedule.

Given its value to Avista's system as a whole, it is proposed to incorporate only uncertainty related to the wholesale energy price into the optimization engine. To create these uncertainty estimates, a statistical model will be developed comparing the forecasted and actual value for the given signal. From this comparison, an error signal for each dispatch period of the forecast horizon will be generated, and a model of that error will be formed. Using this model, the standard deviation of the error for each period in the forecast will be calculated and added as a weighting factor in the optimization function. Periods with high standard deviations of forecast error will induce a penalty for price-based energy transactions during those periods. This penalty will also be weighted by a user-specified risk tolerance.

The distribution network model provided by Avista in Synergi software format was converted by WSU into GridLAB-D format for analysis of the impact of ESS real and reactive power on network operation. Validation of the converted model was performed by comparing power flow results between GridLAB-D and Synergi.

A dynamic model of the Avista system was developed by approximating the dynamics of the conventional generators using a lumped model to analyze the impact of ESS real power injection on dynamic performance in terms of frequency deviation. Two dynamic disturbance cases were studied: one is a step increase in load, and the other is ramping up of load. Among the three different strategies of ACE signal allocation between the ESS and conventional units, the strategy that allocates the highest amount of ACE to the ESS demonstrated best performance for both disturbance cases.

To study the usefulness of the reactive power capability of the ESS in supporting voltage of the Avista distribution network, time series power flow analysis was performed. A voltage-sensitivity-based reactive power control strategy was developed. Validation of the proposed control strategy for several test scenarios, including summer and winter days, demonstrate the ability of the ESS for supporting voltage along the feeder. Scenarios involving high load and PV penetration are also studied. Limitation of inverter reactive power capability may result in not achieving the target voltage in a high load scenario. In addition to a heavy load scenario, multiple solar PV penetration scenarios have been studied to understand the impact of PV generation on voltage profiles and the interaction with ESS inverter reactive power control. The results would be useful to better understand the voltage sensitivities of Avista network with real and reactive power and, hence, to develop mechanisms for optimal and coordinated voltage control.

11.0 References

Synergi Electric. n.d. "Synergi Electric 5.2 User Guide." Accessed at <https://www.dnvgl.com/services/power-distribution-system-and-electrical-simulation-software-synergi-electric-5005>.

Yunzhi C, M Tabrizi, M Sahni, A Povedano, and D Nichols. 2014. "Dynamic Available AGC Based Approach for Enhancing Utility Scale Energy Storage Performance," *IEEE Transactions on Smart Grid*. 5(2):1070–1078.

Pacific Northwest National Laboratory

902 Battelle Boulevard
P.O. Box 999
Richland, WA 99354
1-888-375-PNNL (7665)

www.pnnl.gov